W-PM-WS3-3

Tryptophan as a Structural Probe in Peptides and Proteins, Mary D. Barkley, Department of Chemistry, Louisiana State University, Baton Rouge, LA 70803

The amino acid tryptophan is a superb intrinsic probe of peptide and protein structure because its fluorescence is so sensitive to environment. A complex fluorescence decay is usually observed for single tryptophans in polypeptide chains, presumably reporting the heterogeneous microenvironment of the the indole chromophore. The environmental sensitivity derives from two sources: two overlapping electronic transitions with different polarity in the first absorption band and multiple nonradiative decay channels.

We have used constrained tryptophan derivatives to dissect the different nonradiative processes of indole. First, the complex fluorescence decays reflect ground-state heterogenity which leads to excited-state heterogeneity. Second, the nonradiative rate of indole includes contributions from several environmentally sensitive pathways: solvent quenching, excited-state proton transfer, and excited-state electron transfer. Solvent quenching refers to the major temperature-dependent nonradiative process that occurs in all indoles in protic solvent. Two types of excited-state proton transfer reactions occur in indoles at neutral pH in the presence of a strong proton donor: intramolecular and intermolecular. Intra- and intermolecular proton transfer rates can be estimated from photochmical reaction yields for H-D exchange at aromatic carbons. Excited-state electron transfer has not been detected directly, but inferred from solute quenching experiments and substituent effects. Preliminary studies suggest that the electron transfer rate is independent of temperature.

W-PM-WS3-4

BIOSYNTHETIC INCORPORATION OF TRYPTOPHAN ANALOGS IN PROTEINS: EXCITING PROSPECTS FOR PROTEIN INTERACTION STUDIES. ((A. G. Szabo[1,2], C. W. V. Hogue[2], and J. Brennan[2])) [1]Institute for Biological Sciences, National Research Council, Bldg. M54, Montreal Rd., Ottawa Canada, K1A 0R6, [2]Department of Biochemistry, University of Ottawa, 451 Smyth Rd., Ottawa Canada, K1H 8M5.

Protein-protein interactions are ubiquitous in biochemistry and biology and often play a key role in cellular function. The understanding of the molecular details of these interactions are important to the elucidation of their role in biological processes. NMR spectroscopy and X-ray crystallography can provide atomic details of the structure and interactions in proteins. Because of practical limitations many problems involving protein-protein interactions are not amenable to study by these methodologies. In many of the studies of the structure and dynamics of proteins and their interactions, the information required for a sufficient understanding of their relationship to the function of the system can be localized to selected segments of the protein. The intrinsic fluorescence of tryptophan (TRP) in proteins has been shown to be a convenient method to obtain selective and useful local structural information. However, TRP fluorescence may appear to be limited in studies of protein-protein interactions where there is more than one TRP residue in the interacting proteins. Recently we demonstrated that 5-hydroxytryptophan with its distinct spectroscopic properties could be used to investigate protein-protein interactions. We have also shown how using 7AW, 5HW, and 4FW in studies of tryptophanyl-tRNA synthetase gave new mechanistic details of its function. Ross and coworkers, appreciated the significant potential of this approach and incorporated 5HW into bacteriophage λcI repressor and studied its interaction with operator DNA. In this presentation highlights of photophysical studies of the TRP analogs and their use in correlating the interrelationship of the structure, dynamics and function of proteins will be discussed. (Financial Support from the Natural Science and Engineering Research Council of Canada is acknowledged.)

WORKSHOP 4: THEORY AND MOLECULAR DYNAMICS COMPUTATIONS OF THE LIPID-PROTEIN SYSTEM: INTERACTION WITH EXPERIMENTAL FACT

W-PM-WS4

W-PM-WS4

No abstracts submitted.

TRANSFORMATION/PROLIFERATION

W-Pos1

DO TIME VARYING WEAK MAGNETIC FIELDS CAUSE CELL TRANSFORMATION?

((G. Katsir[1], S. C. Nemschitz-Baram[1], Y. Tal[2] and A. H. Parola[1])) Departments of Chemistry[1] and Virology[2], Ben-Gurion University of The Negev, Beer-Sheva, Israel 84105.

Proliferation of chicken embryo fibroblasts (CEF) was assayed by colorimetric method ([3-(4,5-dimethylthiazol 2-yl)]-2,5 diphenyltetrazolium bromide, MTT test) after exposure to sinusoidally varying magnetic field (SVMF), for 24 hours. There is an increase in cell proliferation (up to 42% at 100Hz/7 gauss) after exposure to SVMF; furthermore we see a direct correlation between the intensity of the fields (7, 6, 5 gauss/100Hz) and the rate of cell proliferation. Changing the frequency (100, 60, 50Hz/ 7 gauss) showed a similar correlation, which in all cases was higher then that of the sham exposed cells.

Normal rat fibroblast cells (F111) were infected by minute virus of mice (MVM), known to have a cytopatic effect on transformed cells (E. Guetta, M. Mincberg, S. Mousset, C. Bertinchamps, J. Rommelaere and J. Tal (1990) J. Virol., 64, 458-462). Exposure of viraly infected cells to SVMF (100Hz / 7 gauss / 4 days) resulted in complete extinction of all exposed cells, while sham exposed cells exhibited a normal growth patern. Isolating viral DNA (Hirt assay) showed increased viral DNA (Southern Blot and Autoradiography) in exposed cells as compared to unexposed ones.

Primary or 'normal' cells exposed to SVMF seem to undergo cell transformation. The methods in the present study complement and strengthen those observed before (A. H. Parola, N. Porat and L. A. Kiesow (1993) Bioelectromagnetics, 14, 215-228).

W-Pos2

MOLECULAR SPECIES OF PHOSPHOLIPIDS IN A MURINE STEM CELL LINE RESPONSIVE TO ERYTHROPOIETIN. ((S. Clejan[1,3], C. Mallia[2], D. Vinson[1], and B. Beckman[2,3])) Tulane University School of Medicine, Depts. of Pathology and Laboratory Medicine[1] and Pharmacology[2] and Program in Molecular and Cellular Biology[3], New Orleans, LA. 70112

Hematopoietic growth factors such as erythropoietin (Epo) are known to stimulate the proliferation and differentiation of target stem cells through the generation of lipid signalling molecules such as diacylglycerol (DG) and phosphatidic acid (PA). The kinetics of these responses are both rapid and transient while others are slower and sustained. In this study the molecular species of DG, phosphatidylcholine (PC), phosphatidylethanolamine (PE), phosphatidylinositol (PI) and PA were analyzed in a murine stem cell line (B6SUt.Ep) by HPLC. Approximately 16 different molecular species were present in significant amounts with peak 10 (16:0,20:4), 11 (16:0, 18:2) 20 (18:0, 20:4) and 21 (18:0, 18:2) as the predominant ones. In response to EPO DG changed only in quantity and not in the presence or absence of specific species. Two important patterns were formed: one which peaked at 10 sec then decreased while the other peaked only at 40 min. Since the molecular species of phospholipids (PL) may change in response to EPO we determined the effects of EPO at 10 sec, 40 min, and 1 hr on each PL. Minor decreases occurred which corresponded to the increases in DG. Analysis of water-soluble headgroups was carried out by labeling PC and PE in medium which contained 5 μCi/ml [^{3}H]choline and [^{3}H] ethanolamine. There was an increase in choline release at 40 min and 1 hr. whereas ethanolamine was released as early as 10 sec, suggesting also an important role for ethanolamine for DG synthesis, in addition to PC. From the patterns of all molecular species, we could not find any relation between PA and PI. DG and molecular species were similar to some early peaks in PI. We conclude that detailed analyses of molecular species of phospholipids produced in response to EPO suggests two important temporal patterns.

W-Pos3

CALCIUM BUFFER INCORPORATION REVERSIBLY INHIBITS MITOSIS IN NEOPLASTIC MOUSE KERATINOCYTES.

((D.M.Cisbek and D.J.Gross)) MCB Program, UMass. Amherst, Ma. 01003

The roles of calcium in the regulation of cell division remain elusive. Data on calcium's activity during mitosis from a variety of systems is often confusing and occasionally contradictory. One approach to studying the role of calcium in the cell cycle is to prevent the cell from responding to or generating its normal calcium signals. Recently this alteration of calcium has been accomplished with the BAPTA family of calcium buffers. We have applied the AM ester of one BAPTA buffer, 5,5'-difluoroBAPTA/AM, to transformed mouse keratinocytes to observe the effects on the cells' ability to divide. We found that exogenous application of 20mM 5,5'-difluoroBAPTA/AM to normal growth medium (10% FBS in DMEM) of these cells inhibited cell division for up to 6 days. DNA synthesis was likewise inhibited. Viability of the cells was assessed with light microscopy and with fluorescence activated cell sorting (FACS). DNA synthesis was monitored by ^{3}H-thymidine incorporation and by FACS. The cells' DNA content was determined by measuring ethidium bromide fluorescence of permeabilized cells in the FACS. We found 5,5'-difluoroBAPTA/AM-treated cells had a higher proportion of cells in the G2 phase of the cell division cycle, suggesting that the buffering action of 5,5'-difluoroBAPTA/AM may inhibit a crucial Ca^{++} regulated pre-mitotic step. When inhibited cells were returned to medium that did not contain 5,5'-difluoroBAPTA/AM, the cells resumed their prior growth and division pattern. The effects of 20μM 5,5'-difluoroBAPTA/AM on primary mouse keratinocytes will also be discussed.

Supported by NSF # MCB-9304393

W-Pos4

TRANSDUCTION OF THE MITOGENIC RESPONSE EVOKED BY PARATHYROID HORMONE IN GROWTH PLATE CHONDROCYTES IS AT LEAST PARTIALLY PROTEIN KINASE A-DEPENDENT.

((M.J. Zuscik, J.E. Puzas, R.N. Rosier, K.K. Gunter and T.E. Gunter)) Depts. of Orthopaedics and Biophysics, University of Rochester Medical School, Rochester, NY 14642. (Spon. by W.A. Bernhard)

Aside from the well known role of parathyroid hormone (PTH) as a regulator of blood serum Ca^{2+} homeostasis (through its numerous effects on bone and kidney), it is the most potent activator of the proliferative response in growth plate chondrocytes (GPCs). In these cells, as well as in other PTH-target tissues, the hormone is believed to exert its cellular control through an activation of both cAMP metabolism and phosphoinositide (PI) cascading. Since the PTH-evoked mitogenic effect on GPCs is likely to be a critical event in the ultimate lengthening of bone, questions are raised about which of these two signalling pathways, if not both, are involved in the transduction of the proliferative response. To explore this issue, we performed experiments to assess the involvement of protein kinase A (pkA) and Ca^{2+} transients in the transduction of the hormone's effect on the rate of thymidine incorporation into DNA.

Using a a single cell fluorescence technique with fura 2, we found that a 1 hour incubation with 10 μM BAPTA-AM is sufficient to completely chelate Ca^{2+} transients evoked by PTH in GPCs. Nevertheless, we found that a 1 hour incubation with even 30 μM BAPTA-AM is without effect on the hormone's ability to stimulate DNA synthesis. Comparatively, inhibition of pkA activity with H-89 or R_P-cAMPS was found to cause a significant reduction in the ability of PTH to stimulate the rate of thymidine incorporation into DNA. We conclude from these data that the proliferative response evoked by PTH in GPCs does not require Ca^{2+} signals, but rather is at least partially dependent on pkA.

W-Pos5

ACTIVATION OF PHOSPHOINOSITIDE METABOLISM BY PARATHYROID HORMONE IN GROWTH PLATE CHONDROCYTES IS NOT PROTEIN KINASE A-DEPENDENT.

((M.J. Zuscik, T.E. Gunter, K.K. Gunter, R.N. Rosier and J.E. Puzas)) Depts. of Orthopaedics and Biophysics, University of Rochester Medical School, Rochester, NY 14624.

We have previously shown that parathyroid hormone (PTH) stimulates cAMP metabolism and phosphoinositide (PI) cascading in growth plate chondrocytes (GPCs). Work with other cell types suggests that this activation of both signalling mechanisms is mediated through direct links between the hormone's receptor and two separate classes of G-proteins. However, there is published evidence for a stimulation of the PI cascade by a cAMP/protein kinase A (pkA) -dependent mechanism in hepatocytes. We should therefore consider the possibility that the PTH stimulation of PI metabolism (and the resulting Ca^{2+} transients) in GPCs is mediated by pkA rather than through a direct G-protein interaction with the PTH receptor. To explore this issue, we performed experiments using specific pkA activators (dibutyryl cAMP and S_P-cAMPS) and inhibitors (H-89 and R_P-cAMPS). Using fura 2 to monitor the intracellular [Ca^{2+}] in individual cells, we found that unlike the Ca^{2+} response evoked by PTH (which is known to be due to an IP_3-dependent release of intracellular Ca^{2+}), the Ca^{2+} responses evoked by dibutyryl cAMP and S_P-cAMPS are dependent on an extracellular Ca^{2+} source. Furthermore, by measuring IP_3 formation with a protein binding assay, it was found that while PTH increases IP_3 pool size, activation of pkA by these same cAMP analogs is without effect. Finally, it was found that specific inhibition of pkA with H-89 or R_P-cAMPS does not effect the ability of PTH to evoke its normal Ca^{2+} response. We conclude from these findings that the PTH stimulation of PI metabolism in GPCs is not pkA-dependent, but rather is likely due to a direct G-protein link with the receptor.

W-Pos6

STRUCTURE OF A SUPERANTIGEN: STAPHYLOCOCCAL ENTEROTOXIN C_3 AT 2.3Å.

(Y-I. Chi, G.A. Bohach*, and C.V. Stauffacher), Dept. of Biological Sciences, Purdue Univ., West Lafayette, IN 47907 & *Dept. of Bacteriology and Biochemistry, Univ. of Idaho, Moscow, ID 83843

Staphylococcal enterotoxins, which are the causative agents in toxic shock and food poisoning, have been shown to be superantigens, stimulating T-cell proliferation in the absence of antigen. We have solved the X-ray crystallographic structure of the SEC_3 toxin at 2.3Å resolution. The SEC_3 structure was determined by MIR phasing and solvent flattening from a triclinic crystal. The overall structure reveals two unequal sized domains separated by deep clefts. The small domain shows the oligomer binding fold and has an extended disulfide loop implicated in emesis. Residues important in T-cell receptor and MHC II binding localize to a shallow cavity and adjacent groove in the molecule. Refinement and extension to higher resolution (current R = 17.9%, rms bond length = .012Å, rms bond angle = 1.9°) is underway.

W-Pos7

REGULATION OF CELL PROLIFERATION IN HA-RAS ONCOGENE EXPRESSING NIH-3T3 FIBROBLASTS

((E. Wöll, R. Ritter, F. Lang)) Dept. of Physiology, University of Innsbruck A-6020 Austria - Europe

NIH 3T3 fibroblasts expressing the Ha-ras oncogene (+ras) are able to grow in 0.5% FCS (fetal calf serum) in contrast to transfected cells not expressing the oncogene. In addition, +ras cells develop oscillations of intracellular calcium concentration (Ca_i) and concommitant activation of Ca-dependent K-channels upon addition of 0.5% FCS or growth factors such as bradykinin. These oscillations are abolished by nifedipine. The same concentration of nifedipine is also able to inhibit proliferation of +ras cells in 0.5% FCS, whereas calcium channel blockers not interacting with Ca_i oscillations do not alter cellular growth. Another hallmark of +ras cells is their more alkaline intracellular pH (pH_i) as compared to -ras cells. This alkalinization is due to a set point shift of Na/H exchange. Addition of bradykinin to +ras cells increases pH_i even more. HOE 694, a novel blocker of Na/H exchange, is able to inhibit this alkalinization and abolishes growth of +ras cells in FCS-depleted media. Furthermore, expression of Ha-ras oncogene leads to an increase in cell volume. Addition of bradykinin to +ras cells leads to cell shrinkage. This effect is abolished in the presence of both, barium and ochratoxin-A, a novel inhibitor of chloride channels. This same manoeuver inhibits alkalinization upon addition of bradykinin. These evidences lead to the conclusion that K- and Cl-channels are activated by oscillatory increase in Ca_i, leading to a loss in intracellular osmolytes and, therefore, cell shrinkage. Ha-ras oncogene expressing cells subsequently activate Na/H exchange to gain cell volume leading to intracellular alkalinization which seems to be a prerequisit to cellular growth.

W-Pos8

TEMPORAL RELATIONSHIP OF NUCLEAR AND CYTOPLASMIC FREE CA^{2+} ALTERATIONS INDUCED BY PDGF ISOFORMS.

((P.A. Diliberto, S. Krishna, P. Wodnicki and B. Herman)) Dept. of Cell Biology & Anatomy, Univ. of North Carolina, Chapel Hill, NC 27599.

One of the early events in the mitogenic signaling pathway of platelet-derived growth factor (PDGF) is the transient elevation of intracellular Ca^{2+}. We have recently identified increases in nuclear free Ca^{2+} (Ca^{2+}_n) to be a major component of the PDGF-induced intracellular Ca^{2+} response. Confocal laser scanning microscopy was used to analyze alterations in nuclear (Ca^{2+}_n) and cytoplasmic (Ca^{2+}_c) free calcium levels induced by PDGF isoforms in BALB/c3T3 fibroblasts loaded with the calcium-sensitive fluorescent indicator, Fluo-3. In quiescent cells, Ca^{2+}_n levels were lower than surrounding Ca^{2+}_c levels. Both AA-PDGF and BB-PDGF caused transient increases in Ca^{2+}_n that surpassed Ca^{2+}_c. BB-PDGF stimulation resulted in the generation of Ca^{2+}_n oscillations while AA-PDGF was found to induce primarily monophasic Ca^{2+}_n responses. Detailed analyses of these PDGF-induced Ca^{2+}_n alterations with respect to concurrent Ca^{2+}_c changes were performed by confocal line-scanning with a temporal resolution of 0.1 sec. The onset of Ca^{2+}_n and Ca^{2+}_c increases were found to occur simultaneously, with no evidence of Ca^{2+}_c changes preceeding those of Ca^{2+}_n. During an oscillatory Ca^{2+} response in which the magnitude of the nuclear Ca^{2+} change was twice that observed in the cytoplasm, the rate of rise of Ca^{2+}_n was 1.5-fold faster than Ca^{2+}_c. Ca^{2+}_n returned to prestimulation levels at approximately the same time as Ca^{2+}_c, but at a faster rate. These findings support a mechanism for PDGF-induced Ca^{2+}_n increases involving direct and active processes of Ca^{2+}_n regulation that occur in addition to, but temporally associated with, Ca^{2+}_c alterations. We hypothesize that PDGF isoform-induced changes in Ca^{2+}_n may serve as a mechanism by which isoform-specific cellular signaling events (i.e. induction of growth-related gene expression) are manifested.

This work was supported by grants from the NIH, ACS, AHA, and Pfeiffer Fndn.)

W-Pos9

KINETICS OF PRIMARY SIGNAL TRANSMISSION IN MITOGENIC STIMULATION OF CULTURED FIBROBLASTS

((Mary N. Stamatiadou)) Institute of Biology, NCRNS Research Center "Demokritos", Aghia Paraskevi, Athens, Greece.

The overall kinetics of mitogenic stimulation of quiescent 3T3 cells by macromolecular growth factors are examined during the early process of primary signal transduction to initiation of DNA synthesis. The temporal profile of signal transmission in the prereplicative phase of stimulated 3T3 cells indicates a cumulative time integral activation of cells that increases with time and reaches a plateau after about 9 hours. The length of latency to maximal activation is independent of growth factor concentration, while the magnitude of that activation is quantitatively related to the concentration of growth factors in the culture medium. A continuous exposure of cells to growth factors for at least 9 hours is required for cells to express a maximal mitogenic response. This primary signal transduction appears to be temporally filtered by at least a simultaneous lateral dissipative process involving internalization of unoccupied cell surface receptors through release of inositol triphosphate and diacylglycerol via the corresponding kinase cascade system that controls cellular response to growth factors (e.g., protein kinase C for epidermal growth factor). The rate of reappearance of unoccupied reptors on the cell surface may have an effect on response kinetics, which shows up in the consecutive cell cycle in which a shortening of latency to maximal activation is observed.

NEURAL FUNCTION

W-Pos10

TRANSIENT PERTURBATIONS PRODUCE LONG-TERM CHANGES IN THE ELECTRICAL ACTIVITY OF NEURON R15 IN *APLYSIA*.

((H.A. Lechner, D.A. Baxter and J.H. Byrne)) Dept. of Neurobiology and Anatomy, Univ. of Texas Medical School at Houston, Houston, TX 77030.

By examining a mathematical model of the bursting R15 neuron in *Aplysia*, it was shown that multiple stable modes of oscillatory electrical activity can coexist at a given set of parameters, and that transient synaptic inputs can induce a shift from one mode to another (Canavier et al. *J. Neurophysiol.* 69: 2252-2257, 1993).

We have begun to test the predictions of the model by making intracellular recordings from R15. To mimic the effects of transient synaptic input, we applied brief (0.5-1.5 s) constant depolarizing current pulses (5-10 nA) at various times during the burst phase and the postburst afterhyperpolarization. Also we examined the extent to which mode shifting was affected by different levels of steady-state bias current and bath application of serotonin (5-HT, 10 μM). The transient depolarizing pulses were able to switch the electrical activity of R15 between bursting and beating modes. These transitions persisted for up to 10 min. Although we have not performed a complete parametric analysis, mode shifts were more readily obtained in the presence of 5-HT or depolarizing bias current.

Our results resemble the permanent modeshifts predicted by the model neuron. Also they indicate that persistent changes, or mode transitions, do not require alterations in the biophysical properties of neurons and that the effects of modulatory agents may increase (or decrease) the sensitivity of the neuron to synaptic input by regulating its eligibility for multimodal activity.

W-Pos11

FORSKOLIN INCREASES INACTIVATION RATE OF POTASSIUM CURRENTS IN NEUROBLASTOMA CELLS VIA A cAMP-INDEPENDENT PATHWAY.

((J.K.W. Blandino and D.W. Johns)) Cardiovascular Division, University of Virginia School of Medicine, Charlottesville, VA 22908.

Forskolin (FSK) is often used to activate adenylate cyclase (AC). We examined the ability of cAMP to inhibit voltage-activated potassium current (I_k) by FSK in differentiated neuroblastoma (Neuro 2A) cells. FSK reduced I_k in a dose-dependent manner with threshold at 0.1μM. For a 200ms step potential to +90mV from a holding potential of -80mV, in paired single cell experiments, bath application of 10μM FSK reduced the peak and steady-state I_k by 40.4±8.4% and 63.9±5.0% (mean±sem, n=7, $p<0.001$), respectively. In control conditions I_k inactivation was predicted by a single exponential. After FSK, the time constant of inactivation decreased from 919±173ms (n=7) to 372±95ms (n=4, $p<0.05$). I_k was not affected by either 8-bromo-cAMP or IBMX. However, 10μM 1,9-dideoxyforskolin (1,9-ddFSK), a FSK analog which does not activate AC, mimicked the effect of FSK on I_k.

Five minutes of incubation with 10μM FSK produced a 9-fold rise in extracellular and 8-fold rise in intracellular cAMP (n=6) while 10μM 1,9-ddFSK had no effect on these values (n=6).

In conclusion, forskolin suppresses voltage-activated potassium currents and augments the inactivation of I_k. These effects are not mediated by the production of cAMP.

W-Pos12

EVIDENCE FOR A SODIUM-DEPENDENT OUTWARD CURRENT IN CULTURED STELLATE GANGLION NEURONS OF THE GUINEA-PIG.

((R. Hendriks and D.L. Kreulen)) NHLBI, NIH, Tucson, AZ 85724. (Spon. by R.Greuner)

The stellate ganglia form part of the upper mammalian sympathetic nervous system. We used whole cell patch clamp techniques to study a range of inward and outward currents in cultured stellate ganglion neurons of the guinea-pig that were between 20 and 48 hours old, after dissociation. Standard internal pipette solutions consisted of (mM): KCl, 144.5; (ATP)-Na_2, 4; (EGTA), 3.5; HEPES, 4 (pH 7.4, adjusted with NaOH). Externally, the cells were perfused with buffered (HEPES, pH 7.4) Krebs. Two inward currents were identified; a tetrodotoxin (TTX) - sensitive sodium current and a calcium current that was blocked externally with cadmium ($CdCl_2$ 0.1mM). Both currents were completely blocked by either. Substitution of internal (pipette) KCl with CsF (140mM), $CsCl_2$ (144mM), or N-methyl-D-glucamine (NMG:120mM) ± TEA-Cl (35mM) revealed a persistent outward current that activated at potentials more positive than -50 mV. The reversal potential for this current was around -60mV. The current remained when the internal CsF concentration was lowered to 80mM and TEA- Cl (20mM) plus NaF 20mM were added. Dependence of this residual outward current on internal currents was determined by blocking inward sodium currents with external TTX (1μM) or NMG (1 mM) and calcium currents with external $CdCl_2$ 0.1mM. The external addition of TTX under conditions of both internal CsF and $CsCl_2$ substitution reduced the residual steady - state outward current by about 75%. A similar effect was not observed when $CdCl_2$ was added to the external perfusate. Furthermore, when the external perfusate was changed to (mM): Na-glutamate, 140; $ZnSO_4$, 1.2mM; $MgSO_4$, 2.5mM; $CaCl_2$, 1.6mM; $CdCl_2$, 0.1mM; HEPES, 4mM (pH7.4), the residual outward current could be markedly attenuated. We therefore conclude that a sodium - dependent outward current is present in stellate ganglion neurons of the guinea-pig and that this current is possibly carried by chloride ions. Supported by HL14136 & HL27781.

W-Pos13

INCREASED INTRACELLULAR SODIUM CONCENTRATION OF ASTROCYTES INDUCED BY ARACHIDONIC ACID ACCOUNTS FOR ITS INHIBITORY EFFECT ON GLUTAMATE UPTAKE

((T-I Peng[1] and S-S Sheu[2])) Program in Neuroscience[1] and Department of Pharmacology[2], University of Rochester, Rochester, NY 14642. (Sponsored by V. K. Sharma)

Inhibition of glutamate uptake of astrocytes by arachidonic acid (AA) has been implicated to play important roles in glutamate excitotoxicity found in many pathological conditions of the nervous system, such as ischemia, hypoxia and trauma. Transport of glutamate into the cells occurs via a Na^+ -- glutamate cotransporter which utilizes the Na^+ concentration gradient as a driving force for the uptake mechanism. In this report, we studied whether there is a change of intracellular sodium concentration ($[Na^+]_i$) induced by AA, and whether this change of $[Na^+]_i$ accounts for the glutamate uptake inhibition. An astrocyte cell line (RBA-1), which was derived from primary culture of neonatal rat cerebrum, was used in this study. To measure $[Na^+]_i$, cells were loaded with the Na^+ sensitive fluorescent probe SBFI, and fluorescent signals from single cells were recorded by a photomultiplier tube via fluorescent microscope. Progressive rise of $[Na^+]_i$ was noted from astrocytes treated with low micromolar concentrations of AA. With 15 μM AA for 10 minutes, $[Na^+]_i$ increased from 10 mM to 30 mM. This rise of $[Na^+]_i$ was greatly attenuated by 2 mM Ni^{++}, a finding similar to the AA induced change of $[Ca^{++}]_i$. (Biophys. J. Abstract 61:2,2 p A367 Feb.1992). While 15 μM AA for 10 minutes caused 25% inhibition of glutamate uptake, AA with Ni^{++} resulted in less than 5% inhibition. These results suggest that AA induced glutamate uptake inhibition in astrocytes is not a direct effect on the transport protein, but is mediated secondarily by an increase of $[Na^+]_i$ which diminishes the driving force needed for glutamate uptake.

W-Pos14

IMMUNOLOGICAL IDENTIFICATION OF A BRAIN-SPECIFIC 58 kDa PROTEIN THAT COPURIFIES WITH THE N-TYPE VDCC.

((E. Swider*, W.-L. Lee*, D.J. Suicu*, T.D. Copeland#, M. Takahashi@, and M.W. McEnery*)) *Dept. of Physiology and Biophysics, Case Western Reserve Univ. Sch. of Med., Cleveland, OH 44106, #ABL-Basic Research Program, NCI-Frederick Cancer Research and Development Center, Frederick, MD 21702, and @Mitsubishi-Kasei Institute, Tokyo, Japan.

Omega-conotoxin GVIA sensitive N-type voltage dependent calcium channel (CTXR) mediates the entry of calcium into neurons to signal the release of neurotransmitters. In addition to its pivotal role as a calcium channel, CTXR is also implicated as a docking-protein for synaptic vesicles, as suggested by immunoprecipitation by antibodies to synaptic vesicle proteins (Takahashi, et al. (1991) Brain Res. **551**: 279; Bennett, et al. (1992) Science **257**: 255; Yoshida, et al. (1992) J. Biol. Chem. **267**: 24925). Our studies of the proteins copurifying with the [^{125}I]omega-conotoxin GVIA binding-230 kDa alpha-1 subunit of CTXR identify four additional major proteins of 140, 110, 70, and 58/60 kDa (McEnery (1993) Meth. Pharmacol. **7**: 3-39). The 58 kDa protein (p58) is characterized further by affinity-purified polyclonal antibodies and is distinct from synaptotagmin, GAP 43, and Na/K-ATPase beta subunits. Western blots of representative fractions obtained throughout CTXR purification indicate p58 copurifies with [^{125}I]CTX binding, in contrast to synaptotagmin. Western blot analysis indicates p58 is abundant in brain homogenate and not identified in peripheral tissues including heart, lung, spleen, kidney or thymus. Anti-p58 antibodies immunoprecipitate greater than 40% of total specific [^{125}I]CTXR from partially purified detergent extracts. These results suggest a tight association between the 230 kDa alpha-1 subunit and p58.

W-Pos15

EFFECTS OF EXTERNAL CATION CONCENTRATION ON MEMBRANE POTENTIAL - COMPARISON OF RAT ASTROCYTES AND HUMAN GLIAL CELLS.

((S. Anderson, T. Brismar and E. Hansson)) Departments of Clinical Neurophysiology and Cell Biology, Faculty of Health Sciences, University of Linköping, S-58185 Linköping, Sweden.

The effects of varied external $[K^+]_o$ on membrane potential (E_m) and I-E curves of astrocytes, prepared from rat, were studied with patch clamp technique (whole cell recordings) and compared with strains of human glial cells and human glioma cell lines (Brismar & Collins,*J. Physiology* 1993, 460, pp.365-383.) Under current clamp E_m was -76±7.5 mV in 3.0 mM K^+ (n=25), -1.1±5.7 mV in 160 mM K^+ (n=17) and hyperpolarized to -97.7±11.7 mV (n=14) in K-free solution. The latter effect contrasted with the depolarization caused by K-free solution in human glial cells. Plotted on a logarithm scale of $[K^+]_o$, E_m changed linerly with a slope of 44 mV per 10 fold change in $[K^+]_o$. Under voltage clamp in 3.0 mM K^+ the conductance (g) in rat astrocytes was 16.0±2.1 nS at E= -80 mV (n=12). In 160 mM K^+ g was 20.0±3.5 nS (n=8). Block of K-channels with 1 mM-Ba^{2+} depolarised the cells by 31.3±3.2 mV (n=4) and g was reduced by ca. 65 % at -80 mV (n=2). Deleting Ca^{2+} from the external reference solution or applying the metabolic inhibitors, DNP (1 mM) and FCCP (1 μM), all resulted in depolarisation. This study confirms that K^+_o has a different effect on E_m in rat astrocytes in primary culture than in humanl glial cells. However, the effects of Ca-free solution and metabolic inhibtors were similar.

(Supported by Swedish MRC grant 14X-04255).

W-Pos16

Na-Ca EXCHANGE REGULATES INTRACELLULAR STORES OF Ca^{2+} IN MOUSE CORTICAL ASTROCYTES.

((V.A.Golovina, L.L.Bambrick, B.K.Krueger, P.J.Yarowsky, and M.P.Blaustein)) Depts. of Physiol. & Pharmacol., Univ. of Maryland Med. Sch., Baltimore, MD 21201

The influence of the plasmalemmal Na^+ electrochemical gradient on the amount of Ca^{2+} sequestered in intracellular Ca^{2+} stores was studied in mouse cortical astrocytes. The cytosolic free Ca^{2+} ($[Ca^{2+}]_{cyt}$) and Na^+ ($[Na^+]_{cyt}$) concentrations were determined, respectively, by digital imaging of fura-2 and SBFI fluorescence. Cyclopiazonic acid (CPA; 5 μM), which inhibits endoplasmic reticulum Ca^{2+}-ATPase and depletes IP_3-sensitive stores, transiently increased $[Ca^{2+}]_{cyt}$ from 113±4 nM to 607±18 nM (n=83 cells). Caffeine (10 mM), which releases Ca^{2+} from an IP_3-insensitive stores, increased $[Ca^{2+}]_{cyt}$ to 200±14 nM (n=41 cells). The transients were evoked 1 min after removing external Na^+ and Ca^{2+} and adding 50 μM EGTA to prevent Ca^{2+} influx. When the Na^+ pump was inhibited with 1 mM ouabain, $[Na^+]_{cyt}$ rose from a resting value of 2.9±0.3 mM to 14.6±0.6 mM (n=27 cells) in 12 min. Pretreatment of the cells with ouabain (1 mM) for 12 min raised resting $[Ca^{2+}]_{cyt}$ to 198±14 mM and, augmented the responses to CPA (to 1620±112 nM, n=68 cells) and caffeine (to 401±36 nM, n=34 cells). In another set of experiments, resting $[Ca^{2+}]_{cyt}$ was increased from 80±5 to 120±11 nM after 3 min in Na^+-free medium containing 1.8 mM Ca^{2+}, but the CPA-evoked Ca^{2+} transient was increased from 707±18 to 1403±71 nM (n=36 cells). These data demonstrate that Ca^{2+} entering the cells via the Na-Ca exchanger is rapidly sequestered in IP_3- and caffeine-sensitive stores. Dissipation of the Na^+ electrochemical gradient, for example by energy depletion or inhibition of the Na^+ pump, may greatly enhance the response of astrocytes to agents that induce Ca^{2+} release from these stores.

W-Pos17

MULTIPLE EFFECTS OF ETHANOL ON NMDA RECEPTOR-CHANNEL KINETICS.

((J.M. Wright, R.W. Peoples, and F.F. Weight)) NIAAA, NIH, 12501 Washington Ave, Rockville, MD 20852.

Effects of ethanol in concentrations from 0.1 to 500 mM were studied in whole cell and excised outside-out patch single channel recordings from cultured mouse cortical neurons. The concentration-response curves of current inhibition in single-channel and whole-cell recordings were not significantly different. Ethanol had multiple effects on the NMDA receptor-channel complex, all of which served to decrease the NMDA-activated currents at the whole-cell level. Overall, ethanol reduced the frequency and duration of openings. However, the details indicated complex mechanism(s) because inhibition depended upon the kinetic state of the receptor-channel. There were 2 exponential distributions of open times: one of 7.9 ms and another of 1.3 ms. The short duration openings were not inhibited by ethanol while the longer ones were reduced 38% by 200 mM ethanol. In addition, the proportion of short events increased in the record. The mean number of events per burst decreased from 1.5 to 1.3. Application of 200 mM ethanol increased the percentage of single isolated openings from 71% to 79% of events. These changes in burst kinetics and mean open time accounted for 90% of the current reduction in excised outside-out patches.

W-Pos18

EXPERIMENTAL AND THEORETICAL STUDY OF LOW-FREQUENCY DISCHARGE OF C-FIBER PAIN RECEPTORS.

((S.Revenko[1], L.Baidakova[1], V.Ermishkin[1], E.Timin[1], M.Valentini[1], L.Selector[2])) [1]National Cardiology Research Center, Moscow 121552, Russia, [2]Columbia University, NY 10032 (Spon. by L.Selector)

Cutaneous C-fiber polymodal mechanoheat (CMH) sensory units of narcotized cats were shown to respond to non-algesive (subnociceptive) chemical stimuli with low-frequency discharge. The discharge frequency of CMH units excited by nociceptive and subnociceptive chemical stimuli were analyzed to find the neurological correlate of nociceptive chemical-induced excitation. The boundary frequency of 2 imp/s is considered as the upper limit of subnociceptive excitation of CMH-units by chemical stimulus. The existence of low-frequency subnociceptive discharge of CMH units makes it possible to achieve local analgesia by inhibition of high-frequency responses in CMH-units without complete block of these sensors. Such frequency-dependent (use-dependent) inhibition of CMH-units was found under the action of Na channel blockers: cardiac antiarrhythmical agents N-propyl-ajmaline and lidocaine. The marked use-dependent inhibition developed during moderate natural mechanical or heat pain stimuli. Under the action of a use-dependent blocker the CMH-units responded to repeated noxious stimuli with progressively weaker discharges which were partially restored during a prolong pause.

A mathematical model was developed to account for the prolonged discharge of C-fibers with gradual dependence of the discharge rate upon the strength of a persistent stimulus. This model has demonstrated the key role of slow permeability changes in C-fiber nerve membrane connected with slow K channels and slow inactivation of fast Na and K channels in determining the firing rate elicited by chemical stimulation.

W-Pos19

NEURAL SPIKE GENERATOR ENTRAINMENT AND STABILIZATION BY REGULARLY SPACED SYNAPTIC INPUT: A CIRCUIT MODEL ILLUSTRATION.

((J. R. Harvey and L. J. Bruner)) Dept of Physics, Univ. of California, Riverside, CA 92521.

Perkel, et al[1] presented a mathematical formulation and computer simulation, as well as measurements on molluscan and crustacean pacemaker neurons, which demonstrated frequency locking of pacemaker firing to regularly spaced synaptic input, either EPSP's or IPSP's. A spike generator circuit model which we have described previously[2] exhibits all of the features they described. The accompanying plot of spike generator frequency *versus* EPSP frequency illustrates a typical "stability zone" over which the spike generator frequency is locked to the much more stable synthesizer derived EPSP frequency. The abrupt reduction in standard deviation of spike generator frequency accompanying locking is also illustrated. The narrow, negative sloped regions marking the transition between free running and locked states of the spike generator exhibit the same seemingly paradoxical behavior noted by Perkel, et al., namely, an increase of EPSP frequency is accompanied by a decrease of spike generator frequency. Locking is expected for regularly spaced IPSP inputs as well, with positive slopes for transition regions and negatively sloped stability zones. All stability zones are straight line segments which extrapolate to the origin of spike generator frequency *versus* PSP frequency plots.

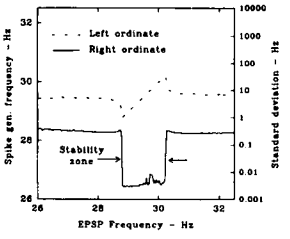

This work is supported by the Office of Naval Research.

1. Perkel, D. H., Schulman, J. H., Bullock, T. H., Moore, G. P., and Segundo, J. P. *Science*, **145**, 61-63 (1964).
2. Bruner, L. J., and Harvey, J. R., *Biophys. J.* **64 (No. 2; Pt 2)**, A99 (1993).

W-Pos20

SYNAPTIC CURRENT NOISE LIMITS THE ABILITY OF SENSORY TRANSDUCTION TO DETECT A CHANGE OF INPUT STIMULUS: THE EXAMPLE OF ELECTRORECEPTION. ((L. J. Bruner and J. R. Harvey)) Dept of Physics, Univ. of California, Riverside, CA 92521.

The electroreceptor organ of marine elasmobranches contains a sensory epithelium of ≈ 10^4 receptor cells innervated by ≈ 10 afferent fibers[1]. Bursting voltage oscillations at ≈ 20 Hz within each receptor cell causes periodic release of glutamate or a related neurotransmitter and associated periodic EPSC's originating at adjacent synapses.[2] Oscillations and associated EPSC outputs from different receptor cells are, however, believed to be asynchronous. Our calculations based on the above data have related the time averaged postsynaptic current from a set of asynchronous synaptic sources, $\overline{I(t)}$, and the temporal variance of that current, $\sigma_I^2 = \overline{(I(t) - \overline{I(t)})^2}$, by the equation;

$$\frac{\sigma_I^2}{\overline{I(t)}^2} = \left(\frac{\overline{(N_{ch})^2}}{\overline{(N_{ch})}^2}\right)\frac{1}{N_s}\frac{1-p_c}{p_c}$$

where averages over N_{ch} are ensemble averages over a population of N_s synapses of the number of neurotransmitter activated channels initially opened within a single synapse by an arriving pulse of neurotransmitter. A statistical analysis of such channel opening is available[3]. Also, p_c is the probability of coincident EPSC's from a pair of asynchronously firing synapses. A numerical estimate based upon electroreceptor morphology[1] and known properties of glutamate activated postsynaptic membrane channels[4] yields $\sigma_I/\overline{I(t)} \approx 0.1$. If we assume that $\overline{I(t)}$ is proportional to input stimulus amplitude, and that $\overline{I(t)}$, by modulating the frequency of the afferent neural spike generator to which it provides input, conveys information to the CNS, then the minimum detectable fractional change of stimulus must be ≈ 0.1 as well. This conclusion also accords with psychophysical data, summarized by the Weber-Fechner criterion[5].

This work is supported by the Office of Naval Research.

1. Waltman, B. Acta Physiol. Scand. 2648, 1-60 (1966).
2. Clusin, W. T. and Bennett, M. V. L. J. Gen. Physiol. 7, 703-723 (1979).
3. Dilger, J. P. and Brett, R. S. Biophys. J. 57 723-731 (1990).
4. Dudel, J., Franke, C. and Hatt, H. Ion Channels, Vol. 3, T. Narahashi, Ed. Plenum. New York. (1992).
5. Uttal, W. R. The Psychobiology of Sensory Coding. Harper and Row, New York. (1973).

W-Pos21

ROLE OF INTRACELLULAR SODIUM IN THE MECHANISM OF DESTABILIZATION OF CALCIUM HOMEOSTASIS IN CULTURED NERVE CELLS AFTER A TOXIC GLUTAMATE OR NMDA TREATMENTS. ((V.Pinelis, M.Segal, V.Grinberg and B.Khodorov)) Inst.of Pediatrics, Moscow, Russia; Weizman Inst., Rehovot, Israel; Inst. of General Pathology, Moscow.

Previous investigations (FEBS LETTERS,324,271-273) led us to suggest that a sustained increase in cytosolic Ca^{2+} after a toxic glutamate (GLU) treatment of cultured nerve cells is mainly due to suppression of Ca^{2+} extrusion, in particular via Na^+/Ca^{2+} exchange system. In the present work the Glu- and NMDA-induced changes in cytosolic Na^+ ($[Na^+]_i$) were monitored by using SBFI fluorescent probe and imaging microscopy. Both GLU and NMDA (50μM in Mg^{2+}-free solution, 15min) induced a marked increase in $[Na^+]_i$ (from 6-8 to 30-45 mM) which persisted after the termination of a treatment. The NMDA-receptor antagonist, APV (100μM) when applied in the post-NMDA period failed to decrease the elevated $[Na^+]_i$. The hypothesis is put forward that a sustained increase in $[Na^+]_i$ induced by GLU or NMDA is caused by inhibition of Na^+ pump, and that, in turn, high $[Na^+]_i$ suppresses the extrusion of internal Ca^{2+} in exchange for external Na^+. Inhibition of Na^+ pump in the post-GLU period is probably due to intracellular acidosis and a decrease in ATP content revealed in our previous studies.

W-Pos22

INHOMOGENEOUS CORRELATION FUNCTIONS FOR A PLANAR MEMBRANE MODEL NEURON. ((W.J. Ellis)) Department of Applied Mathematics, University of Adelaide, Australia. (Spon. by P.C. Jordan)

Structure and movement of molecules in the Debye layers of a neuron is of fundamental importance to the function of a neuron. This paper is an investigation into the distribution of mobile ionic species and dipoles adjacent to the planar membrane walls of a model neuron using electrical double layer theory.

The BBGKY hierarchy of partial differential equations for the correlation functions are truncated with Loeb's closure relation to determine expressions for the number densities and pair correlation functions of the ionic species and dipoles. The results obtained for the pair correlation function indicate a shielding both in the normal and transverse directions.

W-Pos23

SOME IMPLICATIONS OF A MIND-BODY THEORY; WARREN REHM UNIVERSITY OF LOUISVILLE, LOUISVILLE, KY. 40293

An interaction theory for the consciousness-brain (mind-body) problem was published (FASEB,J.7:4,1993). It is postulated that certain patterns of neural activity produce consciousness. This process requires energy and some energy ends up in consciousness - sufficient energy to appropriately modify neural activity. To illustrate: A subject agrees to close a switch when one of the following stimuli is presented - a tap on the wrist (touch), a red object (vision), a hand clap (auditory), etc. Each stimulus produces consciousness (awareness), which in turn changes the activity of appropriate neurons - eventually the motoneurons involved in the muscles controlling the movement of the arm and hand. How can the hypothesis that consciousness is a force be tested? Other forces gravity, electromagnetic, strong and weak are tested by showing their effects on things we can measure. For consciousness such tests are difficult but not impossible. According to J.O. Wisdom (Brit J. Phil SC 2:295, 1952) states "If interaction could be rendered more acceptable, a great part of the reason for holding any of the other theories would disappear."

W-Pos24

β-AMYLOID INDUCES K^+ CHANNEL DYSFUNCTION FOUND IN ALZHEIMER'S FIBROBLASTS. ((R. Etcheberrigaray, E. Ito., C. S. Kim and D. L. Alkon)) *Laboratory of Adaptive Systems*, NINDS, NIH, Bethesda, MD 20892.

It has been demonstrated that potassium channels play a fundamental role in memory storage (Alkon, Sci. Amer. 1989). Since memory loss is the hallmark of Alzheimer's disease(AD), we studied and recently showed that a 113 pS, TEA-sensitive K^+ channel was functionally absent in fibroblasts from AD patients. In addition, the TEA-induced $[Ca^{2+}]_i$ elevation (TEAr) normally observed in control individuals [young(YC), age-matched(AC), and other neurological disorders (NAD)] was never observed in AD fibroblasts (Etcheberrigaray et al., PNAS 1993). Although a direct causal or mechanistic relation has not yet been demonstrated, a number of studies have suggested that β-amyloid(AβP) plays an important role in the pathophysiology of AD. Since the lack of TEAr was AD-specific, and previous research has shown that AβP caused alterations in Ca^{2+} metabolism and/or Ca^{2+} mediated toxicity, we decided to study the effects of AβP on the normal TEA response. Cell lines from AC (N=4) and YC (N=4), previously shown to have normal TEAr were exposed to 10 nM AβP(1-40) for 48 h. Fluorescent Ca^{2+} imaging techniques (Fura 2 AM) were used to assess TEAr. We observed no changes in resting $[Ca^{2+}]_i$ levels as compared to untreated or solvent-only(DMSO) treated cells. Nevertheless, in the AβP exposed fibroblasts, the TEAr was completely abolished or did not meet a criterion response (10% of cells in a line with ≥ 100% elevation) in 6 out of 8 control cell lines, $p < 0.005$ (Fisher exact test). In the two responding cell lines, the $[Ca^{2+}]_i$ elevation was significantly lower than the controls for each cell line, $p < 0.001$. The TEAr was absent in the four AD lines with or without AβP treatment. The high K^+-induced $[Ca^{2+}]_i$ elevation, previously shown to be preserved in AD, was also present in 6 of the 8 treated control cell lines. Patch-clamp was also used to independently investigate the presence/absence of the 113 pS TEA-sensitive channel. Patches were obtained in 12 cells from 3 different AβP-treated AC fibroblasts. The 113 pS channel was absent in all but 1 of the treated cells, while it was previously found in 94% of the AC fibroblasts. Moreover, the only observed 113 pS channel was TEA insensitive. Thus, the results indicate that AβP induces changes that transform normal K^+ channel function in AC and YC fibroblasts into a defective AD-like pattern.

W-Pos25

Temperature effects on the activity of nicotinic acetylcholine receptor heterologously expressed in clonal cell lines. L. P. Zanello, S. Antollini, A. M. Roccamo, I. Bonini de Romanelli and F. J. Barrantes. Instituto Invest. Bioquímicas, Bahía Blanca, Argentina.

Temperature affects the activity of the mouse embryonic muscle-type nicotinic acetylcholine receptor (AChR) channel endogenously expressed in BC3H-1 cells and heterologously expressed in transfected CHO cells (Zanello et al., Biophys. J. 64, A328 (1993). We have comparatively studied the electrical activity of the embryonic receptor (γ-AChR) of the two above mentioned cell lines and the adult form of the same receptor (ε-AChR) heterologously expressed in CHO SPB-1, a thermosensitive mutant of a CHO cell line deficient in the biosynthesis of sphingomyelin. Single-channel patch-clamp recordings were obtained over a range of temperatures (3° to 40°C). De novo synthesis of sphingomyelin in the mutant was modified by varying the culture temperature. The clone SPB-1/A7 grown at 37°C (at which temperature cells have ≈80 % decrease in the biosynthesis of the lipid) exhibit a markedly reduced unitary conductance (23 pS) and longer open times (24.4 ms) in comparison to the AChR channel of cells grown at the permissive temperature of 30°C (75 pS and 12.2 ms). Thermodynamic parameters associated to the processes of conductance and gating of the channel were obtained for all cases. The information stemming from this series of experiments indicate that the physical state of the membrane bilayer affects AChR channel behavior, and that alterations in metabolism, and presumably in cell-surface distribution of single lipid constituents can also affect AChR function in a substantial manner.

W-Pos26

A NOVEL MODE OF INACTIVATION OF NICOTINIC ACETYLCHOLINE RECEPTOR BY A NONCOMPETITIVE INHIBITOR ((Ge Wu and Keith W. Miller)) Department of Anesthesia, Massachusetts General Hospital, and Department of Biological Chemistry and Molecular Pharmacology, Harvard Medical School, Boston, MA 02114.

Most noncompetitive inhibitors (NCIs) for the nicotinic acetylcholine receptor (nAcChoR) exert their effects by blocking the open channel. However, 3-(trifluoromethyl)-3-(m-iodophenyl) diazirine (TID) has been found to label 75% less of the receptor in desensitized state than in resting state (White, B. H., et. al. (1991) J. Biol. Chem. 266, 21595-607). Using a 9 ms $^{86}Rb^+$ efflux assay in native *Torpedo* vesicles, we show that after preincubating nAcChoR with TID for 1 minute or longer, half inhibition (IC_{50}) of acetylcholine (AcCho)-induced $^{86}Rb^+$ flux occurs at 0.4 μM with a Hill coefficient of 0.9. However, when TID (up to 0.3 mM) and 1 mM AcCho are simultaneously mixed with the nAcChoR, no inhibition of $^{86}Rb^+$ flux is observed. Mixing nAcChoR with 10 μM TID for various times and then rapidly mixing with 1 mM AcCho for 9 ms, showed TID inhibited efflux with a half-time of 60 ms. In comparison, we found that octanol, another NCI, inhibits nAcChoR when simultaneously mixed with AcCho under the same conditions. Additivity studies show that TID and octanol exert their inhibition at different sites. We propose 1) TID only inhibits nAcChoR in the resting state since there is no inhibition during the 9 ms $^{86}Rb^+$ flux time even at high TID concentration (750 times greater than the IC_{50}); 2) slow inhibition of the nAcChoR by TID (compared with octanol) implies that either a) its diffusion to the resting channel pore is sterically hindered (directly reaching the binding site inside the pore with steric resistance or crossing the lipid bilayer and reaching the same site from the opposite side of the membrane) or b) it diffuses to a site, possibly within the lipid bilayer, triggering a slow conformational change in the resting nAcChoR state that prevents its transition to the open state.

W-Pos27

THE EFFECT OF THE LIPID BILAYER ON THE AFFINITY STATE TRANSITIONS OF THE NICOTINIC ACETYLCHOLINE RECEPTOR ((Saffron E. Rankin and Keith W. Miller)) Department of Anesthesia, Massachusetts General Hospital, and Department of Biological Chemistry and Molecular Pharmacology, Harvard Medical School, Boston, MA 02114

It has been shown that certain lipids support the affinity state transitions of the nicotinic acetylcholinic receptor (nAcChoR) and furthermore specific bilayer components are required for optimum receptor function (Fong and McNamee, Biochemistry, 1986, 25, 830). The non-competitive inhibitor ethidium bromide is thought to bind with an increased affinity to the receptor in the desensitized state (K_D=3.6x10^{-7}) as compared with its affinity for the receptor in the resting state (K_D=1x10^{-3}) (Herz *et al.*, J. Biol. Chem., 1987, 262, 7238). This phenomenon has been utilized as a means of detecting the ability of the receptor to change from one affinity state to another. The fluorescent signal from ethidium increases upon the addition of carbamylcholine because the receptor undergoes a resting to desensitized-state transition resulting in increased binding of the fluorophore. This carbachol-induced fluorescence enhancement has been observed with the receptor in native and in simulated native (DOPC-PA-Cholesterol; mole ratio 63:12:25) lipid bilayers, but in DOPC alone and DOPC-PA a further increase in fluorescent signal is not observed indicating that the receptor is unable to undergo desensitization. Previous studies have been unable to resolve the various components of receptor conformation changes. Therefore, fast kinetic techniques with the fluorescent agonist Dns-C_6-Cho have been used to investigate further the behavior of the receptor in different lipid milieu. These methods allow resolution of binding to the pre-existing desensitized state and the onset of fast and slow desensitization. The distribution of receptor states is unaffected by the bilayer, however interconversion from one to another appears to require the presence of both cholesterol and PA.

W-Pos28

AGONIST-DEPENDENT PHOSPHORYLATION OF THE HUMAN M2 MUSCARINIC ACETYLCHOLINE RECEPTOR IN INSECT SF9 CELL MEMBRANES
((S.K. DebBurman and M.M. Hosey)) Department of Pharmacology and Institute of Neuroscience, Northwestern University, Chicago, IL 60611. (Spon. by R.L. Chisholm)

Agonist-dependent phosphorylation is proposed to be a critical event that mediates the homologous desensitization of G protein-coupled receptors (GPRs). G protein-coupled receptor kinases (GRKs) specifically phosphorylate GPRs in an agonist-dependent manner. GRK-phosphorylation of GPRs has been difficult to study in membrane preparations for reasons that are poorly understood, and routinely requires the use of purified and reconstituted receptors. In this study we expressed the human m2 muscarinic acetylcholine receptor (hm2 mAChR) in insect Sf9 cells with recombinant baculovirus and analyzed agonist-dependent phosphorylation of the hm2 mAChR in insect cell membranes under different experimental conditions. Pretreatment with 5M urea allowed agonist-dependent phosphorylation of the hm2 mAChR by the purified β-adrenergic receptor kinase 1 (βARK1) with a stoichiometry of phosphorylation of ~2 mol P/mol of receptor. A relatively significant component of phosphorylation of the receptor was however agonist-independent, and, surprisingly GRK-dependent, suggesting that urea may have altered some receptors to a partially-activated conformation. These results provide the first demonstration of the phosphorylation of m2 mAChRs by GRKs in membrane preparations.

W-Pos29

ALLOSTERIC REGULATION OF THE 5-HT_2 RECEPTOR: PUTATIVE ROLE OF TRANSMEMBRANE HELIX 2 ((D. Zhang and H. Weinstein)) Dept.Physiology/ Biophysics, Mt. Sinai Sch. Med., New York, NY 10029 (Spon. F. Landsberger)

Ligand binding of G-protein coupled receptors (GPCRs) was shown to be subject to allosteric regulation by cations. Mutations in α_2-adrenergic and dopamine-D_2 receptors have implicated a conserved Asp in transmembrane helix (TMH) 2 in this process, but it remains unclear how this Asp affects the binding of ligand and what mechanism is responsible for the regulation. We used the structural model of the 5-HT_2 receptor (5HT_2R) described recently [Zhang & Weinstein, J. Med. Chem. 36:934,1993] to explore the mechanistic relation between the TMH2-Asp and the ligand binding site. This 5HT_2R model had been shown to be similar to the TMH bundle of rhodopsin, and to behave in molecular dynamics (MD) simulations of ligand binding in a manner consistent with the known pharmacological properties of the ligands. In this model, the conserved Asp98 in TMH2 (TMH2:Asp98) directly interacts with two other conserved residues TMH7:Tyr380 and TMH7:Asn376 which, in turn, interact directly with TMH7:Ser372 in the ligand binding site to create a hydrogen-bond network connecting TMH2:Asp98 to ligand binding. A hypothesis for the mechanism of allosteric regulation in the 5-HT_2R emerged from a quantitative analysis of the interaction between various ligands and the receptor model. We observed a significant correlation between the experimentally determined ligand affinities and interaction energy terms from the MD simulation results: the sum of ligand-TMH7 interaction energies and the changes in the interaction energy between TMH2 and the other TMHs in the model. This correlation connects ligand binding to the conformational changes in 5HT_2R. The results suggest that specific helix-helix interactions between TMH2 and other TMHs determine the observed allosteric regulations. *Supported by NIH grants DA-06620 and DA-00060.*

W-Pos30

pH-Dependent Interaction of an Intraluminal Loop of the Inositol 1,4,5-Trisphosphate Receptor with Chromogranin A Seung Hyun Yoo and Marc S. Lewis LCB, NIDCD, and BEIP, NCRR, National Institutes of Health, Bethesda, MD 20892

The secretory vesicles of adrenal medullary chromaffin cells have been identified as a major inositol 1,4,5-trisphosphate (IP_3)-sensitive intracellular calcium store, and the calcium storage function of the secretory vesicle was attributed to the high capacity, low affinity calcium binding property of chromogranin A (CGA). It was recently found that CGA interacts with several membrane proteins of the secretory vesicle membrane at the intravesicular pH of 5.5 and dissociates from them at a near physiological pH of 7.5, and that one of the CGA-interacting membrane proteins was tentatively identified as the IP_3 receptor (Yoo, S. H. unpublished observation). In view of the fact that the IP_3 receptors are thought to have 8 transmembrane domains at the C-terminal region with the C-terminus facing the cytoplasm and to exist as homotetramers in the membrane, the possibility that the intraluminal region(s) of IP_3 receptor might interact with CGA in a pH-dependent manner arose. The potential interaction of the IP_3 receptor intraluminal domain(s) with CGA was studied by analytical ultracentrifugation, using the multi-wavelength scanning technique (Lewis *et al.*, Colloid and Polymer Sci., in press) and synthetic intraluminal loop peptides of the IP_3 receptor. The synthetic peptides were labelled with 5-hydroxy tryptophan in order to obtain the spectral difference the method requires. We found the pH-dependent interaction of an IP_3 receptor intraluminal loop (the region between the putative transmembrane domains 7 and 8) with CGA. Specifically, both monomeric and tetrameric CGA bound this loop peptide at pH 5.5 with average ΔG^o values of -6.7 and -23.6 kcal/mol, respectively.

W-Pos31

MODEL FOR THE HORMONE BINDING DOMAIN OF THE ESTROGEN RECEPTOR. ((Pamidighantam V. Sudhakar and Shankar Subramaniam)) Center for Biophysics and Computational Biology, Beckman Institute for Advanced Science and Technology, National Center for Supercomputing Applications, University of Illinois, Urbana, IL 61801

The hormone binding domain of the estrogen receptor is modelled based on the limited sequence homology with 3α,20β-hydroxysteroid dehydrogenase, whose back-bone crystal structure has been reported recently. Side chain placement and spinning were achieved using PROGEN and PROSPIN protocols. The model is tested for the environmental profile characteristics of individual residues using Eisenberg methods and for the protein fold class using a pair distance radial distribution function developed in our laboratory. The homology with t-RNA synthetases that was recognized earlier was used to define the putative ligand binding site in the proposed three dimensional structure. Interaction energies with various hormone agonists and antagonists were evaluated using Sybyl's DOCK program which uses a grid based calculation. The site-directed mutational results are interpreted in the light of the suggested model. (Supported partially by FMC Corporation.)

W-Pos32

ALTERATION OF AGONIST-INDUCED DESENSITIZATION OF RAT SUBSTANCE P RECEPTOR BY MUTAGENESIS AND INOSITOL POLYPHOSPHATES ((N. Sasakawa, M. Sharif, and M. Hanley)) Dept. of Biological Chemistry, UCD School of Medicine, Davis CA 95616-8635.

The rat substance P receptor (SPR) was expressed in *Xenopus* oocytes and examined for substance P (SP)-induced loss of Ca^{2+}-dependent Cl^- current responses. Stimulation with SP (30 nM) elucidated a response of 1670 ± 262, but a second response after 10 min washing was 15 % of first response. This loss of SP responsiveness was not due to loss of calcium from stores in that another stimulant of calcium mobilization, lysophosphatidic acid, could elicit responses after loss of SP responsiveness. Based on earlier claims that inositol hexakisphosphate ($InsP_6$) inhibited rhodopsin inactivation (Neuron, 8, 117-126, 1992), $InsP_6$ and inositol pentakisphosphate ($InsP_5$) were microinjected into oocytes expressing SPR. A time- and dose-dependent reduction in the degree of desensitization of peak current upon a second SP challenge was observed. The maximum preservation (58 %) of second response was obtained by $InsP_6$ and $InsP_5$ (100 μM ; final conc. in oocyte). Progressive mutagenic truncation of SPR also attenuated desensitization. In particular, deletion of 70 residues from C-terminal generated a mutant receptor which had reduced SP-induced desensitization dramatically, whereas a mutant SPR lacking 47 residues retained SP-induced desensitization. These results suggest that a domain between residues 338 and 360 mediates SP-induced desensitization, and that this may be modulated by an endogenous small molecule, $InsP_6$ and $InsP_5$. A model for these interactions and their functional importance will be presented.

W-Pos33

BINDING OF A SOLUBLE TRUNCATED FORM OF moFcγRII TO MEMBRANE-BOUND IgG AS MEASURED BY TOTAL INTERNAL REFLECTION FLUORESCENCE MICROSCOPY. ((D. Gesty-Palmer and N. L. Thompson)) Dept. of Chemistry, University of North Carolina, Chapel Hill, NC 27599-3290.

Total internal reflection fluorescence microscopy has been used to investigate the binding of the soluble extracellular domain of mouse FcγRII (s-moFcγRII) to monoclonal $moIgG_{2b}$ (GK14.1) that is specifically bound to substrate-supported planar membranes of dipalmitoyl-phosphatidylcholine (DPPC) and trinitrophenylaminocaproyldipalmitoyl-phosphatidylethanolamine (TNP-cap-DPPE). The association constant of s-moFcγRII with antibodies bivalently bound to TNP-cap-DPPE/DPPC planar bilayers containing 2-25 mole% hapten was 1.2 μM. Fluorescence recovery curves were best analyzed as a sum of two exponentials. The rates and fractional recoveries were on the order of $1s^{-1}$ (65%) and $0.1s^{-1}$ (35%). The similarity between these results and those previously measured for the binding of IgG to intact moFcγRII reconstituted into substrate-supported planar membranes suggests that conformational restraints which may occur when antibodies are bivalently bound to membranes do not affect the equilibrium or kinetics of IgG-moFcγRII binding. This work was supported by NIH grant GM-37145.

W-Pos34

DIRECT MEASUREMENT OF IgG-Fc RECEPTOR KINETICS: A STUDY USING TOTAL INTERNAL REFLECTION - FLUORESCENCE PHOTOBLEACHING RECOVERY ((H.V. Hsieh, E.D. Sheets and N.L. Thompson)) Department of Chemistry, University of North Carolina, Chapel Hill, NC 27599-3290.

Previously, total internal reflection fluorescence microscopy (TIRFM) was used to directly measure the weak equilibrium dissociation constant (≈ 3 μM) between fluorescently labelled mouse IgG and a mouse Fc receptor (moFcγRII) that had been purified and reconstituted into substrate-supported planar membranes (Hsieh et al., (1992) *Biochemistry* 31: 11562). Here, total internal reflection - fluorescence photobleaching recovery (TIR-FPR) has been used with the IgG-moFcγRII system to examine kinetic dissociation rates. The data were best described by two reversible components (≈ 1.3 sec^{-1} and ≈ 0.06 sec^{-1}) and an irreversible component. Several control experiments, including the variation of photobleaching parameters and the use of two different extrinsic fluorescent probes, confirmed that little or no photoartifacts were present. The kinetic rates for different solution characteristics (e.g., ionic strength) and antibody parameters (e.g., Fc regions, subclass) were examined. In addition, TIRFM and TIR-FPR were used to measure IgG-moFcγRII equilibrium and kinetic dissociation constants in the presence of saturating amounts of hapten and a protein antigen. This work was supported by NIH grant GM-37145 and a Department of Education Fellowship (HVH).

W-Pos35

TMH 2 AND TMH 7 PROXIMITY OF THE GONADOTROPIN-RELEASING HORMONE RECEPTOR.
((W. Zhou[1], C. Flanagan[3], J.A. Ballesteros[2], K. Konvicka[2], J. S. Davidson[3], H. Weinstein[2], R. P. Millar[3] and S.C. Sealfon[1])) Fishberg Ctr in Neurobiology[1], Dept of Physiology and Biophysics[2], Mount Sinai Med Schl, NY, NY10029, MRC Regulatory Peptides Research Unit[3], Univ of Cape Town Med Schl, Observatory 7925, South Africa

The activation of the pituitary gondadotropin-releasing hormone receptor (GnRHR), a member of the seven-transmembrane G-protein coupled receptor (GPCR) family, triggers a cascade of events leading to gonadotropin release and stimulation of the reproductive system. An unusual feature of this receptor, observed in all the mammalian receptors cloned, is the presence of Asn^{87} in the second putative transmembrane helix (TMH) at the location of a highly conserved Asp in the GPCR family, and of Asp^{318} in the putative seventh transmembrane helix where nearly all other GPCRs have Asn. The possibility that these residues interact was suggested by this reciprocal pattern and by a preliminary three-dimensional model of the GnRHR, and was investigated by site-directed mutagenesis. Replacing Asn^{87} in the second transmembrane domain by Asp eliminated detectable ligand binding. A second mutation generating the double mutant receptor $Asp^{87}Asn^{318}$, recreated the arrangement found in other GPCRs and re-established high affinity agonist and antagonist binding. The restoration of binding by a reciprocal mutation indicates that these two specific residues in helix 2 and 7 are adjacent in space and provides an empirical basis to refine the model of the receptor's transmembrane helix bundle.

W-Pos36

Structural Mapping of T Cell Receptor Complexes Using Flow Cytometric Resonance Energy Transfer. ((P. Zhou, D. Holowka, and B. Baird)) Cornell University, Ithaca, NY 14853

The T cell receptor complex (TCR) is composed of at least eight polypeptide chains, $\alpha\beta\gamma\delta\varepsilon_2\zeta_2$ ($or\zeta\eta$). In order to investigate physical proximity of different subunits within this complex and between aggregated receptors, we have separately labeled Leu4, a monoclonal antibody (mAb) specific for the ε chain, with fluorescein isothiocyanate (FITC) or the reactive cyanine dye Cy3. We have also labeled an antibody specific for TCR α/β variable domains, T40/25, with Cy3. We have prepared Fab fragments of all of these labeled mAbs. Quenching of the donor FITC fluorescence was monitored by flow cytometry as a function of time and acceptor concentration. Efficient intramolecular energy transfer (0.22) was observed between bound FITC-Fab Leu4 and Cy3-Fab T40/25, but no transfer was detected between bound FITC-Fab Leu4 and Cy3-Fab Leu4. Separate experiments showed that these latter probes do not bind simultaneously to the *same* TCR, suggesting that the two ε subunits are close together. In contrast to the Fab results, when intact FITC- and Cy3- Leu4 are used, efficient energy transfer (0.19) is detected. Similar results are obtained when phycoerythrin (PE) labeled Leu4 is used as an acceptor. These energy transfer results imply that the formation of dimeric TCR by the Leu4 antibodies causes larger scale aggregation of receptors on the cell surface. The relationship of the large-scale aggregation process to cellular signaling is currently under investigation.

W-Pos37

SINGLE CHANNEL PROPERTIES OF THE NODULIN 26 PROTEIN FROM SOYBEAN NODULE SYMBIOSOME MEMBRANES. ((N. H. Shomer, C. D. Weaver, D. M. Roberts, and C. F. Louis)) Graduate Program in Veterinary Biology, University of Minnesota, St. Paul, MN 55108 and Dept. of Biochemistry, University of Tennessee, Knoxville, TN 37996.

Nodulin 26 is a member of the MIP family of proposed pore-forming proteins which includes the lens membrane protein MP26 and the kidney water channel CHIP. To determine whether nodulin 26 demonstrated ion channel activity, this protein was purified to homogeneity from soybean nodule symbiosome membranes, incorporated into liposomes, and its single channel activity determined in a planar lipid bilayer system. Addition of nodulin 26-containing liposomes to the bilayer chamber resulted in the incorporation of ion channels with an apparent maximum single-channel conductance of 3.1 nS. In addition, several subconductance states of 0.5 nS, 1.1 nS, 1.6 nS, 1.9 nS, and 2.5 nS were frequently observed. Occupancy of these different conductance states was voltage sensitive, with greater occupancy of the 3.1 nS state at voltages less than 30 mV, and greater occupancy of the subconductance states at voltages between 40 and 100 mV. The channels exhibited a permeability ratio $P_{K^+}:P_{Cl^-}$ of 1:1.2, indicating that the channels were weakly anion selective. The large unitary conductance, multiple subconductance states, voltage sensitivity, and anion selectivity of nodulin 26 are all very similar to previously reported properties of MP26 channels. These data suggest that nodulin 26 may be functionally similar to MP26 and may effect ion transport in the symbiosome membrane. Supported by NIH EY-05684, USDA 91-37305-6752, and USDA 93-37304-7884.

W-Pos38

IDENTIFICATION OF AN INTEGRAL COMPONENT OF THE GAP JUNCTION CHANNEL VOLTAGE SENSOR. ((V.K. Verselis, C. Ginter and T.A. Bargiello)) Albert Einstein College of Medicine, Bronx, NY 10461.

The molecular mechanisms underlying the voltage dependence of intercellular channels formed by the family of vertebrate gap junction proteins (connexins) are unknown. Members of the connexin gene family display significant differences in voltage dependence that do not obviously correlate with differences in primary sequence. Through the analysis of chimeras, we have demonstrated that hemichannels formed of two closely related connexins, Cx26 and Cx32, gate for opposite polarities of transjunctional voltage, V_j. In Cx26 junctions, the hemichannel that closes is on the relatively positive side of the junction, whereas for Cx32 it is on the relatively negative side of the junction. We report a single amino acid residue in Cx32 that reverses its gating polarity. Positively charged amino acids at this position maintain Cx32 gating polarity and significantly steepen V_j-dependence. Negatively charged amino acids reverse gating polarity to that of Cx26. Neutral substitutions in Cx32 maintain Cx32 polarity indicating that additional positively charged residues are involved in forming the voltage sensor complex. These data identify a key residue that is likely to form an integral part of gap junction channel voltage sensors and suggest that effect of the charge reversal at this position is to reverse the sign of the voltage sensor in Cx32 and Cx26 thereby dictating gating polarity. The data are consistent with charge movement toward the cytoplasmic end of the channel upon closure.

W-Pos39

SPATIAL COHERENCE OF THERMAL ELECTRICAL NOISE AT THE GAP JUNCTION INTERFACE. ((Paul C. Gailey)) Oak Ridge National Laboratory, Oak Ridge, TN 37831-6070. (Spon. by U.S. Department of Energy)

Electrical noise across gap junctions arises in part due to the net resistance of the junction. For a uniform resistive layer with high-conductivity media on either side, the Johnson/Nyquist (thermal) noise is spatially coherent over large areas. In contrast, a detailed analysis of a model of the gap-junction interface reveals that thermal noise is only partially correlated at different locations on the junction. The degree of correlation depends on the number of channels in the junction and their dimensions. For voltage-sensitive junctions, each channel can be regarded as a separate voltage sensor. Exogenous or endogenous electric fields may be spatially coherent over the dimensions of the cell and induce potentials across gap junctions which are correlated at the different channel locations. Lack of correlation of the voltage noise occurring at different channels reduces the minimum theoretical detection limit of the junction to applied fields by enabling the junction to act as a coincidence detector.

W-Pos40

ASYMMETRY IN V_J-DEPENDENT INACTIVATION OF CARDIAC GAP JUNCTION CHANNELS ((¹K. Banach, ¹R. Weingart, ²P. Meda)) ¹Dep. of Physiology, University of Bern; ²Dep. of Morphology, University of Geneva, Switzerland; (Spon. by P. R. Brink)

A communication deficient rat islet tumor cell line (RIN) was transfected with cDNA encoding for Cx43. A clone with stable expression of Cx43 was selected to study gap junction properties in cell pairs. The dual voltage-clamp method was used to apply junctional voltage gradients, V_j ($V_j=V_2-V_1$; V_1,V_2: membrane potential of cell 1 and cell 2, respectively) and measure junctional currents, I_j. Small V_j gradients (<50 mV) were associated with constant I_j signals. Large V_j gradients (>50 mV) were accompanied by I_j signals exhibiting a time- and voltage-dependency, both being affected by the pulse protocol. Using a non-symmetrical protocol (V_1 was stepped, V_2 kept constant), the plot of normalized conductance, $g_{j(ss)}/g_{j(inst)}$, versus V_j revealed a bell-shaped curve which was well fit by a two-state Boltzmann process. Half maximal inactivation was reached at -77 mV and +66 mV, respectively, implying an asymmetrical gating behavior. This asymmetry was also reflected in the time constants of I_j inactivation, τ_i. At positive V_j, τ_i exhibited a steeper voltage dependence than at negative V_j. Using a symmetrical protocol (V_1 and V_2 were changed simultaneously using steps of equal amplitude but opposite polarity), the V_j-dependent asymmetries disappeared. I.e., the polarity of V_j did no longer affect $g_{j(ss)}/g_{j(inst)}$ (half maximal inactivation at -59mV and +60mV, respectively) and τ_i. The asymmetry in V_j-dependent inactivation of I_j cannot be explained with a conventional V_j-gating. Possible models will be discussed. Supported by SNSF (31-36'046.92)

W-Pos41

MODULATION OF GAP JUNCTIONAL PERMEABILITY IN WHOLE, PERFUSED RAT HEART ((John D. Sedovy and RL White)) Temple University School of Medicine, Philadelphia, PA 19140(Spon. by Steven P. Driska).

Myocytes in the heart are extensively coupled by gap junctions which allow the intercellular diffusion of ions and molecules up to 1 kD. If localized ischemia occurs in a heart, changes are observed in the intracellular concentrations of ions and molecules in the ischemic tissue, but intercellular propagation of damage to perfused areas was reported to be restricted. In isolated cell pairs, substances such as octanol, arachidonic acid, and pH synergistically with Ca_i decrease gap junctional conductance, but few studies have extended these findings to whole heart models. We examined the effects of some pharmacological interventions on intercellular permeability by examining the spread of fluorescent dye in perfused, beating rat hearts. We loaded cells in restricted areas on the epicardial surface of the LV (at 30 min. intervals) with 5(-6)-carboxymethyl rhodamine succinyl ester. During the initial control period, hearts were perfused with MEM equilibrated with 95% O_2/5% CO_2. Under these conditions, hearts contracted at a rate of 180-240 beats/min. and there was extensive intercellular dye spread. Hearts arrested by perfusion with oxygenated MEM containing 50 mM KCl also showed extensive dye spread. However, when hearts were perfused with MEM containing 500 µM octanol or when hearts were perfused with MEM containing 10 mM $CaCl_2$, 10 µM A23187 and equilibrated with CO_2 (pH 6.1), a second application of dye did not spread as extensively. In contrast, 20 min. of ischemia or 20 min. of ischemia followed by 10 min. of reperfusion did not substantially reduce dye spread. We conclude that gap junctions may remain patent in the early stages of ischemia.

W-Pos42

ION PERMEABILITY OF CONNEXIN-SPECIFIC CHANNELS, VARIATIONS ON A COMMON THEME? ((R. D. Veenstra[1], H.-Z. Wang[1], D. A. Beblo[1], E. C. Beyer[2], and P. R. Brink[3])) [1]SUNYHealth Science Center, Syracuse, NY 13210, [2]Washington University, St. Louis, MO 63110, and [3]SUNYHealth Science Center, Stony Brook, NY 11794.

The connexin family of proteins share a common membrane topology and form gap junction channels with distinct conductance and regulatory properties. The classical interpretation of gap junction channels models them as aqueous pores of 8-14 Å in diameter. The conductance and permeability properties of gap junctions are, therefore, determined by the hydrated diameter of the permeant molecule relative to the pore length and diameter. Predictions from channel conductances (43-63 pS) of connexin43 (Cx43) in tissues and transfected cells are consistent with this hypothesis. It follows that higher conductance gap junction channels should exhibit similar fluorescent dye and ionic permeabilities. We have performed conventional dye injections, using 6-carboxyfluorescein (6-CF, M_r = 376 D), and ion substitution (KCl/Kglutamate) experiments (±2 mM 6-CF) to determine the relative anion/cation and dye permeabilities of connexin-specific channels in stably transfected into mouse neuro2A (N2A) cells. Single channel conductances (γ_j) were 357, 178, and 32 pS for connexins-37,-40, and -45 (Cx37, Cx40, and Cx45) in 120 mM KCl. Estimated effective Cl/K permeabilities ($P_{Cl/K}$) were 0.43, 0.26 and 0.00, respectively. The frequency of 6-CF dye transfer exceeded control values (8% of injections in vector-transfected N2A cells using 10 kD rhodamine-dextran) by 28% for Cx37 and 10% for Cx40. These high γ_j and low $P_{Cl/K}$ and dye transfer values are not consistent with the simple aqueous pore model. Other connexin-specific gap junction channels are currently under investigation. Supported by NIH HL-42220, HL-31299, and HL-45466. RDV and ECB are Established Investigators of the AHA.

W-Pos43

IS THE ROLE OF CONNEXIN33 AN INHIBITORY ONE? ((M. Chang, G. Dahl and R. Werner)) Departments of Biochemistry & Mol. Biol. and Physiology & Biophysics, U. of Miami, School of Med., Miami, FL 33101

Functional expression of gap junction proteins can be obtained conveniently with the paired oocyte cell-cell channel assay. So far all gap junction proteins (connexins) have been found to make functional channels either by themselves or in the form of hybrid channels (two hemichannels of different connexin composition). Connexin33 appears not to follow this rule, expression of cx33 does not yield functional channels, and attempts to identify a pairing partner for cx33 to form hybrid channels also fave failed so far.

The chance observation was made that cx33 inhibits functional expression of other connexins in a connexin-specific way. While expression of cx38 and cx32 remains unaffected by coinjection into oocytes of cx33 mRNA together with mRNAs of these connexins, junctional conductance obtained with cx43 is moderately reduced whereas coinjection of cx33 mRNA at equimolar concentrations almost completely abolishes cx37 expression.

The fact that testis is the only tissue found to express significant levels of cx33 mRNA together with cx37 and cx43 suggests a possible functional role for an inhibitory connexin. A model is proposed where cx33 limits a cell's capability to make functional channels by allowing heterologous channels with other cells to be formed while homologous channels are disallowed. Such a mechanism would permit asynchronous maturation of spermatocytes while at the same time allowing communication between spermatocytes and Sertoli cells.

W-Pos44

STABLE TRANSFECTION AND FUNCTIONAL EXPRESSION OF A GAP JUNCTION PROTEIN, RAT CONNEXIN 37 (CX37) IN A COMMUNICATION DEFICIENT CELL LINE.

((M.N. Waltzman, S. Bai, and D.C. Spray)) Albert Einstein College of Medicine, Bronx, NY 10461. (Spon. by A.C. Campos de Carvalho)

The rat connexin gene family has almost a dozen members and the tissue distribution of mRNA transcribed from these genes has been well documented. Less clear are the physiological properties of many of these connexins. One such gap junction protein is rat Cx37 whose transcript is found most robustly in lung. The coding region of rat Cx37 (generously provided by Dr. David Paul) was subcloned into the mammalian expression vector pSG5 (Stratagen) in preparation for transfection into the communication deficient mouse neuroblastoma cell line N_2A (grown in DMEM, 10% FBS, 1% Pen/Strep). Cotransfection along with a neomycin resistance containing vector, pSV7neo, was mediated by $CaPO_4$-DNA precipitation followed four hours later by a two minute 10% glycerol shock. Geneticin resistant colonies were isolated, grown in selective media, and harvested for Northern Blot analysis. Clones which were positive for expression of Cx37 mRNA were then assayed for functional expression using dual whole-cell voltage clamp. We have obtained recordings of both macroscopic and unitary junctional conductances in several different Cx37 positive clones. Macroscopic junctional conductance is voltage-dependent with a moderate voltage-insensitive component (g_{min} ~ 20%); V_0 for the voltage dependent component is in the range of 35-45mV. Unitary conductance is very large (~ 250pS) at low transjunctional voltages, but unitary conductance is reduced at higher driving forces, presumably accounting for g_{min}. Thus, Cx37 channels possess a substate with reduced voltage sensitivity compared to that of the fully open state.

W-Pos45

HUMAN CONNEXIN 43 (hCx43) PHOSPHORYLATION SITE MUTANTS: UNITARY CONDUCTANCE AND VOLTAGE SENSITIVITY OF CHANNELS IN STABLE TRANSFECTANTS.

((L.K. Moore, A.P. Moreno, G. I. Fishman, and D. C. Spray.)) Albert Einstein College of Medicine, Bronx, NY 10461. (Spon. by L. Moore)

Cx43 is the most ubiquitous gap junction channel protein; expression is particularly prominent in the cardiovascular system and brain. In several types of mammalian cells expressing Cx43, either endogenously or after stable transfection, voltage sensitivity of junctional conductance (g_j) is weak ($V_o \approx 50$ mV; g_{min}, the proportion of g_j that is not voltage sensitive, ≈ 0.4), and unitary junctional conductances (γ_j) are of three sizes: ≈ 30, $\approx$ 60-70, and $\approx$ 90-110 pS. The smallest γ_j value apparently represents a voltage-insensitive subconductance state corresponding to g_{min}, the largest γ_j value to dephosphorylated Cx43, and the intermediate channel size to phosphorylated Cx43. Using site-directed mutagenesis we have created two mutants to further explore the role of the cytoplasmic carboxy-terminus in determining channel conductance state. Replacement of the hypothesized serine phosphorylation sites (SER 368, SER 373) with alanine resulted in a shift of the channel populations to the larger conductance state, although a moderate number of 60 pS events were still observed. This supports our belief that the largest conductance represents the dephosphorylated channel. The second mutation replaced the carboxy terminus of highly voltage sensitive Cx32 with the Cx43 carboxy terminus (rat Cx32 amino acids 1-229/hCx43 283-382). The channel populations of these transfectants resembled those observed with wild type human Cx43. The voltage/conductance relationship, however, was intermediate between that observed in wild type Cx32 or Cx43. These results support the role of serine phosphorylatable sites in determination of Cx43 channel conductance, and possibly suggests that the carboxy terminus may influence the voltage-dependence observed in different connexin proteins.

W-Pos46

ELECTRICAL AND DYE COUPLING IN IMMORTALIZED HIPPOCAMPAL NEUROBLASTS: CORRELATION WITH DIFFERENTIATION. ((M. Morales, R. Rozental, M.F. Mehler, R. Dermietzel, J.A. Kessler and D.C. Spray)) A. Einstein Coll. Med., Bronx, NY 10461. (Spon. by D.C. Spray).

We previously showed that the type and extent of expression of gap junctions changes in developing and mature brain tissues (*PNAS* **86**, 1989). To evaluate changes in coupling during neuronal ontogeny, we have used murine hippocampal primary cultured neurons and immortalized murine embryonic (E17) hippocampal progenitor cells (MK31) (*Nature* **362**, 1993) treated with cytokines. Cells maintained at 39°C (nonpermissive for T antigen expression) were well coupled (Lucifer yellow spread, dual whole cell recordings). Unitary junctional conductances of naive cells were predominantly 60 pS (n=7) and junctional conductances (g_j) were $\approx$ 7 nS (n=84). G_j was reversibly reduced by 1 mM halothane. Immuno-reactivity to connexin 43 (Cx 43) was localized in naive cells coexpressing immature neurofilament proteins. However, as neuroblasts differentiated into neurons under the influence of cytokines, the extent of dye coupling, the strength of g_j and the amplitude of unitary conductances progressively changed. Furthermore, Cx 43 was not observed in primary cultured neurons. Thus, differential expression of gap junctions appears to occur during *in vitro* differentiation of neuronal cells.

W-Pos47

FUNCTIONAL CONSEQUENCES OF PREVENTING PHOSPHORYLATION OF GAP JUNCTION PROTEIN CONNEXIN43 IN NORMAL RAT KIDNEY CELLS WITH BREFELDIN A. ((H.C. Haspel, E.P. Grine, G.E. Callender, E.L. Hertzberg*, and P.R. Brink)) Physiology & Biophysics, SUNY, Stony Brook, NY 11794 and *Neuroscience, AECOM, Bronx, NY 10461. (Spon. by R.T. Mathias)

Treatment of normal rat kidney (NRK) cells with brefeldin A (BFA) alters intracellular membrane trafficking. Musil and Goodenough [Cell 74:1065 (1993)] have demonstrated that BFA can prevent both the phosphorylation and movement to the plasma membrane of connexin43 (CX43) in NRK cells and proposed that this prevents assembly of CX43 into functional gap junctions. We have examined the effects of BFA on junctional coupling in both epithelial (NRK-52E) and fibroblastic (NRK-49F) NRK cells. Immunoblotting of cellular membranes demonstrated that BFA (5 μg/l, 5 h) causes the content of phosphorylated CX43 to diminish by ~50% and >80% in the NRK-52E and NRK-49F, respectively. Immunofluorescence localization of CX43 in BFA treated NRK cells indicates minimal loss of macula staining at cell borders in either cell line. In contrast, intracellular staining for CX43 is increased slightly in NRK-52E and greatly in NRK-49F. Fluorescent dye transfer from microinjected cells demonstrated that BFA minimally decreases gap junction function in NRK-52E and incompletely blocks dye transfer in NRK-52E. These results indicate that although the phosphorylation of CX43 is significantly diminished by BFA treatment of NRK cells the content of functional cell surface gap junctions is minimally altered. This suggests that "spare" or "stable" pools of functional connexins may exist in NRK cells. Supported by NIH (HL-31299) and NYA-AHA.

W-Pos48

MODULATION OF Cx43 EXPRESSION BY ACTIVATION OF PROTEIN KINASE C IN VASCULAR SMOOTH MUSCLE CELLS. ((X-D. Huang, D.R. Hathaway and M. L. Pressler)) Krannert Institute of Cardiology, Indiana University & Roudebush VAMC, Indianapolis, IN

We have previously described cell-cycle dependent changes in localization and expression of the gap junctional protein connexin43 (Cx43) in cultured bovine aortic smooth muscle (BASM) cells. We now report modulation of Cx43 expression and intercellular coupling of BASM cells by activation of protein kinase C (PK-C). Quantity and distribution of Cx43 were analyzed using a confocal microscope. BASM cells (≤ 7 passages; 10,000 cells/cm^2 plating density) were examined 72 hrs after plating ± stimulation by 1 μM phorbol dibutyrate (PDB 0, 1, 2, 24 hrs). Transient (1-2 hrs) exposure to PDB resulted in marked (87%) reduction of immunoreactive Cx43 in proliferating cells (n=9; P<0.01). Studies of Lucifer Yellow dye transfer showed coincident changes in intercellular communication: dye coupling was reduced from 85% (control) to 18% (PDB × 2 hrs; P<0.02). In contrast, immunoreactive Cx43 was no different from control after prolonged (24 hr) exposure to PDB. Additional assays showed that >90% of PK-C activity was depleted after 1 μM PDB was present for 24 hrs. The results suggest that activation of PK-C reduces intercellular communication in BASM cells by downregulation of Cx43. Studies are in progress to determine if PK-C may modulate the trafficking of Cx43 between the membrane and cytosol.

W-Pos49

FUNCTIONAL PROPERTIES OF CHICK CX56 IN *XENOPUS* OOCYTE PAIRS.((L. Ebihara[1], E. Steiner[1], E.C. Beyer[2])) [1]Department of Pharmacology,Columbia University, NY, NY 10032. [2]Department of Pediatrics, Washington University, St. Louis, Mo 63110.

Chick connexin56 is a gap junctional protein found in the chick lens. It is more closely related to rat connexin46 than to any other known gap junctional protein. We studied the functional properties of cx56 expressed in *Xenopus* oocyte pair system using the dual two microelectrode voltage clamp technique. In order to eliminate endogenous coupling, the oocytes were treated with antisense oligomers against *Xenopus* cx38. Cx56 formed gap junctional channels which were sensitive to transjunctional voltage(V_j) but insensitive to inside-outside voltage. The steady-state G_j-V_j relation could be described by the Boltzmann equation with A=.11, V_o = ±42 mV, V_{min} = .23. Gap junctional coupling could be reversibly blocked by cytoplasmic acidification. In addition, cx56 mRNA-injected oocytes developed a large, time and voltage dependent, nonjunctional current which activated on depolarization. The kinetics of activation and deactivation of the nonjunctional current resembled those of the cx46-induced nonjunctional current. However, the steady-state current-voltage relation was shifted to more positive potentials.

W-Pos50

LIPID DIFFERENTIATION IN GAP JUNCTIONS. ALKENYL ACYL AND ALKYL ACYL ETHANOLAMINE GLYCEROPHOSPHOLIPIDS IN GAP JUNCTION ENRICHED MEMBRANES OF BOVINE LENS ((Barbara Malewicz, Christoph G. Baumann and Wolfgang J. Baumann)) The Hormel Institute, University of Minnesota, Austin,MN 55912.

As gap junctions (GJ) reside and function in the lipid milieu of the plasma membrane, the role that lipids play in GJ assembly and structure has become the focus of much interest (for a review, see Malewicz, Kumar, Johnson and Baumann, *Lipids 25*, 419-427, 1990). To assess lipid differentiation in GJ domains, GJ enriched membrane fractions were isolated from bovine lens by Tris and urea treatment. Enrichment in GJ structures and 26 kDa protein (MP26) was monitored by EM and SDS-PAGE, respectively. We found that cholesterol (Chol) was by far the most abundant lipid component in GJ-enriched lens membranes (832.7 nmol/mg protein) and was more predominant than all phospholipids (PL) combined (682.7 nmol/mg). In the course of isolating the GJ-enriched membranes, Chol levels increased 144-fold, PL levels 99-fold, and the Chol/PL ratio increased from 0.84 to 1.22. The greatest differential enrichment (152-fold) was observed for the phosphatidylethanolamine (PE) fraction. ^{31}P NMR analysis showed that the PE fraction (37.3% of total PL) consisted of 29.4% alkyl acyl glycerophosphoethanolamine (GPE), 42.3% alk-1-enyl acyl GPE, and only 28.3% diacyl GPE. In contrast to the PE fraction, the phosphatidylcholine fraction was much less enriched (86-fold) and consisted of 82.7% diacyl species. Our data show that lipid differentiation occurs in the GJ domain of lens fiber cells and that there seems to be a special requirement for alkenyl acyl and alkyl acyl GPE species as well as for cholesterol in the GJ structure. (Supported by GM46277, and the Hormel Foundation).

W-Pos51

Differentiating keratinocytes express different gap-junction proteins and have different junctional selectivity. James E. Hall[†], Janice Brissette[‡], N.B. Gilula[§], Nalin Kumar[‡] and Paolo Dotto[‡]. [†]Department of Physiology and Biophysics, UC Irvine, CA 92717, [‡]Center for Cutaneous Biology, Department of Dermatology Harvard Medical School and Mass. General Hospital East Charlestown MA 02129 and [§]Department of Cell Biology, The Research Institute of Scripps Clinic, La Jolla, CA 92037. (Sponsored by J. E. Hall)

In high calcium medium, mouse keratinocytes undergo terminal differentiation and switch from expressing α_1 (Cx43) and β_2 (Cx26) gap junction proteins to expressing β_3 (Cx31) and β_4 (Cx31.1). We measured dye-transfer and electrical conductance simultaneously on pairs of undifferentiated (low calcium) and differentiated (high calcium for 72 hours) keratinocytes. Junctional conductance was measured using double whole cell patch clamping. External solution was mammalian ringer, internal solution KAspartate, one pipette also containing 10 μM 5,6 carboxyfluorescein. Gap junctional conductance was measured by applying computer-generated voltage protocols to two Axopatch 1C clamps. The current response of both clamps was digitized and stored on disk. A typical protocol was to hold both cells at -40 mV and then step first one and then the other cell to -20 mV. Junctional current was taken as the current which flowed in the cell held at -40 mV. Dye was imaged using a SIT camera. Of five differentiated cell pairs , the average junctional conductance was 16.8 nS with a population standard error of 9.7 nS (lowest value:5.6 nS; highest: 32.2 nS. Of 13 pairs of undifferentiated cells, the average junctional was 20 nS with a population standard deviation of 23 nS (lowest 1 or 2 nS and the highest73.4 nS). None of these five differentiated cell pairs showed dye transfer (five out of five). Conversely nine out of ten undifferentiated cell pairs showed dye transfer. (No assesment of dye transfer was made for three electrically coupled undifferentiated pairs.). Dye transfer between undifferentiated cells occurred even when the junctional conductance was lower than the lowest junctional conductance seen for differentiated cells. Thus the difference in dye transfer cannot be a result of difference in junctional conductance but probably reflects a difference in junctional selectivity.

PORPHYRINS

W-Pos52

Transient Resonance Raman Studies of Ruthenated Cyto c and Heme Model Complexes ((B. Fan, Y. Zhou and M. Ondrias)) Department of Chemistry, University of New Mexico, Albuquerque, NM 87131

As part of an on-going program to probe protein structural dynamics during and subsequent to electron transfer, we have examined a series of cytochromes c and heme c model complexes modified with different ruthenium-based photoinitiators. Initial studies on the equilibrium forms of these systems using absorption, circular dichroism, fluorescence and resonance Raman spectroscopies reveal no detectable structural perturbation upon ruthenation. Preliminary transient Raman studies on these systems indicate that significant photoreduction of the heme occurs upon laser excitation of the covalently attached ruthenium complex. Detailed studies of the dependence of ET efficiency on different initiators and the structural dynamics will be discussed in context of current throries of long-rang electron transfer in proteins. [Supported by the NIH GM33330]

W-Pos53

MODE SELECTIVE ENERGY LOCALIZATION DURING PHOTOEXCITATION OF DEOXYHEMOGLOBIN AND IRON PORPHYRIN MODEL COMPLEXES ((M.C. Schneebeck, P. Gurule, C.M. Cheatum, L.E. Vigil M.R. Ondrias)) University of New Mexico, Department of Chemistry, Albuquerque, NM 87131.

Vibrational energy redistribution may be important in regulating the function of hemes and related macrocycles. Transient resonance Raman experiments reveal a non-Boltzmann vibrational energy distribution among the heme normal modes of deoxyhemoglobin. Within 10 nanosecond excitation pulses, ν_4 exhibits flux-dependent anti-Stokes peak position, Stokes and anti-Stokes linewidths, and anti-Stokes:Stokes ratio. Other modes, most notably ν_7, do not behave in this manner. Spectra of protoporphyrin IX-2-methyl imidazole and of iron octaethyl porphyrin-2-methyl imidazole under similar conditions indicate that specific heme-protein interactions cannot be entirely responsible for this behavior. The dependence of this phenomenon upon excitation energy and upon ligation state is explored.

This research was funded by the National Institutes of Health (GM33330). MCS is a Howard Hughes Predoctoral Fellow.

W-Pos54

Electron Transfer Dynamics of Electrostatic Uroporphyrin /Cytochrome C Complex : A Time-Resolved Resonance Raman Study ((Y. Zhou, B. Fan, J. Wang and M. R. Ondrias)) Department of Chemistry, University of New Mexico, Albuquerque NM 87131

We have examined the photodynamics and electron transfer kinetics of isolated uroporphyrin and electrostatic complexes of uroporphyrin with cytochrome c. Time-resolved resonance Raman spectroscopy has been employed to mornitor the dynamics of photoinduced electron transfer in the system. The results revealed that transient triplet state of uroporphyrin is photogenerated at about 50ns, and then rapidly quenched by electron transfer to cytochrome c. This process could be readily seen in the time-resolved spectra of the heme. Spectra were further quantified by spectral deconvolution. The rate observed for heme photoreduction in the time-resolved spectra is about 10^{-6}s and was well-correlated to the disappearance of uroporphyrin triplet bands. The current results provided a firm quantitative basis for probing structural dynamics at the heme site which may accompany electron transfer. (This work is supported by the NIH GM33330)

W-Pos55

Resonance Raman Study of the Heme-protein Interaction Between a Tripeptide and an Iron Sulphonato-porphyrin. M. H. Wall,[1] R.W. Larsen[2], and M.R. Ondrias,[1] [1]Department of Chemistry, University of New Mexico, Albuquerque, NM 87131, [2]Department of Chemistry , University of Hawaii, Honoloulou, Hawaii

Electron transfer reactions involving donor and acceptors embedded in protein matrices are of prime importance to all life. The role of the protein matrix provides for specific distance and orientation relationships between participating donor and acceptor pairs. As a less complex model to the natural systems, a water soluble iron porphyrin (tetrakis(4-sulphonatophenyl)porphynato-iron and a tripeptide (glycine-histidine-glycine) was synthesized. Resonance Raman has been employed to investigate the structural characcteristics of this species. Comparison of this system with other models demonstrate that the ground state porperties of the iron porphyrin (i.e. ligation state, spin state, and equilibrium geometry) are greatly influenced by the binding of the tripeptide. The results of this study are to be used as a basis for future investigations of intramolecular electron transfer systems involving derivatives of polypeptides with attached electron donors . The current data will be discussed in the context of these future investigations involving the structural dynamics of an electron donor -acceptor pair upon electron transfer. (Supproted by the NIH GM33330 and start-up funds, University of Hawaii , RWL.)

W-Pos56

NICKEL LIPOPORPHYRIN-STEARIC ACID LANGMUIR-BLODGETT FILMS. ((Xingzhi Song[1,2], J. David Hobbs[1], Kelly A. Anderson[1,2], Xiang Xu[1], J. Cesarano[2], John A. Shelnutt[1,2])) [1]*Sandia National Laboratories, Albuquerque, NM 87185,* [2]*University of New Mexico, Albuquerque, NM 87131*

A new detergent porphyrin has been synthesized, incorporated into Langmuir-Blodgett (LB) films, and investigated using UV-visible and Resonance Raman spectroscopy. The nickel derivative of octaacetic-acid-tetraphenylporphyrin-octamethylester-tetraeicosanate (LipoP) has a polar head group composed of the tetraphenylporphyrin macrocycle surrounded by twelve polar ester groups and four hydrophobic tails consisting of twenty-carbon linear alkanes. Spectroscopic studies and molecular mechanics calculations show that the macrocycle is highly distorted from planarity. Extensive steric crowding of the twelve substituent groups effectively precludes π-π aggregation of the porphyrin head groups in organic solutions and also in the stearic acid LB films. Two types of LB films, differing in the surface pressure at which they are transfered to substrates, have been constructed and analyzed. Molecular mechanics calculations and UV-visible absorption measurements suggest that the films differ in the positions of the porphyrin head groups with respect to the stearic acid head groups. In the low pressure (14 mN/m) LB film, the porphyrin moiety resides at the interface of the carboxylates of the stearic acid component (stearic acid : porphyrin = 30:1). In the high pressure (27 mN/m) film, the NiLipoP sets well above the stearic acid monolayer with up to 12 stearic acid molecules filling in underneath the porphyrin head group. Photoactive metal derivatives of LipoP are now being incorporated into the LB films as models of vectorial electron-transport processes across membranes and for biosensor and photoactive device applications.

Supported by United States Department of Energy Contract DE-AC04-94AL85000 and Associated Western Universities Fellowships (XS, JDH, KKA).

W-Pos57

Structural heterogeneity of Nickel octaethylporphyrin (NiOEP) in organic solvents revealed by resonance Raman spectroscopy. ((W. Jentzen, W. Dreybrodt, R. Schweitzer-Stenner)) Inst. of Exp. Physics, Univ. of Bremen, 28359 Bremen, Germany. (Spon. by A. Mayer-Heinricy)

We have measured resonance Raman spectra of Ni(OEP) in solution of CH_2Cl_2 and CS_2 for temperatures between 330 to 190 K. Analysis of the band profiles of the structure sensitive bands ν_3, ν_{10}, ν_{11} and ν_2, ν_{11} reveal two sublines (SL) due to different conformers, the intensity ratios of which show a van't Hoff behaviour with $\Delta H \approx 3$ kJ/mol. For the bands ν_3, ν_{10}, ν_{19} the low frequency SLs are attributed to the more stable conformer. They show temperature independent line widths larger than the high frequency SLs, the linewidths of which increase with temperature. The SLs of the bands ν_2 and ν_{11} show opposite behaviour. The Raman excitation profiles of the SLs ν_{10}, ν_{11}, and ν_{19} reveal a red shift of the Q(0-0)-band resonance for the more stable conformer. From the broad SLs we infer that both conformations show additional structural heterogeneity. This is confirmed by comparison with the Raman spectra of nickel(II) porphine. It also exhibits line doublets both SLs of which exhibit temperature dependent linewidths. Pd(OEP) which due to the larger central metal stabilizes the planar macrocycle shows only single Raman lines with large linewidths for ν_2 and ν_{11} suggesting that only one conformer with additional heterogeneity is existing. We conclude that small central metal sizes and not too bulky substituents are necessary for the macrocycle to exhibit both, different conformers and additional substructures of each located in the pyrrole rings and methin bridges. This seems to be important for the biological function of Fe porphyrins in heme proteins.

W-Pos58

STRUCTURE-FUNCTION RELATIONSHIP IN OXYGEN AND CARBON MONOXIDE BINDING WITH HEME MODELS.

((C Tetreau,[a] D. Lavalette,[a] M. Momenteau,[a] J. Fisher[b] and R.Weiss [b]))
a) INSERM U350 & CNRS URA 1687, Institut Curie, 91405-Orsay France. b) CNRS URA 424, Université Strasbourg 1, 67070-Strasbourg Cedex France.

'Hybrid' heme models are TPP (iron(II)-5,10,15,20-tetraphenylporphyrin) derivatives in which a variable amount of distal steric hindrance is provided by a chain rigidly maintained in a central position by the presence of two lateral pivalamido pickets. The binding of O_2 and CO with 'hybrids' penta-coordinated with nitrogeneous bases has been investigated using laser flash photolysis. We have previously shown the interest of linear free energy relationships (LFER) to compare the reactivity of models with that of O_2-carriers. We now show that six encumbered TPP-derivatives reasonably mimic the reactivity of mammalian hemoproteins with O_2 and CO. The crystal structures of two 'hybrid' carboxyhemochromes have been determined by X-ray diffraction. The results indicate that the mechanism by which steric interaction with CO is released in encumbered TPP derivatives involves a ruffling distorsion of the porphyrin ring, instead of the distorsion of the Fe-C-O unit wich is observed in hemoproteins. This is due to the mode of anchorage of the encumbering structure on the *meso* phenyls of TPP, which allows a direct transfer of the steric constraints to the macrocycle. In conclusion, TPP derivatives fail to reproduce structural aspects in spite of reasonably mimicking the reactivity of hemoproteins. This constitutes an example of the non univocal nature of structure-function relationships.

W-Pos59

RANDOM SEQUENCE MUTAGENESIS: ESTABLISHING PERMISSIBLE AMINO ACID SUBSTITUTIONS WITHIN THE GLYCINE LOOP IN AMINOLEVULINATE SYNTHASE

((Jian Gong and Gloria C. Ferreira)) Department of Biochemistry and Molecular Biology, University of South Florida College of Medicine and Institute for Biomolecular Science, Tampa, FL 33612. (Sponsored by G.C. Ferreira)

5-Aminolevulinate synthase (ALAS) (E.C.2.3.1.37) catalyzes the condensation of succinyl-CoA and glycine to yield 5-aminolevulinate (ALA). This reaction is the first step in the heme biosynthetic pathway in non-plant higher eukaryotes. ALAS requires pyridoxal 5'-phosphate (PLP) as its cofactor, but residues involved in binding and orienting the cofactor have not been identified. A glycine-rich sequence has been found in many PLP-dependent enzymes and nucleotide-binding proteins and has been proposed to be the phosphate-binding motif in some cases. A similar glycine loop has bee identified in ALAS of diverse sources. In this study, we determined the essentiality of each residue within the 11-codon glycine loop (of murine erythroid ALAS) through partial random mutagenesis of the entire loop followed by an efficient biological selection, using a *hemA⁻ Escherichia coli* strain to recover functional unnatural enzymes. We produced and tested 5,444 variants, of which 283 were found to be functional. DNA sequencing results of 226 functional mutants revealed a high degree of flexibility in accommodating different types of amino acids in this loop. However, Arg-149 was conserved through all the functional mutants sequenced, while Gly-142 and Gly-144 can only tolerate alanine replacement. The identification of the permissible amino acid substitutions and conserved residues will provide a structural basis for the functional studies of ALAS.

[Supported by a grant from NSF (MCB-9206574) to GCF. JG is an AHA Predoctoral Fellow #93GSF/9]

W-Pos60

RESONANCE RAMAN SPECTROSCOPY OF (DMSO)(2-MeIm)Fe(II)PPIX: IMPLICATIONS FOR THE EFFECTS OF PORPHYRIN GEOMETRY ON LIGAND PHOTODISSOCIATION DYNAMICS. ((R.E. Nalliah and E.W. Findsen)) Department of Chemistry, The University of Toledo, Toledo, OH 43606.

Resonance Raman and UV-Visible absorption spectra indicate that a (DMSO)(2-MeIm)Fe(II)PP complex is formed in DMSO solutions saturated with 2-methylimidazole. This six-coordinate complex is of interest because of its strained geometry, which is caused by steric hindrance of the methyl group of the 2-methylimidazole ligand at the iron center. At high laser power, transient resonance Raman spectra show the formation of a five-coordinate complex. Other workers have shown that for different mixed-ligand (L)(Im)Fe(II) porphyrin complexes, L photodissociates rather than the imidazole. These observations indicate that the DMSO ligand photodissociates rather than the 2-MeIm. The (DMSO)(2-MeIm)Fe(II)PP photodissociation behavior is distinct from that of $(DMSO)_2Fe(II)PP$. Transient resonance Raman spectra taken with 30-ps pulses show the appearance of the modes of the ground-state five-coordinate (2-MeIm)Fe(II)PP complex within the pulsewidth, while the modes of the ground-state five-coordinate (DMSO)Fe(II)PP complex do not appear in the same time frame. The steric hindrance of the 2-methylimidazole is known to decrease the affinity of the iron for the second axial ligand. The effects of this strained geometry caused by the 2-methylimidazole upon the ligand photodissociation dynamics will be discussed.

W-Pos61

MICELLAR EFFECTS ON METALLOUROPORPHYRINS ((Bryan S. Wicks, Eric W. Findsen)) Department of Chemistry, University of Toledo, Toledo, OH 43606

The study of the interactions between metalloporphyrins and aqueous micellar environments has been motivated by the obvious biomemetic relationship to heme proteins. In this report we examine the all to illusive interphase region of micelles, which is defined as the region between the hydrophobic core of the micelle and the surrounding aqueous environment. We have found that uroporphyrins form electrostatic complexes with positively charged micellar species and thus lend themselves to be excellent spectroscopic probes of the micellar interphase region. Association of uroporphyrin complexes with the micellar surface results in a red shift in both the Soret and Q absorption band maxima that is similar to the behavior observed when uroporphyrin binds to cytochrome c. The results of resonance Raman, fluorescence, electron spin resonance and absorption spectroscopic studies which provide detailed information on the solution forces present at the micellar interface and their effect on porphyrin spectra will be presented.

ENZYMES

W-Pos62

BIOPHYSICAL STUDIES OF ADENOSINE DEAMINASE ((Q. Zeng and M.D. Barkley)) Department of Chemistry, Louisiana State University, Baton Rouge, LA 70803

Adenosine deaminase (ADA) is a key purine salvage enzyme essential for immune competence in humans. The enzyme has been overproduced in moth larvae infected with recombinant baculovirus. The stability of the wild-type and mutant enzymes with active site histidine or glutamic acid replaced by alanine has been determined. A reversible two-state transition occurs in guanidinium chloride denaturation, urea denaturation, and thermal denaturation for all enzymes. In the three sets of denaturation reactions, the unfolding of wild-type ADA occurs at about 1.2 M guanidinium chloride, 5 M urea, and 60° C, respectively. The temperature-dependent or denaturant-dependent stability of ADA is monitored by circular dichroism and thermodynamic parameters have been determined from CD data. ADA catalyzes the deamination of substrate adenosine and binds with its transition state analogues, such as 2-amino purine riboside, purine riboside, with varying efficacy. Being highly fluorescent, 2-amino purine riboside dissociation constant K_d is measured directly using a fluorescence assay. Purine riboside inhibitor binding constant K_d=1.7μM is obtained by competetion fluorescence assay using 2-amino purine riboside. The enzyme kinetics are determined using both HPLC and UV spectrometry methods. All inhibitor dissociation constants measured by fluorescence assay are in reasonable agreement with the literature K_i values.

W-Pos63

PROBING CROTONASE-CATALYZED ß-ELIMINATION IN SOLUTION AND IN THE CRYSTALLINE STATE: A Time-Resolved Fluorescence Study ((P.J. Tonge[1], T.E.S. Dahms[1,2], R. To[1], and A.G. Szabo[1,2]) [1]Institute for Biological Sciences, National Research Council, Ottawa, Ont., Canada, K1A 0R6. [2]University of Ottawa (Spon. H.C. Jarell)

Crotonase (enoyl-CoA hydratase, EC 4.2.1.17) catalyses the reversible *syn* addition of water across the carbon double bond of *trans*-2,3-unsaturated fatty acid acyl-CoA thiolesters. The enzyme from rat liver mitochondria has been cloned and overexpressed in *E. Coli*. Expressed protein is purified using a combination of affinity chromatography and HPLC, and assayed by monitoring the hydration of crotonyl-CoA at 280 nm. The identity and purity of the expressed material was verified by electro-spray ionization mass spectrometry and N-terminal sequencing.

X-ray diffraction quality protein crystals (0.6 mm x 0.6 mm x 0.2 mm) of the wild type and expressed protein in the presence and absence of substrate (crotonyl-CoA), were grown by the vapour diffusion method. The unit cell parameters are: a = b = 68.0 Å, and c = 214.2 Å, with twelve molecules (two hexamers) in the crystallographic unit cell. The space group is $P6_122$ with one molecule in the asymmetric unit.

Crotonase contains a single Tryptophan residue and is therefore suitable for time-resolved fluorescence studies. The fluorescence decay of the enzyme both in solution and in the crystalline state is best described by triple-exponential decay kinetics. In the presence of crotonyl-CoA, the decay times are shorter and there is significant fluorescence quenching, suggesting that the Trp residue is to the active site. In the crystal, the relative proportion of each decay-time shows little variation with orientation of the crystal with respect to the vertically polarized laser beam. This observation is consistent with the large number of molecules (twelve) in the crystallographic unit cell. Time-resolved fluorescence data of crotonase will be compared in the presence and absence of substrate both in the crystalline state and in solution.

W-Pos64

FLUORESCENCE ANISOTROPY DECAY MEASUREMENTS OF THIOREDOXIN SINGLE TRP MUTANTSAND COMPARISON WITH MINIMUM PERTURBATION MAPPING PREDICTIONS. ((Norberto Silva, Jr., Christopher Haydock and Frank Prendergast)) Mayo Clinic, Guggenheim 14, Rochester, MN 55905.

Proteins are fluctuating structures that cover a wide range of motion and timescales. The nsec-psec dynamics of Trp residues can be investigated through their time-resolved fluorescence anisotropy decay. Trp residue librational motion is characterized, in the Lipari-Szabo formalism, by an order parameter (S^2) and a "wobbling diffusion" correlation time (ϕ_{TW}). This can be interpreted as a Trp residue undergoing free diffusion in a cone-like environment. We wish to consider the predictions of a realistic environment modeled by molecular simulations where we assume the fluorescence anisotropy decay is primarily due to isomerization of Trp about its $\chi_1\chi_2$ dihedral angles. The simulations are performed on W31 and W28 of thioredoxin using the technique of minimum perturbation mappings (MPM). Calculated order parameters and interconversion rates between isomers are compared with the time-resolved fluorescence intensity and anisotropy decay results of single Trp mutants of oxidized and reduced thioredoxin (C32-C35 form a disulfide bridge near W31 and W28). Experimental results on oxidized TRX show that W28 is completely restricted in motion while W31 displays subnanosecond fluctuations. The MPM predicted difference in internal mobility is very sensitive to uncertainties in Trp and neighbor residue rotamer populations. Furthermore, the simulations suggest that the motions of W31 abouts its χ_1 dihedral angle contributes to the observed fluorescence anisotropy decay of oxidized W28F TRX. Comparison of theory and experiment is also discussed in the case of reduced TRX. (Supported by GM34847.)

W-Pos65

SPECTROSCOPIC IDENTIFICATION OF INACTIVE, MEMBRANE-BOUND STATES OF THE EXTRACELLULAR PLA_2. ((W.R. Burack, M.E. Gadd and R.L. Biltonen)) Depts. of Pharmacology and Biochemistry, University of Virginia 22908

The activity of extracellular PLA_2 toward bilayer phospholipid is extremely sensitive to the physical state of the substrate. Therefore, we use this system to model the possible effects of membrane structure on enzymatic activity. PLA_2's activity toward certain zwitterionic phospholipid bilayers is characterized by a period of slow product accumulation (the lag) followed by the onset of rapid activity (the burst). The burst is associated with the lateral phase separation of reaction products and substrate. Here we characterize the state of the enzyme during the lag phase. Using vesicles composed of binary mixtures of DPPG and DPPC, we create conditions under which all enzyme is bound during the lag period. The change in intrinsic fluorescence of PLA_2 upon binding to vesicles depends on the mole fraction of DPPG, suggesting that the state of the enzyme on the surface is determined by the composition of the bilayer. Therefore, either a distribution among bound states of PLA_2 is affected by compostion, or the state of PLA_2/membrane interaction varies continuously with compostion. In either case, there are multiple kinds of bound states. Using vesicles to which all enzyme is initially bound, simultaneous recordings of fluorescence and activity show that the spectroscopic and catalytic properties of PLA_2 can be varied independently. These data show that not only are there inactive states of PLA_2 on the surface, but also indicate that the burst in activity cannot be attributed entirely to recruitment of PLA_2 to the vesicle surface. (Supported by NIH)

W-Pos66

EVIDENCE FOR THE MODULATION OF *PSEUDOMONAS AERUGINOSA* EXOTOXIN-A INDUCED PORE FORMATION BY MEMBRANE SURFACE CHARGE DENSITY. ((D.M. Rasper and A.R. Merrill)) Guelph-Waterloo Centre for Graduate Work in Chemistry, Dept. of Chem. & Biochem., Univ. of Guelph, Guelph, ON, Canada N1G 2W1.

The lipid requirement for the binding of wild-type *Pseudomonas* Exotoxin A (ETA) to model endosomal membrane vesicles was evaluated by using a fluorescence quenching technique. The binding of toxin to model membrane vesicles (0.1 μm dia.) composed of various molar ratios of POPC and POPS was pH-dependent with maximal binding observed at pH 4.0. Analysis of the binding curves indicated that the interaction of ETA with the membrane bilayer is dominated by a set of high affinity binding sites (K_d 2 - 8 μM; 60:40 mol:mol, POPC:POPS large unilamellar vesicles, LUV). Binding of toxin was highly pH-dependent but affected only slightly by increasing POPS content and was ionic strength independent. Toxin-induced pore formation in the lipid bilayer, as measured by the release of the fluorescent dye, calcein, from LUV was pH-dependent with optimal dye release occurring at pH 4.0. The rate of dye release decreased rapidly with increasing pH and approached zero at pH 6.0 and higher. The pK_a for this process ranged from 4.3 - 4.5. Calcein release was also sensitive to changes in the ionic strength of the assay buffer with maximal release occurring at 50 mM NaCl. Higher ionic strength media resulted in a dramatic reduction in the rate indicating that the toxin-induced pore is modulated by ionic interactions. Further evidence for the role of electrostatic interactions between the toxin and membrane was provided by the effect of POPS on the kinetic properties of the pore. Maximal dye release (pH 4.0) was observed for vesicles composed of 60 mole % POPS. At higher vesicle POPS content (i.e., 100 mole %), the rate of dye release was reduced by 6-fold compared with 60 mole % POPS and 2-fold compared with 20 mole % POPS. The toxin-induced membrane permeabilization was temperature dependent with an activation energy (E_a) near 14 kcal/mole (58.5 kJ/mole). A break point in the Arrhenius plot for toxin-induced pore activity indicated that the permeabilization process was sensitive to the physical state of the membrane bilayer. [supported by the Medical Research Council of Canada, (A.R.M.)]

W-Pos67

pH DEPENDENCE OF THE KINETICS OF SITE DIRECTED MUTANTS OF E. COLI ASPARTATE TRANSCARBAMYLASE ((X. Yuan, V.J. LiCata, and N.M. Allewell)) Department of Biochemistry, University of Minnesota, St. Paul, MN 55108

Aspartate transcarbamylase (ATCase) from *E. coli* has been widely studied as a model allosteric system. Although it is known that ATCase switches between two major conformational states, T and R, and that this allosteric transition is pH dependent [Pastra-Landis, et al., *J. Biol.Chem.* 253:426 (1978)], details of the coupling between pH and the allosteric transition at the molecular level remain elusive. Previously we found that the pH dependence of the estimated kinetic parameters of six catalytic chain mutants of ATCase allowed the mutants to be classified as either T-like or R-like [Yuan, et al. *Biophys. J.*. 64:A165 (1993)]. We have examined Y165F a T-like, or low activity mutant, and Y240F, an R-like mutant, in greater detail. Both mutations are at the c1-c4 interface, which is involved in propagation of homotropic cooperativity. Data have been collected over a very wide range of substrate concentration (0-350 mM aspartate) allowing us to analyze the data using a Michaelis type equation which incorporates both cooperativity and un-competitive substrate inhibition. Full titration curves for the mutants and wild type enzyme have been collected at 10 different pH's (pH 6.2 to pH 9.9). Although we find similarities between Y240F and wild type enzyme, and a different pH dependence for Y165F, attempts to classify mutants as either T or R state are not clear cut. We present interpretations of the roles of Y240 and Y165 in the T to R transition, and deviations of the functional behavior of the mutants from the two state model.

Supported by NIH grant DK-17335.

W-Pos68

CHOLESTEROL ESTERASE EXHIBITS ENHANCED HYDROPHOBICITY AT THE ACTIVE-SITE AND DIMER INTERFACE IN COMPARISON WITH HOMOLOGOUS TRIACYLGLYCEROL ACYL HYDROLASES. ((D. Ghosh,[1] V.Pletnev[1,3], Z. Wawrzak,[1] W. L. Duax,[1] R. Kaiser,[2] H. Jornvall,[2] W. Pangborn[1] and M. Erman[1])) [1]Medical Foundation of Buffalo, Buffalo, NY. [2]Karolinska Institutet, Stockholm, Sweden. [3]Permanent address: Shemyakin Inst. of Bioorganic Chem., Moscow, Russia. (Spon. by D. Dorset)

Cholesterol esterase (ChE; EC 3.1.1.13) from *Candida cylindracea* is a cholesteryl ester hydrolase that specifically uses cholesterol linoleate as the substrate. The active dimeric form of the enzyme has been crystallized from polyethylene glycol in the space group P1 (a=58.565Å, b=88.685Å, c=58.585Å, α=93.29°, β=113.72°, γ=95.98°). The three-dimensional structure of the enzyme has been determined by molecular replacement techniques using the structure of acetylcholine esterase as the search model. The structure containing 1,068 amino acids in two identical polypeptide chains has been partially refined at 2.0Å. The current R-factor is 0.25 for 48,114 reflections, $F>2\sigma(F)$, with protein atoms only. The resolution is now being extended to 1.86Å. The recently determined chemical sequence of the enzyme (Kaiser, R. *et al.*, submitted) is 89% homologous to *Candida* lipase 1, a monomeric triacylglycerol acyl hydrolase. Nearly half of the amino acids that are different in the ChE structure are distributed either near the Ser-His-Glu triad or in a flap that sits over the active site and comprises the dimer interface. Most of these changes in sidechains result in additional hydrophobicity that may be responsible for providing interactions specific for cholesteryl esters. The enhanced hydrophobicity at and underneath the flap may necessitate the dimerization of the molecule not previously observed for lipases from the same family. Research is funded by NIH Grant DK26546 and also by a Mae Stone Goode Trust grant.

W-Pos69

X-RAY ABSORPTION SPECTROSCOPY OF THE CO(I) INTERMEDIATE INVOLVED IN ACETYL COENZYME A SYNTHESIS BY *CLOSTRIDIUM THERMOACETICUM*. ((J.J. Wu[a], M.D. Wirt[a], M. Kumar[a], S.W. Ragsdale,[a] and M.R. Chance[a])) *Albert Einstein College of Medicine, Bronx, NY 10461, [a]University of Nebraska, Lincoln, NE 68583.*

The corrinoid/iron-sulfur protein (C/Fe-SP) from *Clostridium thermoaceticum* cycles between a methyl-Co(III) and Co(I) form as it transfers a methyl group from methyltetrahydrofolate to carbon monoxide dehydrogenase as a step in acetyl-CoA synthesis. Extended X-ray Absorption Fine Structure (EXAFS) and x-ray edge spectroscopy of the active Co(I) state of the C/Fe-SP indicates a four-coordinate (distorted) square-planar structure where the best fit gave average Co-N(equatorial) distances of 1.87 ± 0.01 Å, corresponding to 4.2 ± 0.3 ligands. The x-ray edge spectrum of Co(I) C/Fe-SP contains a moderate intensity 1s-4p + shake-down transition and no 1s-3d peak (shake-down (SD) transitions are indicative of square-planar geometries). X-ray edge results for the methyl-Co(III) form, reported earlier, are consistent with a base-off methylcobamide structure. The absence of a ligated benzimidazole base in the methyl-Co(III) state is important since the base-off form is expected to predispose the Co-C bond toward heterolytic cleavage to form four-coordinate Co(I). Additionally, we have examined first derivative x-ray edge spectra of Co(I) C/Fe-SP relative to edge spectra of a cobalt foil as an indicator of effective nuclear charge (ENC) on cobalt. The Co(I) C/Fe/SP edge position at 7720.5 ± 0.3 eV is consistent with (but 0.5 eV lower in energy than) previous trends noted for free cobalamins. This reduction in ENC for protein bound cobalt may be related to the mechanism the enzyme utilizes to facilitate conversion of the methyl-Co(III) C/Fe-SP species to Co(I). This research is supported by USDA Grant 91-37200-6897 (MRC) and NIH Grant RO1-GM-39451 (SWR).

W-Pos70

PREDICTING HIGH-FREQUENCY EPR OF METALLOPROTEINS: FOUR-DIMENSIONAL GRAPHICAL REPRESENTATIONS APPLIED TO THE METALLOENZYME LIPOXYGENASE. ((K.S. Doctor, B.J. Gaffney and H.J. Silverstone)) Departments of Chemistry, Johns Hopkins University, Baltimore, MD 21218

Iron and other S>1/2 metal ions have multiple energy levels that become closely spaced when the Zeeman and zero field splitting terms in the spin Hamiltonians are of similar magnitudes. In this case, angular dependence of transitions and transition probabilities for electron paramagnetic resonance become complex. We have recently introduced graphical representations of the angular dependence of EPR spectral information by combining representation of the magnetic field relative to molecular coordinates with a color code for transitions probability (J. Phys. Chem. **1993**, 97, 3028-3033). Here, we extend this approach to prediction of the EPR spectra of ferric lipoxygenase at high frequencies (to 250 GHz) and examine optimum angles and frequencies for measuring EPR of single crystals of ferric iron proteins.

W-Pos71

HOMOLOGY MODELING OF SOYBEAN-2, 5-HUMAN, 12-HUMAN AND 15-HUMAN LIPOXYGENASES ((S.T. Prigge, J.C. Boyington, B.J. Gaffney and L.M. Amzel)) Department of Biophysics and Biophysical Chemistry, The Johns Hopkins University School of Medicine, Baltimore, MD 21205. (Spon. by Eaton Lattman)

Lipoxygenases are a unique class of non-heme iron-containing dioxygenases widely distributed across plants, animals, fungi and yeast that catalyze the hydroperoxidation of polyunsaturated fatty acids using molecular oxygen. In mammals, this pathway is used in the biosynthesis of leukotrienes and lipoxins, two families of potent physiological effectors. The three-dimensional structure of 839 residue soybean lipoxygenase-1 is being used to model several homologous lipoxygenases from soybeans and humans. The highly homologous soybean isoenzyme lipoxygenase-2 (85% identity and 94% similarity) was modeled using the package Quanta in an attempt to understand differences in substrate specificity. The region from residues 142 to 674 of human 5-lipoxygenase (24% identity and 46% similarity) is being modeled to elucidate its positional specificity. Due to low homology with soybean lipoxygenase-1, a distance-based algorithm has been written to place sidechains in 5-human lipoxygenase. Human 12-lipoxygenase and human 15-lipoxygenase will be modeled in a similar way.

W-Pos72

STRUCTURAL STUDIES OF QUINONE REDUCTASE BY X-RAY CRYSTALLOGRAPHY ((R. Li[1], M.A. Bianchet[1], P. Talalay[2], L.M. Amzel[1])) [1]Department of Biophysics and Biophysical Chemistry, [2]Department of Pharmacology and Molecular Sciences, The Johns Hopkins University School of Medicine , Baltimore MD 21205, USA

Quinone reductase[NAD(P)H:(quinone acceptor) oxidoreductase] is an FAD-containing protein that catalyzes the obligatory two-electron reduction of quinones with reductants of NAD(P)H. The enzyme protects animal cells against quinone carcinogens by preventing the formation of semiquinone radicals, and may be involved in the vitamin K-dependent blood coagulation cascade. Monoclinic crystals in $P2_1$ of the rat liver quinone reductase have been obtained by cocrystallization with Cibacron Blue, a potent inhibitor of the enzyme. I2 crystals(a=72.0, b=107.0, c=88.4, β=92.6°) with one dimer per asymmetric unit have been obtained in the presence of duroquinone, a substrate of the enzyme. Native and derivative data sets have been collected to 2.3Å on a Nicolet Area detector. Mercury and platinum derivatives were used to produce a 2.7Å MIR map in which secondary structure elements were evident. The phases were improved by solvent flattening and averaging over the two-fold non-crystallographic symmetry. The resulting map has been traced and shows that the folding pattern of one of the two domains is similar to that of flavodoxin. The molecular structure determination of the 273- residue protein complexed with substrate, inhibitor and FAD is proceeding using the improved phases. *(Supported by NIH Grants GM45540 and CA44530)*

W-Pos73

INVESTIGATION OF CO INHIBITION OF Mo- AND V-NITROGENASE. ((L.M. Cameron, R.C. Tittsworth and B.J. Hales)) Louisiana State University, Chemistry Department, Baton Rouge, LA 70803. (Spon. by B.J. Hales)

Nitrogenase, consisting of two proteins, catalyzes the reduction of small molecules including N_2, C_2H_2 and H^+, in a process likely to involve the two types of metal clusters in the component 1 protein. Neither the substrate binding site nor the pathway of electron transfer to substrate has been established.

CO inhibits all substrate reductions except that of H^+, by Mo-nitrogenase. A much higher ppCO (1-2 orders of magnitude) was required to inhibit the V-nitrogenase of *Azotobacter vinelandii* than the *A.v.* Mo-nitrogenase, consistent with previous reports (1). Unexpectedly, V-nitrogenase-catalyzed C_2H_6 formation from C_2H_2 increased under low ppCO, but showed a greater sensitivity to CO under higher ppCO than did C_2H_4 formation. CO induces EPR signals from Mo-nitrogenase under high electron flux (2). We observed similar signals from Mo-nitrogenase but not from V-nitrogenase under low electron flux conditions, conditions in which almost all component 1 proteins would be in low reduction states (3). In another study, g=1.95 and 1.82 signals were observed from moderate electron flux turnover samples under CO. Similar signals observed from oxidized component 1 protein have been assigned to the P^+ state (3). Further studies with CO will aim to shed light on the roles of metal clusters in substrate reduction by Mo-nitrogenase.

(1) Dilworth, M. J., Eady, R. R. & Eldridge, M. E.(1988) *Biochem. J.* **249**, 745-751.
(2) Davis, L. C., Henzl, M. T., Burris, R. H. & Orme-Johnson, W. H. (1979) *Biochemistry* **18**, 4860-4869.
(3) Fisher, K., Lowe, D. J. & Thorneley, R. N. F. (1991) *Biochem. J.* **279**, 81-85.
(4) Tittsworth, R. C. & Hales, B. J. (1993) *J. Am. Chem. Soc.* **115**, 9763-9767.

W-Pos74

USE OF 2ND DERIVATIVE INFRARED SPECTROSCOPY TO ASSESS THE PURITY & STRUCTURAL INTEGRITY OF COMMERCIAL PROTEIN SAMPLES. ((D.M. Byler[1], C.S. Randall[2] & T.D. Sokoloski[2])) [1]Philadelphia College of Textiles & Science, Philadelphia, PA 19144-5497, & [2]SmithKline Beecham Pharmaceuticals, King of Prussia, PA 19406-0939

Second derivative infrared (IR) spectroscopy [Susi & Byler, BBRC, 1983, 115, 391] can serve as a quick, easy, reproducible, cost-effective method by which to assess the relative purity and structural integrity of protein samples from different sources or lots. For this study, second derivative IR spectra were collected from aqueous solutions of four different commercial samples of the same enzyme, porcine pancreatic elastase (2.2-3.8 mg protein/ 100 µL D_2O, pD = 5.7 to 9.1. (To compensate for differences in solution concentrations and in cell pathlength, all spectra were normalized to the same peak intensity for the 1516 cm^{-1} tyrosine band.) As with other proteins possessing a large fraction of ß-structure, the amide I' region (1700-1620 cm^{-1}) of the four elastase spectra all exhibit a characteristic pair of bands near 1684 (weak) and 1633 cm^{-1} (moderate-to-strong). However, striking variations among the four samples are apparent in the observed intensities of the amide I' bands relative to the 1516 cm^{-1} absorption. This implies that the the four samples differ significantly in the amount of native protein present in each.

Cursory examination of the spectra suggests that two samples exhibit much greater purity and structural integrity than the other two, both with respect to overall intensity of the amide I' protein backbone absorptions and as regards the absence of strong bands not associated with the native protein. By contrast, the other two samples are obviously of much lower quality. In these two spectra prominent bands appear which are clearly absent in spectra of the pure, native enzyme. In one sample, new features near 1562 and 1416 cm^{-1}, together with the low intensity of the amide I' bands, suggest that the sample is either impure and/or that much of the protein has autolyzed into shorter peptide fragments. For the second sample, strong absorption near 1615 cm^{-1} indicates possible denaturation and formation of intermolecular hydrogen bonds.

Summary: In <1 hr (including solution preparation and data collection) one can use 2nd derivative IR spectroscopy to evaluate the purity of a given lot of water-soluble protein. In addition, one may assess whether the protein is truly in its native conformation. Generally, 1 mg of protein/25 µL D_2O is an adequate sample.

W-Pos75

STRUCTURE OF THE PYRROLOQUINOLINE QUINONE-DERIVED RADICAL IN METHANOL DEHYDROGENASE: INFLUENCE OF Sr^{++} SUBSTITUTION, AMMONIUM AND CYANIDE. ((K. Warncke, T.K. Harris†, G.T. Babcock, V. L. Davidson†, & J. McCracken)) Dept. of Chemistry, Michigan State Univ., E. Lansing, MI 48824 & †Dept. of Biochem., Univ. of Mississippi Med. Ctr., Jackson, MS 39216 (Spon. by A. Revzin)

Methanol dehydrogenase (MEDH) catalyzes the oxidation of methanol to formaldehyde with production of two reducing equivalents. The active site cofactor is pyrroloquinoline quinone (PQQ). A stable PQQ-derived organic radical is present in isolated MEDH at room temperature. To gain insight into the structure of this radical and its possible role in catalysis, we have compared results from combined X-band EPR, ^1H electron-nuclear double resonance (ENDOR) and multifrequency- (8.8-13.7 GHz) electron spin echo envelope modulation (ESEEM) spectroscopic studies of MEDH isolated from *Paracoccus denitrificans*. Multifrequency ESEEM studies indicate hyperfine coupling to one ^{14}N nucleus of the two present in PQQ. ENDOR studies of enzyme in ^1H_2O and ^2H_2O clearly resolve 9 ^1H hyperfine couplings (hfcs) of <10 MHz, 4 of which are solvent-exchangeable. Bound Ca^{++} in the native enzyme is obligatorily required for activity. Substitution with Sr^{++} increases V_{max}. There are no significant differences in ESEEM spectra of MEDH substituted with Sr^{++} *vs.* Ca^{++}. Thus, metal ion swapping does not perturb significantly the observed distribution of unpaired spin. However, ENDOR spectra show loss of 2 weak ^1H hfcs (1.6, 2.8 MHz). These hfcs are also ^2H_2O-exchangeable. Ammonium ion and cyanide ion are obligatory activators of MEDH at low concentrations and inhibitors at high concentrations. ESEEM spectra collected from MEDH treated with these reagents (and ENDOR from cyanide-treated enzyme) do not display significant differences from untreated enzyme. These results suggest that ammonium and cyanide are not bonded covalently to the radical. However, ENDOR spectra of ammonium-treated enzyme show 2 new ^1H hfcs (1.5, 2.5 MHz). The two pairs of altered ^1H hfcs each suggest a nearly pure dipolar hf tensor characteristic of ^1H involved in hydrogen bonds. Thus, any effects of Sr^{++} and ammonia on radical participation in catalysis appear to be mediated by changes in the solvation environment of the radical. Molecular orbital calculations are in progress to assist in assignment of the hfcs in order to determine fully the spin density distribution and protonation state.
Supported by: NIH GM-41574 (V.L.D), GM-37300 (G.T.B.), GM-45795 (J.M.)

W-Pos76

Computer Simulations of the Structural Basis of the Ionic Strength Effect on the Activity and Inhibition of HIV-1 Protease

Fredy Sussman+*, Gerald Koelsch* and Jordan Tang*

Protein Studies Program*, Oklahoma Med. Res. Foundation, Oklahoma City, O.K. 73104 and Research and Education Computing+, Oklahoma University Health Sciences Ctr. Oklahoma City O.K. 73104

The activity and inhibition of the HIV-1 Protease is dependent on ionic strength. At pH 5.5, the optimal pH of the enzyme, the Km value for a charged substrate increases from 0.03 mM to 0.6 mM when the ionic strength is decreased from 0.4 to 0.01 M and not significant change in Kcat is observable. The experiments led to the hypothesis that an ion-pair between Asp-30 and Lys-45 forms upon binding of the substrate to the enzyme. The validity of this hypothesis was demonstrated by mutating K45->E and showing that the resulting enzyme does not present a significant salt effect on substrate binding.
We have performed the molecular dynamics simulations on native HIV-1 Protease and on the mutant K45->E. We have shown that the ionic pair between D-30 and K-45 seems to appear in the native structure after lengthy simulations. The emergence of this ion-pair seems to close the 'flap' region of this enzyme. This 'flap' closure is not seen in the simulation of the K45->E mutant. The results seem to indicate that in the presence of salt, (i.e. when no ion pair is formed), the flap would not close down on the inhibitor and form the necessary interactions for the better substrate binding.

W-Pos77

OSCILLATIONS OF GLYCOLYSIS, ATP, AND CALCIUM IN THE PANCREATIC β-CELL. ((P. Smolen and A. Sherman)) NIDDK, NIH, Bethesda, MD 20892.

In addition to the well-known bursting electrical activity in pancreatic islet β-cells, slower oscillations in calcium levels and average electrical activity, with a period *ca.* 2-20 minutes, have been frequently reported. These can be very long bursts of depolarization (Smith), periodic groups of bursts (Valdeolmillos), or continual bursting but with a slow modulation of burst frequency (Henquin). A possible explanation for these is glycolytic oscillations. We first develop a model for glycolytic oscillations based on detailed experimental rate measurements of the enzyme phosphofructokinase (PFK) which catalyzes the conversion of fructose-6-phosphate (F6P) into fructose bisphosphate (FBP), and which is activated by both FBP and AMP, and inhibited by ATP. Then we couple this oscillator with the Smolen-Keizer (Smolen, 1992) model for β-cell bursting. The combined model exhibits all the types of slow oscillations mentioned above. As the glucose level is varied, the model exhibits good dose-response behavior, moving from an electrically silent state through a region of bursting with slow modulation of the burst pattern to, at high glucose, continuous spiking.

W-Pos78

STRUCTURE-REACTIVITY CORRELATIONS WITH THE QUINOPROTEIN AROMATIC AMINE DEHYDROGENASE.
((Y.-L. Hyun and V. L. Davidson)) University of Mississippi Medical Center, Jackson, MS 39216

Aromatic amine dehydrogenase [AADH] is the second enzyme known to possess the tryptophan tryptophylquinone [TTQ] prosthetic group. AADH catalyzes the oxidative deamination of a wide range of primary aliphatic and aromatic amines. Using a steady-state kinetic assay, which employed phenazine ethosulfate as an electron acceptor, V_{max} and K_m values were obtained for a series of p-substituted phenylethylamines and correlated with electronic, steric and hydrophobic substituent constants. Hammett plots of log K_m against these substituent constants indicated that K_m was strongly influenced by resonance effects and hydrophobicity. Long chain aliphatic amines were also substrates with affinity decreasing with chain length. This substrate specificity is the opposite of that exhibited by methylamine dehydrogenase, the other known TTQ enzyme. Unlike phenylethylamine, benzylamine-dependent activity of AADH was not observed in the steady-state assay. However, benzylamines stoichiometrically reduced the TTQ cofactor. This may be explained by a mechanism in which the aromatic ring attached to the *a*-carbon stabilizes the imine intermediate preventing its rapid hydrolysis and subsequent product release during the catalytic cycle. Supported by NIH grant GM-41574.

W-Pos79

A SHIFTING SPECIFICITY MODEL FOR ENZYME CATALYSIS.
((Mark Britt)) INC-14 MS C345, Los Alamos National Laboratory, Los Alamos, New Mexico 87545

A new model for enzyme catalysis (B.M.Britt, *J. theor. Biol.*, in press) challenges the idea that transition state complementarity of enzyme active sites to the reactions they catalyze is the primary source of their catalytic efficacy. The Shifting Specificity model defines a role for the entire enzyme molecule in the catalytic event, unlike most theories of enzyme catalysis which are concerned only with the interaction of the active site with substrate; incorporates the fact that strong substrate binding, contrary to current view, facilitates its turnover; and, suggests a means for the most effective realization of substrate binding energy in the transition state. The basic tenets of the Shifting Specificity model may be expressed succinctly as i) enzymes have evolved to bind substrates, ii) enzyme/substrate complexes have evolved to bind transition states, iii) a stronger interaction of substrate with the enzyme facilitates a more rapid conversion to product. This last effect results from a more efficient modulation of the global enzyme conformation by tight-binding substrates. Nature has selected for this conformational change to transform the enzyme active site from substrate-specific to transition state-specific.

W-Pos80

SINGLE-TURNOVER AND STEADY-STATE KINETIC ANALYSIS OF VACCINIA TOPOISOMERASE I (TOPO I). ((J.T. Stivers, S. Shuman, and A.S. Mildvan)) Johns Hopkins Med. Sch., Balto. MD 21205 and Sloan-Kettering, N.Y., N.Y. 10021.

Topo I catalyzes site-specific DNA strand cleavage and resealing involving a transient 3'-phosphotyrosyl linkage between the DNA and Tyr-274. The rate constants for DNA strand cleavage (k_{cl}), religation (k_r) and for duplex DNA binding and dissociation at the preferred Topo I cleavage sequence (5'-CCCTT-3') in 50 mM Tris-Cl pH 7.5 at 20 °C have been measured. The values of k_{cl} = 0.07 s-1 and k_r = 0.66 s^{-1}, indicate that the internal cleavage equilibrium ($K_{cl} = k_{cl}/k_r$ = 0.1) favors the uncleaved E·DNA complex. The apparent second-order rate constant $k_{cl}/K_m = 8 \times 10^5$ M^{-1} s^{-1} for the cleavage reaction, is 10^2 to 10^3-fold less than the rate of encounter and provides an estimate of k_{on} (DNA). Single-turnover "thio-effects" ($=k_{cl}(phos)/k_{cl}(thio)$) of 4.6 and 115-fold for non-bridging racemic phosphorothioate substituted DNA show cleavage to be rate-limiting. Biphasic cleavage kinetics for this reaction indicates a preference for cleavage of one thio isomer. Multiple-turnover reactions showed an initial presteady-state burst proportional to enzyme, followed by a slower steady-state rate (k_{cat} = 0.006 s^{-1}). The thio substrate showed a smaller burst and no effect on k_{cat} indicating fast chemical steps and rate-limiting product dissociation (K_d = 54 nM) in the steady-state, confirmed by direct measurement of k_{off} (product) =0.01 s^{-1}. $MgCl_2$ (5mM) increases k_{off} (product) by an order of magnitude, explaining Mg^{2+} induced acceleration of DNA supercoil relaxation by this enzyme. No Mn^{2+} binding by the enzyme was found suggesting activation by metal binding to DNA. While nucleophilic attack of Tyr-274 and deoxyribose 5'-OH at phosphorus on Topo I represent about 10^9 and 10^{12}-fold rate enhancements over analogous model reactions, supercoil release is probably not significantly catalyzed.

W-Pos81

RAPID ASSAY, ENRICHMENT AND IDENTIFICATION OF CYTOSOLIC POLY (ADP-RIBOSE) GLYCOHYDROLASE FROM HUMAN PLACENTA
((U.O. Nagl, R. Schneider, B. Auer and M. Schweiger)) Dept. Physiology University of Innsbruck A-6020 Austria - Europe (spon. by M. Ritter)

Many different techniques have been developed to evaluate poly (ADP-ribose) glycohydrolase activity. Their common difficulty is the purification of the substrate poly (ADP-ribose). "Combi assay", a direct combination of ADP-ribosyltransferase assay and Poly (ADP-ribose) glycohydrolase assay, does not claim to be specific as TLC methods but is a quick and easy possibility to determine the disappearance of the substrate by precipitation of the polymer during purification. After four liquid chromatography steps (Phosphocellulose, DEAE-Cellulose, Heparin Sepharose and ss-DNA-Cellulose) we enriched cytosolic Poly (ADP-ribose) glycohydrolase 12 000 fold. Three dominant protein bands remained after polyacrylamid gel electrophoresis and Coomassie staining of molecular weight, 62K, 55K and 27K. This procedure guarantees a highly reproducible, effective enrichment of cytosolic Poly (ADP-ribose) glycohydrolase in only one day! Native isoelectric focusing was finally the tool to separate and identify the enriched Poly (ADP-ribose) glycohydrolase activity directly in the gel. After sodium dodecyl sulfate gel electrophoresis in the second dimension we could adjoin the enzyme activity with the double band in the stained polyacrylamid gel with a molecular weight of 62K and 55K and a pI of 6,3. Polyclonal antiserum was raised in rabbit to the 62K protein band out of the Coomassie stained polyacrylamid gel. IgG purified from this polyclonal antiserum reacted in Western blot analysis with both, 62K and 55K, protein bands. These results show that both protein bands share the same antigenic determinants.

W-Pos82

TRANSPORT RATE LIMITED CATALYSIS ON MACROSCOPIC SURFACES: ACTIVATION OF FACTOR X BY TISSUE FACTOR-FACTOR VIIa IN A CONTINUOUS FLOW ENZYME REACTOR
((H.A.M. Andree, P.B. Contino, D. Repke, R. Gentry and Y. Nemerson)), Dept. of Biochemistry and Medicine, Mt. Sinai School of Medicine of CUNY, New York, NY 10029 and Dept. of Mathematics and Statistics, University of Guelph, Guelph, Ontario, Canada N1G 2W1.

The maximal rate of an enzyme on a macroscopic surface can be controlled by the transport of substrate to the surface. It has been hypothesized that the enzyme density resulting in half-maximal conversion would cover only a small fraction of the surface. We have experimentally confirmed this concept by using a surface-bound enzymatic complex imbedded in a phospholipid bilayer coating the inner surface of glass microcapillaries. We used Tissue Factor (TF), a transmembrane protein that when complexed with a serine protease, factor VIIa, initiates blood coagulation by activating a fluid phase zymogen, factor X. We found that conversion of 150 nM factor X was half-maximal at 0.03-0.06% surface coverage with TF-VIIa. At high TF-densities the factor X conversion was linear with the cube root of the wall shear rate, as predicted by hydrodynamic theory. The apparent K_m in the flow reactor rose linearly with enzyme density. These data suggest that factor X conversion under physiological conditions is often limited by the transport of X towards the reactive surface. In effect, when substrate conversion is limited by transport, half-maximal reaction rates are achieved with sparse enzyme surface coverage. At the transport limit, increasing enzyme density does not increase product formation. This contrasts with three-dimensional catalysis in which velocity always increases with enzyme concentration. Supported by NIH Grant HL-29019

W-Pos83

AT LOW IONIC STRENGTH TISSUE FACTOR IN PHOSPHATIDYLCHOLINE IS MORE ACTIVE THAN WHEN PHOPHATIDYLSERINE IS ADDED.
((D. Repke, H.A.M. Andree and Y. Nemerson)) Depts. of Medicine and Biochemistry, Mount Sinai Medical School of CUNY, New York, NY 10029.

Blood coagulation occurs on cell surfaces, with the phospholipid composition modulating the enzymatic activity. Pure phosphatidylcholine (PC) surfaces have been considered to have little or no activity. We have investigated the activation of factor X by the complex of Tissue Factor-Factor VIIa in a continuous flow enzyme reactor. TF in PC had considerably lower activity than TF in phosphatidylserine (PS)/PC at I=0.165. At low ionic strength, however, a slight decrease of TF:PS/PC activity was seen, while TF:PC activity markedly increased. At 0.01 M NaCl the activity of TF:PC was even higher than the activity of TF:PS/PC. The effect of PS on the activity has been attributed to the binding of factor X to the membrane. At the end of reactions, we were not able to detect factor X on the phospholipids. Taking factor Xa binding as a measure of factor X binding, with TF:PS/PC we find an inverse correlation between binding and catalytic activity, while with TF:PC there is little or no binding and hence no correlation: there is no simple relationship between substrate binding to phospholipids and catalytic activity. Thus, TF in PC can be as efficient as TF in PS/PC when the ionic strength is low ($\approx$0.035). These studies were conducted at a wall shear rate of 1600 sec^{-1}; hence convection has no effect on collisions between X and TF:VIIa (Péclet number $<$0.007). We conclude that the enhancing effect of PS cannot be attributed to simple substrate concentration at the membrane surface.

Supported by Grant HL-29019 from the National Institutes of Health

W-Pos84

KINETICS INVESTIGATION OF D-LACTATE DEHYDROGENASE OF *ESCHERICHIA COLI* STUDIED BY STOPPED-FLOW AND ^{1}H-NMR SPECTROSCOPY

((Z.-Y. Sun, S. R. Dowd, and C. Ho)) Dept. of Bio. Sci., Carnegie Mellon Univ., Pittsburgh, PA 15213

The mechanism of the enzymatic reaction by which D-lactate is oxidized to pyruvate by D-lactate dehydrogenase (D-LDH) of *E. coli* has been studied by using a stopped-flow spectrophotometer (OLIS) and ^{1}H-NMR spectroscopy. Under anaerobic conditions, the kinetics of the reaction of ~ 0.02 mM D-LDH with 0.5 mM substrate D-lactate in the presence of lysolecithin can be characterized by three rate constants having typical values of 288, 5.8 and 0.9 sec^{-1}. The fastest rate is D-lactate-concentration dependent, and hence is related to the formation of the enzyme-substrate complex. ^{1}H-NMR experiments show that the Cα-proton of D-lactate, but not of L-lactate, undergoes exchange with solvent in the presence of D-LDH, and that the enol of pyruvate may be involved in the reaction pathway. These steps are necessary, but not sufficient, to show the existence of a two-step one-electron transfer mechanism. A possible semiquinone intermediate having an absorption peak at 380 nm is detected when D-LDH is mixed with D-lactate and a nitroxide spin-labeled compound. The rate constants of the reaction by which reduced D-LDH is oxidized by nitroxides in the presence of lysolecithin increase with increasing membrane permeability of these compounds, indicating that the environment of the enzyme-bound FAD is hydrophobic. [This work is supported by a research grant from the NIH (GM-26874).]

W-Pos85

WILD TYPE AND MUTANT (R)-3-HYDROXYBUTYRATE DEHYDROGENASE EXPRESSED IN INSECT CELLS. ((David Green*, Andrew R. Marks**, Sidney Fleischer and J. Oliver McIntyre)) Vanderbilt University, Nashville, TN 37235; *Johns Hopkins School of Medicine, Baltimore, MD 21218; **Mt. Sinai School of Medicine, New York, NY 10032.

(R)-3-Hydroxybutyrate dehydrogenase (BDH) is a lipid-requiring mitochondrial enzyme with an absolute requirement of phosphatidylcholine (PC) for function. PC serves as an allosteric activator to enhance NAD(H) binding to BDH. Analysis of the primary sequence of BDH (determined by molecular cloning) predicts that lipid binding and substrate specificity are contributed by the C-terminal third of the protein [Marks et al., *J.Biol. Chem.* 267:15459 (1992)]. We have now expressed catalytically active BDH in insect cells (Sf9, *Spodoptera frugiperda*) transfected with BDH-cDNA in baculovirus. Expressed human heart BDH is active and requires PC for function since activity is lost upon digestion with phospholipase A_2 and restored by reconstitution with PC vesicles. The measured enzyme kinetic parameters (K_ms for NADH and (R)-3-hydroxybutyrate, R-HOB) of expressed BDH are similar to those for bovine heart or rat liver BDH in mitochondria. Replacing Cys-242 (the only cysteine in the C-terminal domain) with serine by site-directed mutagenesis resulted in a 10-fold increase in K_m for R-HOB with no change in the K_m for NAD^+, indicating a role for Cys-242 in substrate binding. Deletion of 12 C-terminal amino acids from BDH resulted in the complete loss of enzymic activity, consistent with recent carboxypeptidase cleavage studies which showed a requirement of the C-terminal for catalysis and a role in lipid binding. Structure-function studies are in progress to further define the substrate and the lipid binding/activation domains of BDH. (NIH HL 32711)

HEME PROTEINS I

W-Pos86

FAR UV TIME-RESOLVED CIRCULAR DICHROISM AND ABSORPTION STUDIES OF CARBONMONOXYMYOGLOBIN. ((Befei X. Chen, Sarah J. Paquette & David S. Kliger)) *Department of Chemistry & Biochemistry, University of California, Santa Cruz, California 95064*

Time-resolved absorption studies (TROD) of hemeproteins have traditionally focused on the Soret and near IR regions. In our far UV time-resolved circular dichroism (TRCD) studies of MbCO only small changes in ellipticity were detected from 0*ns* to 500μ*s*. However, parallel TROD studies show unusual kinetics and spectral dynamics. Preliminary global analyses of TROD data indicate that formation of a positive ΔOD 215*nm* band at late times from a negative ΔOD 205*nm* band, present at early times, is due to spectral and temporal convolution of two transients (τ=400 μ*s* & 270*ms*).

Results of far UV-TROD experiments on metMb, metMbN_3^-, HbCO and ferri- and ferrocytochrome *c* suggest that the observed spectra are due to localized heme changes that occur after ligand photolysis. Several porphyrins (hemin, heme-CO, 1-methylimidazole-heme-CO and 5'-deoxyadenosylcobalamin) have been examined to determine the effect of a bulky axial ligand, such as the proximal histidine in MbCO and the lower axial 5,6-dimethylbenzimidazole ligand in 5'-deoxyadenosyl-cobalamin, on the far UV-TROD spectra. *This work is supported by National Institutes of Health Grant GM-35158.*

W-Pos87

CYCLIC VOLTAMMETRY OF CYTOCHROME c OXIDASE ((A. Sucheta and Ó. Einarsdóttir)) Department of Chemistry and Biochemistry, University of California, Santa Cruz, CA 95060

A dynamic electrochemical technique of cyclic voltammetry at pyrolytic graphite electrodes has been used to study the redox potentials of bovine heart cytochrome oxidase. The goal of this approach is to observe reversible and direct (unmediated) electron transfer between the electrode and redox active prosthetic groups in the enzyme. This approach augments mediated electrochemical methods in which electrons are passed to or from the protein under study by mediators, whose efficacy is dependent on the equilibrium thermodynamics of the electron transfer reaction between the mediator and the protein. Various materials that enhance the interactions between cytochrome oxidase and the electrode were explored to ensure the structural and functional integrity of the enzyme. The effects of respiratory inhibitors such as cyanide and carbon monoxide on the observed redox potentials were investigated. The electron-transfer kinetics between cytochrome c and cytochrome oxidase in presence and absence of oxygen were explored and specific voltammetric features assigned to electron exchange between the redox partners. Simultaneous measurements of the redox potentials using cyclic voltammetry and optical absorption spectra of the cytochrome oxidase are in progress. Supported by NIH grant R29 GM45888.

W-Pos88

INTRAMOLECULAR ELECTRON TRANSFER AND CONFORMATIONAL CHANGES IN CYTOCHROME c OXIDASE. ((K.E. Georgiadis, N.-I. Jhon, and Ó. Einarsdóttir)) Department of Chemistry and Biochemistry, University of California, Santa Cruz, CA 95060

The kinetics of intramolecular electron transfer and conformational processes in cytochrome oxidase have been studied at room temperature following photodissociation of CO bound to mixed-valence (cytochrome a_3^{2+}-CO Cu_B^+ cytochrome a^{3+} Cu_A^{2+}) and fully reduced enzyme complexes. Transient absorption difference spectra were collected in the UV-visible and the near-infrared regions on time scales of nanoseconds to milliseconds using a gated optical spectrometric multichannel analyzer. A global exponential fitting routine employing a singular value decomposition method was used to analyze the transient difference spectra at various times following photolysis. Global analysis of the mixed-valence transient difference spectra in the visible region gave five kinetic intermediates with apparent lifetimes of 1.1 μs, 4.3 μs, 83.1 μs, 14.1 ms and 46.6 ms. Similar rates were obtained for the Soret region. It was possible to fit the data to a kinetic model involving a sequential pathway. This model comprises a conformational change, presumably at cytochrome a_3, followed by electron transfer from cytochrome a_3 to cytochrome *a*, with subsequent electron transfer to Cu_A^{2+}. The 14 ms rate is attributed to the CO recombination and the 46 ms rate to a structural change. Based on this model, the microscopic rate constants and absorption spectra of the intermediates present in the conformational and electron transfer dynamics of the mixed-valence cytochrome oxidase have been determined. Supported by NIH grant R29 GM45888.

W-Pos89

SELF-ASSOCIATION OF THE ISOLATED SUBUNITS OF *LUMBRICUS TERRESTRIS* HEMOGLOBIN. ((David W. Ownby and Austen F. Riggs)) Dept. of Zoology, University of Texas, Austin, TX 78712.

The gigantic hemoglobin (Hb) of the earthworm *L. terrestris* (≈4000 kDa) has four O_2-binding chains: *a*, *b*, and *c* (forming a disulfide-linked trimer *abc*) and chain *d*, as well as linker chains which have a structural role. The O_2-binding subunits have been isolated by size-exclusion chromatography of the Hb dissociated at high pH; 76 and 97% of the linkers were removed from the *abc* and *d* fractions, respectively. Association of the subunits as a function of pH, Ca^{2+}, and protein concentration was studied by determination of the weight-average molecular mass (M_w) of the carbon-monoxy (HbCO) derivatives by laser light scattering. *Chain d*: *d* is largely dimeric between pH 6.5 and 9.0 and 0.2-1.4 mg/ml protein, and associates to at least d_4 in the presence of Ca^{2+}. *Trimer (abc)*: Self-association of the trimer is open-ended with M_w values corresponding to $(abc)_i$, where i>10 ($M_w > 5.5 \times 10^5$). The association is maximal at pH 6.0; $(abc)_2$ is the predominant form at pH 9.0. Association of $(abc)_i$ is also enhanced in the presence of Ca^{2+}. *Trimer (abc) + chain d*: *abc* and *d* were recombined on a 3:1 molar heme basis at pH 6.5. The self-association equilibrium gave a weight-average molecular mass of ≈2 x 10^5 Da, with partial dissociation at low concentration. Calcium caused the M_w to increase with concentration, and 7% of the total *abc* + *d* product appeared in a peak of $M_w > 4 \times 10^6$. Supported by NSF Grant MCB-9205764 and NIH Grant GM-35847.

W-Pos90

OXYGENATION EQUILIBRIUM STUDIES OF CROSS-LINKED Ni-Fe HYBRID HEMOGLOBINS. ((A. Tsuneshige and T. Yonetani)) Department of Biochemistry and Biophysics, University of Pennsylvania, PA 19104-6089

To understand the phenomenon of cooperativity in hemoglobin (Hb) it is crucial the characterization of intermediate species of ligation. Both the use of Ni-substituted Hb that mimics a permanent deoxy heme and the cross-linking between both the α subunits to prevent dimerization and recombination of dimers, constitute important tools for the preparation of these intermediate species. We have re-examined the oxygenation characteristics of symmetric Ni-Fe hybrid Hbs —$\alpha(Ni)_2\beta(Fe)_2$ and $\alpha(Fe)_2\beta(Ni)_2$— and found that their oxygen affinities along pH change were different from previous reports [1]: while the O_2 affinity of these two hybrids were low and similar at acidic pH levels, the affinity of $\alpha(Fe)_2\beta(Ni)_2$ increased dramatically at alkaline pH levels while that of $\alpha(Ni)_2\beta(Fe)_2$ remained relatively low. A comparable trend was also observed in asymmetric hybrids of the type 1(Ni)-3(Fe). It was also found that other hybrid Hb systems (such as Zn-Fe, Mg-Fe, Cu-Fe, and even porphyrin-Fe [2]) in which the substitutions occurred in the α subunits, showed behaviors strikingly similar to that of $\alpha(Ni)_2\beta(Fe)_2$.

Supported by Research Grant (HL14508 from NIHLB, NIH)

[1] Shibayama, N., Morimoto, H. & Miyazaki, G. (1986) *J. Mol. Biol.* **192**, 323-329. [2] Fujii, M., Hori, H., Miyazaki, G., Morimoto, H. & Yonetani, T. (1993) *J. Biol. Chem.* **268**, 15386-15393

W-Pos91

THE ROLE OF HIS(FG3) AND LEU(F4) IN LIGAND BINDING TO SPERM WHALE MYOGLOBIN. ((E. Chien, J.D. Müller, G.U. Nienhaus R. Philipp and S.G. Sligar)) Department of Biophysics, Biochemistry, Chemistry and Physics, University of Illinois at Urbana-Champaign

Site-directed mutants of sperm whale myoglobin were constructed to probe the functional role of the highly conserved residues in the proximal side. His(FG3) at position 97 and Leu(F4) at position 89 are highly conserved among the globins and are believed to play an important role in controlling ligand binding. We have mutated His(FG3) to Phe and Leu(F4) to Ile. Binding of CO to these mutants was studied by flash photolysis at various pH's from 293K to 10K. At pH 7, replacement of Leu(F4) by Ile has little effect on CO rebinding, while replacement of His(FG3) by Phe decreases the rate by 50%. As pH is decreased from 7 to 5, CO recombination to these proximal mutants increases by 150 to 200% while the rates for distal mutants His(E7)Gly and His(E7)Val increases by only 11-25%. The results indicate that His(FG3) plays an important role in regulating ligand binding to sperm whale myoglobin but the pH dependence of CO recombination is probably determined primarily by the distal histidine, His(E7). Supported by NIH grant GM31756 and Molecular Biophysics Training grant GM08276.

W-Pos92

A MOLECULAR MECHANICS AND RESONANCE RAMAN INVESTIGATION OF THE CONSERVED NONPLANAR HEME DISTORTION IN CYTOCHROMES *C*.

((J. D. Hobbs[1], K. K. Anderson[1,2], L. Luo[3], J. M. E. Quirke[3], R. W. Larsen[4] and J. A. Shelnutt[1,2])) [1]*Fuel Science Department 6211, Sandia National Laboratories, Albuquerque, NM 87185.* [2]*University of New Mexico, Albuquerque, NM 87131,* [3]*Florida International University, Miami, Fl 33199.* [4]*University of Hawaii, Honolulu, HI 96822.*

The importance of nonplanar macrocyclic conformations in the biological function of tetrapyrrole containing proteins has become increasingly evident. An analysis of high-resolution X-ray crystal structures of cytochromes *c* isolated from seven species reveals the presence of a conserved nonplanar distortion of the heme that is induced through the covalent linkages between the heme peripheral substituents and two cysteine amino acid residues of the protein. Molecular dynamics and energy minimization calculations of yeast iso-1-cytochrome *c* starting from the crystal coordinates of the oxidized form suggest that this distortion is maintained by the protein tertiary structure. Resonance Raman and molecular mechanics studies of metallo-octaethylporphyrins and meso-nitrooctaethylporphyrins suggest a way to measure the energetic and functional properties of protein induced nonplanarity in *c*-type cytochromes and metal-reconstituted cytochromes.

Supported by U.S. DOE Contract DE-AC04-94AL85000 and Associated Western Universities Fellowships (JDH and KKA).

W-Pos93

CONFORMATIONAL RELAXATION AND GEMINATE REBINDING IN CARBOXYHEMOGLOBIN. ((M. Yang, J.Wang, J. Huang, Y. Lu, M.R. Chance, and J.M. Friedman)) Dept. of Physiology & Biophysics, Albert Einstein College of Medicine, Bronx, NY 10461 (Spon. by J. Friedman)

Agmon and Hopfield [1] proposed that conformational relaxation in photodissociated hemeproteins can result in a time dependent increase in the enthalpic barrier controlling geminate recombination(GR). Scott and Friedman [2] reported pH dependent variations in the tertiary relaxation of COHbA on a fast enough time scale to influence the nanosecond GR. They proposed that the Agmon Hopfield theory might be operative in this case although it is usually considered in the context of low temperature experiments. Findsen et al.[3] showed that increasing the viscosity slows and eventually stops the submicrosecond tertiary relaxation in COHbA. In an attempt to more clearly establish the relationship between tertiary relaxation and geminate recombination, we have built upon these earlier results by systematically varying viscosity, pH, effector concentration, hemoglobin type and temperature in parallel experiments focussing on either the tertiary relaxation or the geminate recombination. Conformational relaxation studies include time evolution of the 760 nm photoproduct absorption band and associated kinetic hole burning experiments. A detailed model that is based on the results of these studies and includes conformational relaxation and ligand motion will be presented.

1. J. Chem. Phys. (1983) 79, 2042
2. JACS (1984) 106, 5677
3. Biochemistry (1988) 27, 8719

W-Pos94

ELECTRON-NUCLEAR COUPLINGS TO THE PROXIMAL HISTIDINES IN OXY COBALT-SUBSTITUTED DISTAL HISTIDINE MUTANTS OF HUMAN MYOGLOBIN. ((H. Caroline Lee[1], Dou Yi[2], Masao Ikeda-Saito[2] and Jack Peisach[1,3]))Depts. of [1]Molecular Pharmacology, [3]Physiology & Biophysics, Albert Einstein College of Medicine, Bronx, NY 10461; [2]Dept. of Physiology & Biophysics, Case Western Reserve University, Cleveland, OH 44106.

Electron spin echo envelope modulation (ESEEM) spectroscopy was applied to oxyCo distal histidine ($His^{E7,64}$) mutant (His→Leu, Val, Gly, Gln) and wild type human myoglobins to investigate electron-nuclear couplings to the N_ϵ of the proximal histidine ($His^{F8,93}$). ^{14}N nuclear hyperfine and ^{14}N nuclear quadrupole couplings decrease in the order: H64L > H64V > H64G ≈ H64Q > H64H. For the four mutants, an increase in the polarity in the E7 side chain is accompanied by a decrease in F8 ^{14}N couplings. For H64H, the smaller couplings than those found for the mutants can be attributed to the presence of a hydrogen bond between the distal histidine and the bound O_2, detected by ESEEM measurements in D_2O. From the relative orientation of the g, ^{14}N nuclear hyperfine and nuclear quadrupole tensors, based on computer simulation of spectra, the Co-O-O bond angles are similar in H64H, H64Q and H64G; while those in H64V and H64L are more obtuse. The relative orientation of the O-O bond and the proximal histidyl imidazole in H64G and H64Q are different from that in H64H.

W-Pos95

ELECTRON SPIN ECHO ENVELOPE MODULATION (ESEEM) STUDY OF Fe-Co HYBRID HEMOGLOBINS. ((H. Caroline Lee[1], Antonio Tsuneshige[2], Takashi Yonetani[2] and Jack Peisach[1,3]))Depts. of [1]Molecular Pharmacology, [3]Physiology & Biophyics, Albert Einstein College of Medicine, Bronx, NY 10461; [2]Dept. of Biochemistry & Biophysics, University of Pennsylvania, Philadelphia, PA 19104.

ESEEM spectroscopy was applied to fully oxygenated symmetric Fe-Co hydrid hemoglobins (Hb) to investigate electron-nuclear coupling to the N_ϵ of the proximal histidine of oxyCo α- and oxyCo β-subunits. Both ^{14}N nuclear hyperfine and nuclear quadrupole coupling are smaller in the α- than in the β-subunits. The differences in couplings can be attributed to the presence of a hydrogen bond to bound O_2 in the oxyCo α-subunits, detected as hyperfine-coupled deuterons by ESEEM in D_2O-exchanged samples, but not detected in oxyCo β-chains. The differences in ^{14}N and ^{2}H couplings between the oxyCo α- and oxyCo β-subunits are consistent with the observed larger O_2 affinities for oxyCo and oxyFe α-subunits. The relative orientations of the g, ^{14}N nuclear hyperfine and ^{14}N nuclear quadrupole tensors in the hybrid hemoglobins, determined by computer simulation of spectra, revealed differences in Co-O-O bond angles and in the relative orientation between the O-O bond and the proximal histidine for the two types of oxyCo subunits. These differences correlate with those found for the oxyFe subunits as obtained by X-ray crystallography.

W-Pos96

ELECTRONIC AND COORDINATION STRUCTURE OF COBALTOUS MYOGLOBIN AT LOW pH.

((H. Caroline Lee[1], and Jack Peisach[1,2]))Depts. of [1]Molecular Pharmacology, [2]Physiology & Biophysics, Albert Einstein College of Medicine, Bronx, NY 10461.

EPR and ESEEM spectroscopy were used to characterize the electronic and coordination structure of the metal center of cobalt-substituted myoglobin at low (2.5-4.5) pH. At pH 2.5, in the absence of O_2, no ^{14}N hyperfine splitting was observed in the EPR spectrum, indicating that the proximal histidine was dissociated from Co. Upon oxygenation, an EPR spectrum characteristic of an oxyCo-L complex (where L is an nitrogenous ligand) was observed, indicating the re-association of the proximal histidine to Co upon binding of O_2. Analogous changes in proximal histidine-ligation upon CO binding was observed for the ferrous protein. Application of ESEEM spectroscopy to oxyCoMb at low pH found decreases in hyperfine and quadrupole couplings to the proximal histidyl imidazole, as compared to neutral pH, probably due to an increase in the ionicity of the $Co\text{-}O_2$ bond in the presence of a protonated distal histidine. ESEEM measurements in D_2O did not detect any hyperfine-coupled deuterons, suggesting that the hydrogen bond between the distal histidine and bound O_2, present at neutral pH, was absent at low pH, as proposed by X-ray crystallography of the FeCO protein. The absence of distal hydrogen bonding is also consistent with the reduction of O_2 affinity at low pH.

W-Pos97

BIOCHEMICAL-BIOPHYSICAL STUDIES OF HUMAN NORMAL AND MUTANT HEMOGLOBINS EXPRESSED IN *E. COLI*.

((N.T. Ho, T.-J. Shen, M. Zou, P.D. Sun, V. Simplaceanu, H.-W. Kim, and C. Ho)) Dept. Biol. Sci., Carnegie Mellon Univ., Pittsburgh, PA 15213

We have designed a plasmid (pHE2) which can produce unmodified human adult hemoglobin (Hb A) in *E. coli*, and have constructed several mutant Hbs by site-directed mutagenesis. The mutants expressed in our system are (i) single-site mutants, α20His→Glu, α50His→Glu, α72His→Glu, and (ii) a quadruple mutant (α96Val→Tyr, β99Asp→Asn, β101Glu→Asp, β104Arg→Leu). In all cases, two major peaks have been eluted from a Mono S chromatographic column. The Hb from peak a of recombinant Hb A is identical to Hb A in structure (determined by ^{1}H-NMR) and function (O_2 binding), while the Hb from peak b shows perturbation around the heme group by ^{1}H-NMR and has a higher O_2 affinity and slightly lower cooperativity than those of Hb A. However, peak b can be converted to Hb A in structure and function when it is oxidized, reduced, and put through the column again. ^{1}H-NMR spectra show that the Hb from neither peak a nor b of the single-site mutant Hbs is identical to Hb A in structure. Hb from both peaks also has higher O_2 affinity and lower cooperativity compared to Hb A. When Hb from either peak of the single-site mutant Hbs was oxidized, reduced, and passed through the column, the O_2 affinity was found to be essentially unchanged, but the cooperativity improved to normal values. In the quadruple mutant Hb, ^{1}H-NMR spectra show that Hb from both peaks a and b exhibit structural alterations in the heme pockets and in the $\alpha_1\beta_2$ subunit interface. Hb from both peaks also has extremely high O_2 affinity and low cooperativity. [Supported by a NIH grant (HL-24525)]

W-Pos98

DESIGN OF MUTANT HEMOGLOBINS BY MOLECULAR DYNAMICS AND STRUCTURAL INVESTIGATION BY ^{1}H-NMR SPECTROSCOPY

((H.-W. Kim*, T.-J. Shen*, N. Ho*, M. Zou*, D.-P. Sun*, V. Simplaceanu*, M. Madrid+, and C. Ho*)) Dept of Biol. Sci., Carnegie Mellon University; +Pittsburgh Supercomputing Center, Pittsburgh, PA 15213. (Spon. by S. R. Dowd)

Human abnormal hemoglobins (Hbs) with an amino acid substitution at the β99Asp position possess greatly reduced cooperativity and increased oxygen affinity relative to those of human Hb A. Crystallographic studies have shown that β99Asp is H-bonded to α42Tyr and α97Asn in the $\alpha_1\beta_2$ interface of deoxy-Hb A, suggesting that the essential role of β99Asp is to stabilize the deoxy-Hb molecule by making intersubunit H-bonds. If additional substitutions are introduced in the local environment of the β99 mutants to create new H-bonds in the $\alpha_1\beta_2$ region, it is possible that the cooperativity for the oxygenation of these Hbs can be restored. We have designed such mutants by molecular dynamics simulation. For Hb Kempsey (β99Asp→Asn), in which the amino acid residue replacing β99Asp preserves the H-bonding ability, the simulations indicate that H-bonds involving the β99Asn position can be induced either by introducing mutations into positions surrounding the β99 position, or by replacement of α42Tyr by a strong H-bond acceptor such as Asp. One of these designed mutants, (α96Val→Tyr, β99Asp→Asn, β101Glu→Asp, β104Arg→Leu), has been expressed in *E. coli* and has been tested for its structural perturbations using ^{1}H-NMR spectroscopy. This recombinant Hb shows the typical absorption spectrum of Hb A, and exhibits high affinity for oxygen. The ^{1}H-NMR spectrum of the CO form shows only small changes in the tertiary structure and the heme properties compared to those of Hb A. The ^{1}H-NMR spectrum of the deoxy form shows siginificant changes on the proximal histidyl resonance and the hyperfine-shifted resonances. Most of the characteristic exchangeable resonances of Hb A are present except the resonance from the H-bond between α42Tyr and β99Asp. The contribution of these results to our understanding of the structure-function relationship in Hb will be discussed. [Supported by a NIH grant (HL-24525)]

W-Pos99

THE CONTRIBUTION OF SURFACE HISTIDINES IN THE α-CHAIN TO THE BOHR EFFECT OF HUMAN NORMAL ADULT HEMOGLOBIN

((D. P. Sun, M. Zou, H.-W. Kim, N. T. Ho, V. Simplaceanu, T.-J. Shen, C. Ho)) Biological Sciences, CMU, Pittsburgh, PA 15213

In our laboratory, we have used ^{1}H-NMR spectroscopy to study the contribution of histidyl residues to the total Bohr effect of human normal adult hemoglobin (Hb A). We have monitored the variation of proton resonances from C2 and C4 protons of histidyl residues of Hb A as a function of pH and buffer conditions. In order to assess the contribution of individual histidyl residues to the total Bohr effect, we need to assign each of these proton resonances to individual histidyl residues. By applying site-directed mutagenesis to an *E. coli* Hb expression plasmid, we have constructed six recombinant mutant Hbs, in each of which a single histidyl residue is replaced by a glutamyl residue. The mutated histidyl residues are in the α-chain at the 20th, 50th, 72nd, 89th, 112th, and 122nd position from the NH_2-terminal. By comparing the ^{1}H-NMR spectra of Hb A with those of the recombinant mutant Hbs, we can assign the aromatic resonances arising from the C2 and C4 protons of the six histidyl residues. From the change of the pK value of each histidyl residue, which occurs when Hb A changes from the CO-ligated state to the deoxy state, we can calculate the contribution of individual histidyl residues to the total Bohr effect of HbA. We will discuss the effect of these results to our understanding of the molecular basis of Bohr effect. [Supported by a grant from the NIH(HL-24525)]

W-Pos100

IDENTIFICATION OF PHOTOLYSIS-SENSITIVE VIBRATIONAL MODES IN MbCO AND MbO_2 USING FTIR SPECTROSCOPY.

((D. Durst, L.M. Miller, and M.R. Chance)) *Albert Einstein College of Medicine, Bronx, NY.*

FTIR spectroscopy of liganded and photoproduct states of MbO_2 and MbCO at cryogenic temperatures reveals significant structural information in the 1050 to 1150 cm^{-1} region of the infrared spectrum. This region contains contributions from the heme moiety, histidylimidazole side chains, and the dioxygen stretching frequency of MbO_2, all of which are affected by photolysis. For MbCO and MbO_2, we observe liganded modes at 1080 and 1096 cm^{-1} that shift to lower frequencies upon photolysis and a third liganded mode (MbCO, 1107 cm^{-1}; MbO_2, 1105 cm^{-1}) that shifts to a higher frequency upon photolysis. As the ligand rebinds, these modes revert back to their original liganded positions. In addition, we observe an 1115 cm^{-1} mode that is unique to compounds in which the iron atom is out of the heme plane. FTIR spectra of heme model compounds: $iron^{III}$ octaethylporphyrin, $iron^{III}$ protoporphyrin IX, and $(4\text{-MeIm})_2$FeOEP have aided in the assignment of the first two modes to heme peripheral vinyl groups and the third to the distal or proximal histidylimidazole. We propose that the bandshifts are due to the motions of the heme and histidylimidazole side chains upon photolysis. Additionally, this infrared region also contains a contribution from ν(O=O) in MbO_2 spectra. We present photolysis and isotopic substitution experiments which support the theory that ν(O=O) couples with a distal and/or proximal histidine mode. The dioxygen stretching frequency appears at 1105 cm^{-1}, overlapping a histidylimidazole mode at the same frequency. This work was supported by the NIH grant #HL-45892.

W-Pos101

X-RAY EDGE STRUCTURAL HOLEBURNING OF MbCO.

((L.M. Miller, E. Scheuring, A. Xie, M.R. Chance)) *Albert Einstein College of Medicine, Bronx, NY.*

MbCO has been shown to have various conformational substates that bind carbon monoxide at different rates. The structures of these substates and the intermediates involved in the process of ligand binding to myoglobin are poorly understood. X-ray absorption spectroscopy is an excellent technique for directly examining the heme environment of these intermediates. The x-ray absorption spectrum of the MbCO photoproduct at 20 K shows a shift of the x-ray edge position to a lower energy; this trend is consistent with a "deoxy-like" character. Successive x-ray absorption spectra taken as MbCO recombines represent particular distributions of MbCO structural intermediates. By subtracting a liganded MbCO spectrum from each partially recombined Mb*CO spectrum, only structural characteristics of the photoproduct distribution remain. Interestingly, as the sample recombines, the position of the photoproduct distribution maximum shifts to lower energy, indicating that the part of the photoproduct distribution that has a higher barrier to recombination (i.e. recombines at a higher temperature), is more "deoxy-like" in character. These "structural holeburning" results provide direct evidence for the presence of multiple intermediate states involved in MbCO recombination. Structures of these intermediates can be predicted by making systematic structural changes in the Cambridge Crystallographic Data Base structure of MbCO and/or deoxy Mb. Then, the ab initio EXAFS code, FEFF (v. 5.05), can simulate theoretical x-ray absorption spectra from these data. The theoretical spectra that fit best to the experimental photoproduct data are indicative of plausible structures of the MbCO photoproduct. This work was supported by the NIH grant #HL-45892.

W-Pos102

EFFECTS OF pH, METAL SUBSTITUTION, AND DISTAL HISTIDINE SUBSTITUTION ON THE PHOTOLYSIS-SENSITIVE VIBRATIONAL MODES IN MbCO AND MbO_2 USING FTIR SPECTROSCOPY.

((B. Sclavi, L. M. Miller, D. Durst, and M. R. Chance)) *Albert Einstein College of Medicine, Bronx, NY.*

The 1050-1150 cm^{-1} region of the MbCO and MbO_2 infrared spectra contains several bands that are sensitive to ligand photolysis and thus provide structural markers of intermediate states that are involved in the process of ligand binding to myoglobin. These modes have been attributed to motions of the heme peripheral vinyl groups, and the distal and/or proximal histidylimidazole. Also, a ring-vinyl stretch has been identified as a marker of heme planarity. Therefore, we have addressed the sensitivity of the band positions, intensities, and recombination rates to changes in pH, metal substitution, and distal histidine substitution. We observe position and intensity differences in the heme peripheral vinyl modes upon substitution of a cobalt heme for the iron heme, presumably due to variations in the electron-density contributions from the two metals to the porphyrin π-system. Mutant MbO_2, in which the distal histidine is replaced by a glutamine, reveals a histidylimidazole mode similar to the native MbO_2, identifying this band as a proximal histidine mode. We also observe pH-dependent structural variations in heme planarity of the MbCO photoproduct state, observed through pH-sensitive ring-vinyl stretch modes. Kinetic analysis of the recombination patterns reveals two-state transitions in the peripheral vinyl modes and supports multiple steric and electronic environments of the proximal histidine, each having distinct rebinding kinetics. This work was supported by the NIH grant #HL-45892.

W-Pos103

CHLORIDE MASKS EFFECTS OF OPPOSING POSITIVE CHARGES IN Hb A and Hb HINSDALE (ß139 ASN→LYS) THAT CAN MODULATE COOPERATIVITY AS WELL AS OXYGEN AFFINITY. ((C. Bonaventura, M. Arumugam, R. Cashon, J. Bonaventura and W.F. Moo-Penn[$])) Duke University School of the Environment Marine Laboratory, Beaufort, NC 28516 and [$]Center for Infectious Diseases, Centers for Disease Control, Atlanta, GA 30333.

The substitution of lysine for asparagine at ß139 (H17) in Hb Hinsdale brings two positively charged residues into opposition in the central cavity. Unrecognized effects of chloride on Hb Hinsdale led to it being considered a variant with lowered oxygen affinity and decreased anion sensitivity (Moo-Penn et al., 1989). When examined in a chloride-free at pH 7, the oxygen affinity of Hb Hinsdale is very high (Log P_{50} = -0.6) and cooperative interactions are greatly reduced (n_{50} = 1.3) due to a new high affinity anion binding site. A comparison of the properties of Hb A, Hb Hinsdale, Hb Deer Lodge (ß2 His→Arg) and Hb Abruzzo (ß143 His→Arg) shows that in all these proteins the presence of opposing positive charges in the central cavity allows for anionic modulation of cooperativity as well as oxygen affinity and that even the low chloride concentrations in bis-Tris buffers partially obscure their functional properties.

W-Pos104

CHLORIDE AND WATER BINDING TO HEMOGLOBIN AS A PROBE OF NOVEL HEMOGLOBIN STRUCTURES IN SOLUTION. ((M.F. Colombo)) Dept. of Physics, UNESP, S.J. Rio Preto, SP, Brazil, 15054-000. (Spon. by M. Prouty).

The effect of neutral solutes on Hemoglobin (Hb) oxygen affinity has previously been interpreted by us in terms of a linkage between oxygen and water binding to the protein. We re-examined the effect of Cl on Hb oxygenation, taking into account the coupled changes in water and chloride activities, in order to determine the number of chlorides and waters associated with oxygen uptake. We found that the Cl effect on Hb oxygenation, measured at both constant and variable water activities, could be described by the release of 1 Cl and the binding of 65 extra waters. Further investigation at lower Cl concentrations now reveals a more intricate inter-dependence between changes in hydration and Cl binding linked to oxygenation. The O2 affinity of chromatographically pure HbA0 at varying Cl and fixed water activities is found insensitive to [Cl] up to 5mM, but highly dependent for [Cl] > 20 mM. The sensitivity of Hb oxygenation to [Cl] > 20 mM indicate that almost 2 Cl ions are released from deoxy-Hb. The sensitivity of oxygenation to water activity shows that twice as much extra water is bound with Hb oxygenation at [Cl] > 20 mM than seen at [Cl] < 5 mM. These results are consistent with a substantial change in deoxy Hb conformation associated with Cl binding. Supported by FAPESP.

W-Pos105

DYNAMICS OF OXYGEN PENETRATION AND DIFFUSION INTO HORSE SKELETAL MYOGLOBIN AS REVEALED BY ZINCPROTOPORPHYRIN IX FLUORESCENCE. ((J. Carrero[1], D.M. Jameson[2] and E. Gratton[1])) [1]Laboratory for Fluorescence Dynamics, Dept. of Physics, Univ. of Illinois at U-C, 61801; [2]Univ. of Hawaii at Manoa, Biochemistry & Biophysics, Honolulu, 96822.

Oxygen quenching of tryptophan fluorescence in a number of globular proteins provided some of the early experimental evidence of conformational fluctuations in proteins. Gratton et. al. (*Biophys. J. 45*:789, 1984) derived a model for oxygen quenching of internally buried fluorophores in proteins called the dynamic model for oxygen quenching. For this study, that model is used to analyze the dynamics associated with conformational fluctuations of oxygen entry and to obtain thermodynamic parameters associated with these fluctuations. We used Zincprotoporphyrin IX reconstituted myoglobin and performed oxygen quenching experiments at temperatures of 5, 10, 15, 20, 25 and 30°C. The data was fit to the above model and k^+ (oxygen entry rate), k^- (oxygen exit rate) and χ (oxygen migration rate) were obtained for each temperature, along with the activation energies associated with k^+ and k^-. The protein-to-solvent partition coefficient, α, was also obtained at each temperature along with the thermodynamic variable ΔG associated with this partition. The parameters k^+, k^-, χ, and α have also been determined for the sample in 40% sucrose, to compare the effect of viscosity on these parameters. The effect of this viscous solvent on dynamics of oxygen entry is discussed. Comparison of the Stern-Volmer plots for the raw lifetime data with the steady-state emission spectra demonstrates the existence of quenching of a "quasi static" nature. The fit of the calculated Stern-Volmer plot to the experimental data indicates that the dynamic model accurately represents the oxygen quenching process in Horse Skeletal myoglobin in all the temperature and viscosity ranges investigated. Supported by NIH GM18051 (JC); NIH RR03155 (EG); and NSF DMB9005195 (DMJ).

W-Pos106

HEMOGLOBIN OXIDATION/DENATURATION AND LIPID PEROXIDATION IN HEMOGLOBIN-LIPID VESICLE MIXTURES

((Merita Dias and L. W.-M. Fung))
Department of Chemistry, Loyola University of Chicago, Chicago, IL, 60626.

The binding of oxygen to hemoglobin (Hb) gives oxygenated Hb (oxyHb). However, oxyHb may be oxidized to generate oxygen radicals. The generation of oxygen radicals in human erythrocytes may lead to Hb denaturation and lipid peroxidation. We have studied the interaction of Hb with bovine brain phosphatidylserine unilamellar vesicles at 37 °C as a function of time. These lipid vesicles, in the absence of lipid peroxidation, promote Hb oxidation. Various molecular species (lipid vesicles, Hb and lipid-Hb complex) in the mixtures after incubation for a specific time period have been separated by column gel filtration. The apparent molecular weights of these species have been determined. The UV and visible spectra of these species provide means to distinguish between lipid and protein components and between oxidized and reduced heme components. Lipid peroxidation products have also been detected in some of the mixtures. A detailed understanding of the mechanisms of the individual chemical reaction in oxyHb-lipid mixtures should contribute to our understanding of red cell destruction and of senescent cell elimination from the circulation under both normal and pathological conditions. (Supported by NIH and American Heart Association of Metropolitan Chicago.)

W-Pos107

A NOVEL DIFFERENTIAL STOPPED-FLOW TITRATION CALORIMETER: DETECTION OF CMC AND HEMOGLOBIN-LIGAND INTERACTIONS. ((M.D. Chávez[1], N.L. Gershfeld[2], C.P. Mudd[3], and R.L. Berger[1]))
(1) Lab. of Biophys. Chem., NHLBI, NIH, Bethesda, MD 20892, U.S.A.
(2) Lab. of Phys. Biol., NIAMSD, NIH, Bethesda, MD 20892, U.S.A.
(3) Appl. Clin. Eng. Sec., BEIB, NIH, Bethesda, MD 20892, U.S.A.

The integration of two independent computer controlled injection devices into a differential stopped-flow, heat-conduction microcalorimeter allows for ratio mixing of the reagents. Experiments can now be performed over a wide range of concentrations with the same materials. Thus, reactions involving biological samples with batch dependencies can be accurately normalized and studied. The total volume for each run is 160 μl with accuracy down to ±2 μj. Assuming a 5 kcal/mol reaction, only 80 μl of a ~100 μM solution is required per run. Hence, a complete set of experiments is achieved with small scale samples. Two acid-base reactions, dilution of two micellular solutions to detect the CMC, and the titration of hemoglobin with chloride salts and oxygen have been done to illustrate the flexible applications of the instrument.

W-Pos108

MULTILINKED HUMAN HEMOGLOBIN. ((H. Huang)) Chemistry Department, Loyola University Chicago, Chicago, IL 60626.

Crosslinkers, such as bis(3,5-dibromosalicyl) fumarate, have been used to specifically modify hemoglobin in order to produce potential blood substitutes (J.A. Walder et al, 1979). Multilinkers, which react simultaneously with three or more sites on the protein's surface, have the potential for greater control over the stability and functional properties of the modified hemoglobin. The trilinker, trimesoyl tris(methyl phosphate) which reacts at β_1 82 Lys, β_1 1 Val and β_2 82 Lys (R. Kluger et al, 1990), increased thermal stability of hemoglobin by 15 °C. Another tetralinker was designed using computer graphics and molecular dynamics. It would crosslink between two β 82 and two β 1. Thus, the crosslinked hemoglobin should contain both intra- and interchain crosslinks. (Supported by a grant from the Research Corporation.)

W-Pos109

INFRARED LINEAR DICHROISM OF SINGLE CRYSTALS OF MYOGLOBIN. J.T. Sage[1], D. Ivanov[1], M. Keim[1], J.R. Powell[2], S.A. Asher[3], and P.M. Champion[1]. [1]Northeastern Univ.; [2] Bio-Rad Laboratories; [3] Univ. of Pittsburgh.

Using an IR microscope coupled to an FTIR spectrometer, we have performed linear dichroism measurements on single crystals of MbCO. This allows us to directly characterize the CO orientation in the principal conformational states A_0, A_1, and A_3. This approach contrasts with IR photoselection measurements, for which the interpretation depends on a known or assumed angular distribution of photolyzed heme sites. On the {100} and {001} faces of monoclinic crystals and the {001} face of orthorhombic crystals, the projected CO dipoles of the A_0, A_1, and A_3 bands lie within a range of 4° or less. This suggests that differing steric interactions of the ligand with the distal pocket result in minimal distortion of the Fe-CO unit. At pH5.3 and 4.8, the relative intensity of the three CO bands in monoclinic crystals is consistent with reported solution measurements. In orthorhombic crystals at pH5.6, both A_3/A_1 and A_0/A_1 intensity ratios are significantly enhanced relative to solution. However, the A_3/A_1 ratio is less than unity in all cases. Larger values of this ratio observed in previous studies of polycrystalline samples suggest that the structure of the distal pocket is sensitive to differences in sample handling.

W-Pos110

MICROSCOPIC OBSERVATIONS OF SICKLE HEMOGLOBIN (HbS) FIBER GROWTH, MELTING, NUCLEATION AND DOMAINS IN REAL TIME. ((R.W. Briehl)) Albert Einstein College of Medicine, Bronx, NY 10461.

The double nucleation model for HbS fiber kinetics (Ferrone et al, J. Mol. Biol. 183:611, 1985) derives from macroscopic data on vast numbers of fibers. Here we observe the processes of the model (homogeneous and heterogeneous nucleation and fiber elongation) directly on individual fibers in real time, and also show the mechanisms of fiber melting and domain growth by differential interference contrast (DIC) microscopy. CO HbS was photolyzed to deoxyHbS by epi-illumination; intensity was adjusted to control kinetics, and to reverse reactions. Initial nucleations were spatially random (and in different locations upon repeat after melting), often separate from any surface and showed random, diffusive, movement, all consistent with homogeneous character. Earliest observed post-nucleation structures were about 1μm long and usually roughly linear. Heterogeneous nucleation on existing fibers was much more frequent than homogeneous, produced "decorated" fibers, was highly sensitive to light intensity and ranged from total absence to branches every few microns. Free fibers grew and melted at both ends; melting did not occur by breakage. Growth and melting were reversible; rates depended (but much less strongly than nucleation) on light intensity. Early domains had two-fold symmetry that became radial. For slow fiber growth fibers in domains were radial and not cross-linked. At increased illumination, fibers cross-linked rapidly and domains filled in. Slow domain melting restored two-fold symmetry. (Supported by grant HL 07451 from NHLBI).

W-Pos111

YEAST CYTOCHROME *C* PEROXIDASE-CATALYZED OXIDATION OF YEAST ISO-1 FERROCYTOCHROME *C* BY HYDROGEN PEROXIDE: IONIC STRENGTH DEPENDENCE OF THE STEADY-STATE AND TRANSIENT-STATE RATES. ((A.L. Matthis and J.E. Erman)) Department of Chemistry, Northern Illinois University, DeKalb, IL 60115.

The cytochrome *c* peroxidase-catalyzed oxidation of yeast iso-1 ferrocytochrome *c* by hydrogen peroxide has been investigated at pH 7.5 between 10 and 200 mm ionic strength as a function of cytochrome *c* concentration by both steady-state and stopped-flow techniques. The oxidation of iso-1 ferrocytochrome *c* by cytochrome *c* peroxidase compound I has a complex concentration dependence which varies significantly with ionic strength. The rates appear to have two phases, one at lower cytochrome *c* concentrations which saturates, and a second bimolecular phase, observed at higher cytochrome *c* concentrations, which does not saturate. The saturation rate of the low concentration phase varies from 17 s^{-1} at 10 mM ionic strength to 1900 s^{-1} at 200 mM ionic strength. The reduction rate of cytochrome *c* peroxidase compound II (generated by the initial reduction of compound I in the stopped-flow studies) to the native enzyme depends upon the initial compound I concentration and is independent of both ferrocytochrome *c* concentration and ionic strength. The concentration dependence of the steady-state velocity parallels the rate of compound I reduction in the stopped-flow studies. The data can be rationalized by mechanisms involving both one- and two-cytochrome *c* binding site models for cytochrome *c* peroxidase.

W-Pos112

X-RAY CRYSTALLOGRAPHIC STRUCTURES AND BINDING SITE ANALYSES OF SPERM WHALE MYOGLOBIN N-ALKYL ISOCYANIDES ((R.D. Smith, M.L. Quillin, G.N. Phillips, Jr. and J.S. Olson)) Dept. of Biochemistry and Cell Biology, Rice University, Houston, TX 77251

X-ray crystallographic structures of sperm whale myoglobin n-alkyl isocyanide complexes have been solved as part of our ongoing efforts to elucidate the mechanisms of ligand binding to myoglobin. Previously, crystal structures of these complexes had been solved for native sperm whale myoglobin, which crystallizes in space group $P2_1$ (K.A. Johnson, et al, J. Mol. Biol. vol. 207, 459-463, 1989 and K.A. Johnson, Doctoral Dissertation, Rice University). Subsequently, it was observed that recombinant sperm whale myoglobin crystallizes at pH 9 in space group P6 and has different intermolecular contacts. In order to examine the effects of pH and intermolecular contacts on the distal pocket, we have re-examined, sperm whale myoglobin n-alkyl isocyanide crystal structures using the recombinant protein. To date, six structures at pH 9 have been solved and analyzed: native myoglobin n-butyl isocyanide in space group $P2_1$; recombinant myoglobin n-alkyl isocyanides (n=1-4) in space group P6; and mutant V68F myoglobin ethyl isocyanide in space group P6. The binding site conformations have been analyzed in terms of both ligand and side chain geometry to yield steric information about the size and flexibility of the myoglobin binding pocket under different pH and crystal packing conditions.

Supported by a Robert A. Welch Foundation Predoctoral Fellowship (RDS); a National Science Foundation Predoctoral Fellowship (MLQ); the William M. Keck Foundation and NIH AR40252 (GNP); and the Robert A. Welch Foundation and NIH GN35649 (JSO).

W-Pos113

HEME LOSS FROM MYOGLOBIN AND HEMOGLOBIN AND ITS RELATION TO PROTEIN STABILITY. ((M.S. Hargrove, M.L. Quillin, G.N. Phillips, Jr, and J.S. Olson)) Department of Biochemistry and Cell Biology, Rice University, Houston, TX 77251.

In order to develop an assay for hemin dissociation, His^{64}(E7) was replaced by Tyr in sperm whale myoglobin producing a holoprotein with a distinct green color due to an intense absorption band at 600 nm. Val^{68}(E11) was replaced by Phe in the same protein to increase its stability. When excess $Tyr^{64}Val^{68}$ apoglobin is mixed with either metmyoglobin or methemoglobin, the solution turns from brown to green, and the absorbance changes can be used to measure complete time courses for hemin dissociation from either holoprotein. This assay has been used to measure rates of hemin dissociation from native metmyoglobin, four myoglobin mutants (Ala^{64}(E7), Ala^{68}(E11), Phe^{68}(E11), and Glu^{45}(CD3)), native methemoglobin, valence hybrid hemoglobins, and two mutant hemoglobins (αGly^{64}(E7) and βGly^{64}(E7)). Two kinetic phases were observed for hemin dissociation from native human hemoglobin at pH 7.0 and 37°C. Valence and mutant hybrid hemoglobins were used to assign the faster phase ($k = 7.8 \pm 2.0\ hr^{-1}$) to hemin dissociation from ferric β subunits and the slower ($k=0.6 \pm 0.15\ hr^{-1}$) to dissociation from α subunits. The corresponding rate for wild-type metmyoglobin is $0.007 \pm 0.001\ hr^{-1}$.

A disulfide bond was incorporated into sperm whale myoglobin in an effort to create an even more stabile apoglobin. Stabilities of native myoglobin and several myoglobin mutants were measured in the holo and apoglobin forms to determine the role of heme in stabilization.

Supported by NIH GM08280 (MSH and MLQ), AR40252 (GNP), GN35649 (JSO), the Robert A. Welch Foundation, and the W.M. Keck Center for Computational Biology.

W-Pos114

DIELECTRIC ASYMMETRY IN THE PHOTOSYNTHETIC REACTION CENTER

((Martin A. Steffen, Kaiqin Lao, and Steven G. Boxer)), Department of Chemistry, Stanford University, Stanford, CA 94305-5080

The three dimensional structure of the bacterial photosynthetic reaction center (RC) reveals a high level of structural symmetry, with two nearly equivalent potential electron transfer pathways. Surprisingly, the RC is functionally asymmetric, and electron transfer occurs only along one of the two possible pathways. In order to discover factors which contribute to this symmetry breaking, the internal electric field in the RC when charge is separated (P+Q-) was probed using bandshifts of the monomeric chromophores. The sensitivity of each probe chromophore to an electric field was calibrated by measuring the Stark effect spectrum in an external electric field. The internal electric field in vacuo was calculated by using the x-ray structure of the RC and detailed information on the charge distribution on the two ions. By combining this and the Stark effect data, we calculate the predicted band shift in vacuo. A quantitative comparison of the observed shift and that predicted from vacuum electrostatics gives information on the effective dielectric constant which screens the charges on P+ and Q-. This reveals a significant asymmetry in the dielectric strength of the protein complex along the two potential electron transfer pathways, with a substantially higher dielectric strength (about 3X) along the functional pathway. This dielectric asymmetry could be a dominant factor in determining the functional asymmetry of electron transfer in the RC. An analysis of the polarity of amino acid residues around the reactive chromophores reveals a number of residues which have not previously been implicated in RC symmetry breaking.

W-Pos115

PROTEIN DYNAMICS AND THE PATHWAY OF ELECTRON TRANSFER IN PHOTOSYNTHETIC REACTION CENTERS STUDIED BY FEMTOSECOND INFRARED SPECTROSCOPY

((S. Maiti, G. C. Walker, B. R. Cowen, R. S. Pippenger, C. C. Moser, P. L. Dutton and R. M. Hochstrasser)) Department of Chemistry and Department of Biochemistry and Biophysics, University of Pennsylvania, Philadelphia, PA 19104

Protein and chromophore dynamics following near infrared excitation of the photosynthetic reaction center of Rb. sphaeroides have been investigated by ultrafast infrared (IR) spectroscopy. Changes in the infrared spectrum in the region of 1600 - 1960 cm^{-1} were measured with a 400 femtosecond time resolution. The transient IR method is ideally suited to studies of the protein relaxation induced by photoexcitation and the primary charge separation and a full study of this region explores both chromophore and amide transitions of the protein. It has been possible to measure the IR spectrum of the protein in the transient photoexcited state (P*) for the first time. Bandwidth limited risetimes of P* vibrational bands have been resolved. Transient absorption has also been measured in the region where neutral and reduced bacteriochlorophyll shows static absorption differences in model systems, in search of clear spectral evidence for the direct participation of the accessory bacteriochlorophyll in the electron transfer process.

This work was supported by grants from NIH and NSF.

W-Pos116

FTIR DIFFERENCE SPECTROSCOPY OF THE PHOTOREDUCTION OF THE INTERMEDIARY ELECTRON ACCEPTOR IN RB. SPHAEROIDES BACTERIAL REACTION CENTER

E. Nabedryk, J. Breton
SBE/DBCM, C.E.N. Saclay, 91191 Gif-sur-Yvette Cedex, France

The photoreduction of the bacteriopheophytin *a* intermediary electron acceptor H_L in *Rb. sphaeroides* reaction center (RC) has been monitored by light-induced FTIR difference spectroscopy at 10°C. The H_L^-/H_L spectrum is very comparable to that obtained for *Rps. viridis* RC (1), reflecting similar interactions of H_L with the protein in both RCs. It shows negative signals at 1745, 1733, 1688, 1677 and 1655 cm^{-1}, a main positive signal at 1591 cm^{-1} as well as small positive bands at 1465 and 1372 cm^{-1}. The redox-induced FTIR difference spectrum of the bacteriopheophytin *a* anion in THF (2) shows only two negative signals at 1743 and 1703 cm^{-1} attributed to changes of absorption of the 10a ester and 9-keto carbonyls, respectively. In the H_L^-/H_L spectrum of *Rb. sphaeroides* RC, two peaks at 1688 or 1677 cm^{-1} are candidates for the 9-keto C=O of H_L, corresponding to a hydrogen bonding interaction with the protein. For both *Rps. viridis* and *Rb. sphaeroides* RCs, X-ray crystallography has provided evidence for Glu L104 interacting with the 9-keto C=O of H_L. As previously described in *Rps. viridis* (1), the band at 1733 cm^{-1} in the H_L^-/H_L spectrum of *Rb. sphaeroides* RC is interpreted in terms of the 10a ester C=O of H_L hydrogen bonded to the side chain of Trp L100. The 1745 cm^{-1} band could arise from the contribution of the side chain of Glu L104.

(1)Nabedryk et al., (1988) in "The Photosynthetic Bacterial Reaction Center" Vol. 149, p.237 (Plenum) (2) Mäntele et al., (1987) in "Progress in Photosynthesis Research" Vol.I , p.329 (Martinus Nijhoff)

W-Pos117

KINETICS AND FREE ENERGY GAPS OF ELECTRON TRANSFER REACTIONS IN *RHODOBACTER SPHAEROIDES* REACTION CENTERS*.

((V. Nagarajan, W. Parson, D. Davis and C. Schenck)), Depts. Biochem., Univ. Washington and Colorado State Univ.

The rates of light-driven electron transfer reactions in the bacterial reaction center (RC) are examined in mutant strains in which Tyr (M)210 is replaced by Phe, Ile and Trp. The spectra of absorbance changes between 700 and 975 nm, following excitation by 0.6 ps pulses at 605 nm, are analyzed globally by singular value decomposition, and various kinetic models are evaluated. The first electron transfer step speeds up with decreasing temperature in wild-type RCs, remains unchanged in the Phe mutant, and slows down in the Ile and Trp mutants. In the Ile and Trp mutants at 80 K, the signals in the 850 to 975 nm region include an apparent shift of the stimulated emission or absorption spectrum of P*. Most of the electron transfer to the photoactive bacteriopheophytin (H_L) probably occurs from the relaxed form of P*.

The midpoint potential (E_m) of the P/P+ redox couple is measured by an electrochemical technique, and the free energy change (ΔG) associated with the formation of the $P+H_L^-$ radical pair from P* is also determined by measuring the amplitude of the fluorescence on the ns-time scale after blocking forward electron transfer from H_L. The free energy of $P+H_L^-$ is elevated by an amount comparable to that calculated from the increase in the E_m of P in the Ile mutant, and by 16 meV more than this in the Phe and Trp mutants.

Nonadiabatic electron transfer theory is used to relate the rate constant of the formation of $P+H_L^-$ to ΔG. The altered temperature-dependence of the reaction in the mutants cannot be explained adequately on the assumption that the mutations only alter the overall ΔG, but it can be accounted for by assuming that the mutations also increase the free energy of an additional state ($P+B_L^-$) that serves as both a kinetic and virtual intermediate. The requisite increases in the free energy of $P+B_L^-$ are greater than the measured changes in the free energy of $P+H_L^-$.

*Support by NIH and NSF.

W-Pos118

CALCULATION OF ELECTRON TRANSFER PROPERTIES OF RUBREDOXIN VIA MOLECULAR DYNAMICS SIMULATIONS.

((R. B. Yelle and T. Ichiye)) Department of Biochemistry/Biophysics, Washington State University, Pullman, WA 99164-4660.

Molecular dynamics simulations have been carried out on the iron-sulfur protein rubredoxin from *Clostridium pasteurianum*, in both its oxidized and reduced forms. The simulations were done using explicit water molecules and counterions. Both simulations are in good agreement with the crystal structure, the average structures of the protein having root mean square deviations of 1.25 Å and 1.79 Å respectively, from the crystal structure. The electrostatic potential at the redox site was calculated for the different types of polar and charged groups (solvent, counterions, protein backbone and sidechains). The results show that there is a substantial increase in the electrostatic potential upon reduction, mostly due to the increased solvation at the redox site. The structural changes contributing to this increase will be described. In addition, the activation free energy for the self-transfer reaction

$$Rd^{2-} + Rd^{*1-} \dashrightarrow Rd^{1-} + Rd^{*2-},$$

which was calculated using Marcus theory and probability theory, will be discussed.

W-Pos119

STABILITY OF PLASTOCYANIN TO ACID pH.

((E.L. Gross, B. Pan, B. Li, and Brown, L.)) Dept. of Biochemistry and the Biophysics Program, The Ohio State University, Columbus, OH, 43210

Plastocyanin (PC) is a 10 kD "blue" copper protein which functions as an electron carrier in photosynthesis shuttling electrons from cytochrome f to P700 in Photosystem I. It is located in the lumen of the thylakoid where it experiences pH values $\leq$ 5 upon illumination of the thylakoid.

The retention of the blue copper center was determined as a function of time at different pH values. For oxidized parsley PC, the copper center was stable for at least 48 hours above pH 5.2. The amount of native PC remaining at equilibrium decreased at lower pH with a highly cooperative transition centered at pH 5.0. Reduced PC is more stable than the oxidized form. The amount of native PC remaining at equilibrium at pH 4.5 was 62% for reduced PC compared to 0% for the oxidized form. Inverse rate constants for denaturation (1/k) at pH 4.5 were 8.5 and 9 hours for reduced and oxidized PC, respectively.

The rate of reoxidization of reduced PC is slowed at low pH due to protonation of the His 87 ligand to the copper (pK = 5.7 for parsley) (Sinclair-Day et al. J. Chem. Soc. Chem. Commun. 1985:505-507 (1985)). As a consequence, PC will be predominantly in the more stable reduced form under these conditins which serves to stabilize the PC molecule in the lumen of the thylakoid.

W-Pos120

LIGAND BINDING IN BLUE COPPER PROTEINS. ((D. Ehrenstein, M. Engelhard†, M. Filiaci, B. McMahon, G.U. Nienhaus, and B. Scharf†)) Physics Dept., Univ. of Illinois, Urbana, IL 61801 and †Max-Planck-Institut für Ernährungsphysiologie, Rheinlanddamm 201, 4600 Dortmund, GERMANY.

Azurin (Az) and halocyanin (Ha) are blue copper proteins that can serve as model systems for studying the binding of small ligands to proteins and confirming the generality of protein dynamics principles learned from heme-protein experiments. Although their physiological function is electron transfer, they form photodissociable complexes with nitric oxide (NO) at low temperatures and thus are rare examples of non-heme protein-ligand systems that can be studied with flash-photolysis. We have previously shown that the rebinding kinetics of NO to Az following photolysis are surprisingly similar to the well-known heme-protein data; here we show that HaNO is somewhat different. The low- and high- temperature Ha rebinding data agree well with Az and most heme-proteins, but at intermediate temperatures (90 – 190 K) there is an unusual power law process, with almost constant slope over this entire temperature range. This suggests a rebinding model other than a simple activated, enthalpy-limited process is necessary.

W-Pos121

MULTIEXPONENTIAL FLUORESCENCE DECAY OF HOLOAZURIN IN THE CRYSTALLINE STATE: Further Evidence for Tryptophan Conformational Heterogeneity ((A.G. Szabo[1], X. Lee[2] and T.E.S. Dahms[1,3])) [1]Institute for Biological Sciences, National Research Council, Ottawa, Ont., Canada, K1A 0R6. [2]Department of Cancer Biology, Cleveland Clinic Foundation Research Institute, Cleveland, Ohio, USA 44195 [3]University of Ottawa (Spon. J.D. Brennan)

Pseudomonas fluorescence (Pfl) holoazurin is a blue copper-containing protein which contains a single tryptophan (Trp) residue. The *Ps. aeruginosa* and *Pfl* holoazurins have been studied extensively by several groups using time-resolved fluorescence spectroscopy. Multiexponential decay kinetics of Trp-48 in these holoazurins was rationalized in terms of conformational heterogeneity in the protein (Szabo *et al.*, 1983). This view has not been totally accepted despite the case presented by Hutnik and Szabo (1989) showing that the long decay time was not due to an apoprotein contaminant.

The sequence of *Pfl.* holoazurin has recently been determined (Lanthier and Yaguchi, unpublished results) and the mass of the HPLC purified material was confirmed by electro-spray ionization mass spectrometry. Holoazurin crystals of X-ray diffraction quality (0.6mm x 0.6 mm) have facilitated structure determination to 2.05 Å resolution (Lee *et al.*, unpublished results).

The fluorescence of the HPLC purified material is best described by three decay times both in solution and in the crystalline state with each decay-associated spectra dominated by the shortest decay component. Their relative contributions show significant variation with change in orientation of the protein crystal with respect to the vertically polarized laser beam. This confirms that Trp-48 *of Pfl.* holoazurin is conformationally heterogeneous in solution and in the crystalline state. These results obtained from highly purified holoazurin confirm earlier work from this laboratory, clearly showing that the long decay component must originate from a Trp conformation in which the residue is remote from the Cu^{2+} ligand site.

W-Pos122

THE CRYSTAL STRUCTURE OF HOLOAZURIN FROM *PSEUDOMONAS FLUORESCENS* AT 2.05 Å RESOLUTION ((X. Lee[1], T.E.S. Dahms[2,3], D.W. Zhu[4], P. Lanthier[2], M. Yaguchi[2] and A.G. Szabo[2,3])) [1]Department of Cancer Biology, Cleveland Clinic Foundation Research Institute, Cleveland, Ohio, USA 44195 [2]Institute for Biological Sciences, National Research Council, Ottawa, Ont., Canada, K1A 0R6. [3]University of Ottawa [4]McGill University (Spon. C.M.L. Hutnik)

The azurins comprise a homologous class of blue copper-containing proteins which function as redox partners in bacterial electron transfer. The holoazurin of *Pseudomonas fluorescens (Pfl.)* has recently been crystallized, producing X-ray diffraction quality crystals (Lee *et al.*, in press). The unit cell parameters are: a = 31.95 Å, b = 43.78 Å and c = 78.81 Å. The space group is $P2_12_12_1$ with one molecule in the asymmetric unit. The entire amino acid sequence of *Pfl.* holoazurin has been determined and the calculated mass was confirmed by electro-spray ionization mass spectrometry (Lanthier and Yaguchi, unpublished results).

The structure has been solved to 2.05 Å resolution by molecular replacement using the atomic coordinates of the *Alcaligenes denitrificans* holoazurin structure (Baker, 1988). The R-factor is 22.5 using the data from 8.0-2.05 Å without the water molecules modelled into the structure. The structure consists of eight beta strands and one alpha helix which is similar to the other homologous azurin structures. The Cu^{2+} ion is in the centre of a plane formed by ND1 of His-46, ND1 of His-117 and SG of Cys-112. The SD of Met-121 and the carbonyl oxygen of Gly-45 form axial ligands on either side of the plane. This ligand conformation is more bipyramidal than distorted tetrahedral. The structure of *Pfl.* holoazurin will be compared to the structure of the other homologous azurins from the Brookhaven Protein Data Bank.

W-Pos123

EPR OF REDUCED PHTHALATE DIOXYGENASE REDUCTASE ((L.Wang, D. Gatti, D. Ballou, W.R. Dunham* and R.H. Sands*)) Biol.Chem. and Biophys. Res. Div.*, U. of Mich., Ann Arbor, MI 48109-1055

The Phthalate Dioxygenase system is one of a group of systems that carry out the dihydroxylation of unactivated aromatic compounds to give *cis*-dihydrodiols of benzenoid compounds. Phthalate Dioxygenase Reductase (PDR) contains one FMN and one plant-type [2Fe-2S] center and belongs to the family of electron transferases called the FNR family. The systems couple the normal 2-electron carriers [NAD(P)H, $FMNH_2$, quinones] to the 1-electron iron-containing proteins in respiratory and other systems. X-ray(2Å) crystallographic results on PDR show the flavin and [2Fe-2S] sites within 5 Å to each other, similar to Trimethylamine Dehydrogenase (TMADH) previously studied. With the two moities (FMN and [2Fe-2S]) PDR can accept up to three electrons. The isolated 1-electron reduced flavin group shows a g=2 semiquinone signal 1.9 mT wide. The 1-electron reduced [2Fe-2S] center displays a g=1.94 EPR signal below 90 K. The EPR of the spin-coupled combination will be discussed as well as the quantitative relationships with the optical data. The EPR of a $3e^-$-reduced single crystal of PDR (space group:R3) records three resonances for every crystal orientation. The linewidths of these signals reflect "g-strain" similar to that from the frozen aqueous solutions. Attempts to place the G-tensor on the x-ray crystal structure will be demonstrated.

This work was supported by NIH GM20877 and NIGMS J.A. Shannon Award

W-Pos124

THE SOLUTION STRUCTURE OF PUTIDAREDOXIN FROM ^1H AND ^{15}N NMR

((Teresa Lyons and Thomas Pochapsky)) Brandeis University, Departments of Chemistry and Biology, Waltham, MA 02254-9110. (Sponsored by John Lisman)

Putidaredoxin (Pdx) is a 106-amino acid Fe_2S_2 electron transport protein originally isolated from *Pseudomonas putida*. It transfers two electrons in discrete steps to cytochrome $P\text{-}450_{cam}$, which in turn reduces camphor to 5-*exo*-hydroxycamphor in the first step of camphor metabolism. The structure of $P\text{-}450_{cam}$ is known, so the structure of Pdx, as $P\text{-}450_{cam}$'s electron transfer partner, is of interest. Pdx has not been crystallized to date. The *camB* gene which encodes Pdx has been cloned (Koga et al., *J. Biochem.* **106**, 831, 1989). We placed the *camB* gene under a *T7* promoter on a plasmid and transformed it into an *E. coli* strain that contains the gene for T7 RNA polymerase under a *lacUV5* promoter, making Pdx expression indirectly IPTG-inducable. We have determined the secondary and tertiary structure of Pdx using 2D and 3D homo- and heteronuclear NMR techniques (Ye and Pochapsky, *Biochemistry* **31**, 1961, 1992). Assignments of all detectable ^1H resonances have been made. ^{15}N assignments have recently been made from 3D ^1H-^{15}N NOESY-HMQC and TOCSY-HMQC spectra. We present a model for the solution structure of Pdx based on ^1H-^1H nOes, chi angles from ^1H coupling constants, Fe-S cluster ligand geometry modelled from known ferredoxin structures, and molecular dynamics.

W-Pos125

REDUCTIVE QUENCHING OF RUTHENIUM(II) POLYPYRIDINE COMPLEXES COVALENTLY LINKED TO METALLOPROTEINS. ((D. H. Heacock II, B. Durham and F. S. Millett)) Department of Chemistry/Biochemistry, University of Arkansas, Fayetteville, AR 72701.

Intra-complex electron transfer reactions rely on the presence of sacrificial redox reagents to facilitate unidirectional electron flow through the protein systems under study. In the past, EDTA has been used successfully as an electron donor in studies of this type. However, the presence of a net -3 charge at pH 7 on EDTA makes it unsuitable for studies requiring extremely low salt solutions (I < 0.1 M). Several small organic molecules with neutral or -1 charges have been identified that act as highly efficient sacrificial electron donors to ruthenium polypyridine labeled cytochrome c. Selection criteria are presented for identification of potential sacrificial redox reagents in other systems. Intramolecular electron transfer by a reductive quenching mechanism is followed spectroscopically at wavelengths specific for Ru(I) and Fe(II). Rate constants of 2.6×10^5 s^{-1}, 3.5×10^5 s^{-1}, 5.9×10^5 s^{-1} and 1.0×10^6 s^{-1} have been determined for derivatives of cytochrome c labeled at lysines 86, 87, 8 and 7, respectively.

This work supported by NIH Grants GM20488 and RR07101.

W-Pos126

COMPARISON OF OXIDIZED AND REDUCED PLASTOCYANIN IN PHOTOINITIATED ELECTRON TRANSFER FROM RUTHENIUM DERIVATIVES OF CYTOCHROME C.
((M. Harris, R. Gales, B. Durham, and D. Davis)) Dept. of Chemistry and Biochemistry, Univ. of Arkansas, Fayetteville, AR 72701

Plastocyanin (PC), is a type I copper protein that accepts electrons from cytochrome f (cyt f), in the photosynthetic chain. Until recently cyt f was not well characterized so cytochrome c (cyt c), was chosen to replace cyt f to study the electron transfer properties of PC. PC is known to interact with Ru(dcbpy)(bpy)$_2$ derivatives of horse heart cyt c in a 1:1 electrostatic complex. The Ru-label is covalently linked to various lysine residues and allows the photoinduced intracomplex electron transfer rates and association constants to be determined. Analysis of temperature dependent studies have allowed the calculation of activation parameters for this system. PC is easily reduced, so native, oxidized PC has been replaced by reduced PC, and it has been shown that intracomplex electron transfer can still occur. Interestingly, the electron transfer rate decreases with increasing concentrations of reduced PC, while with increasing concentrations of oxidized PC, the rate increases. Although the steady state form of PC in the lumen of the thylakoid membrane is not known, studies of reduced PC will give insight into its function in electron transfer.

W-Pos127

ELECTRON SPIN ECHO MODULATION AS A PROBE OF INTRAMOLECULAR CHARGE DISTRIBUTION CHANGES IN AZURIN.
((C.J. Bender, M. van de Kamp, G.W. Canters, J. Peisach)) Einstein College of Medicine, Bronx, NY 10461 and Leiden University, 2300 RA Leiden.

The relative magnitude of superhyperfine terms attributed to the non-coordinated nitrogen of ligand histidines to the Type I copper of azurin sets a condition whereby the spectrum of the electron spin echo modulation resolves pure quadrupole transitions. Quadrupole spectra reflect the valence shell orbital occupancy and local electric field, therefore the ^{14}N quadrupole spectrum of the non-coordinating ligand histidine nitrogen can be used as a probe of intramolecular charge at the copper site. Spin echo detected spectra of azurin and mutants M44K and M121Q resolve subtle differences in superhyperfine parameters from remote and local changes in the amino acid residues affecting the copper site. Our results indicate that quadrupole parameters e^2Qq and η differ among the forms of the protein: w.t. parameters of 1.60 MHz and 1.0 (e^2Qq and η), shift to 1.54 MHz and 0.78 (M44K, remote mutation) and 1.44 MHz and 1.02 (M121Q, mutation of weak ligand to Cu). These, plus small shifts in the effective isotropic hyperfine coupling constant of the remote nitrogen suggest that the mutations do influence the charge distribution at the metal binding site and that electron spin echo spectroscopy may be used as an analytical method to probe these small changes.

W-Pos128

PROTEIN:PORPHYRIN INTERACTIONS AND ELECTRON TRANSFER ACTIVITY OF ANIONIC PORPHYRIN:MYOGLOBIN COMPLEXES.
((R. W. Larsen and D. H. Omdal)) Dept. of Chemistry, Univ. of Hawaii at Manoa, Honolulu HI, 96822.

Intercomplex electron transfer (ET) reactions in biological systems play a critical role in bioenergetic process in all known organisms. The rates of intermolecular ET reactions are modulated by thermodynamic driving force, inner- and outer-sphere reorganizational energy, donor:acceptor orientation, and the nature of the intervening medium. In addition, conformational factors which influence protein:protein binding and recognition contribute to "gating" of ET in protein:protein complexes. In order to better understand intermolecular ET reactions we have investigated a series of model system designed to mimic intermolecular ET in proteins. One such system consists of anionic porphyrins electrostatically complexed to the surface of various proteins which contain rings of positively charged amino-acids with the same dimensions as the porphyrin charge ring. The model system to be presented is that of 4-carboxyphenyl porphyrin electrostatically bound to the surface of horse heart metMb. Equilibrium spectral characterization indicates significant electronic perturbations localized on the porphyrin. This systems also displays photo-induced ET activity with a forward rate (i.e, porphyrin to protein) >10^4 s^{-1} and a back rate (protein to porphyrin cation radical) of ~150 s^{-1}. These results will be discussed in the context of current ET mechanisms.

FLUORESCENCE MICROSCOPY

W-Pos129

ANALYSIS OF THE TRUE 3-DIMENSIONAL POINT SPREAD FUNCTION AND ITS EFFECTS ON QUANTITATIVE FLUORESCENCE MICROSCOPY
P.K. Gasbjerg, A. Horowitz, R.A. Tuft, W.A. Carrington, F.S. Fay, and K.E. Fogarty.* Biomedical Imaging Group, UMASS Medical Center., Worcester Ma., and *Rosenthal Ctr., Brandeis U., Waltam Ma.

The achievable infocus point spread functions (PSFs) of objective lenses used in high resolution fluorescence microscopy, as well as other contrast modes, are usually specified under ideal conditions and at the coverslip when applicable. Variations of the actual 3-D PSF from the theoretical arise when focussing into media (the specimen and its environment) different from the ideal, and result in loss of resolution. These losses affect measurements obtained from confocal and deconvolved optical sections of molecular distributions inside fixed and living cells. We examined the 3-D PSF in common specimen environments, PBS(H_2O) and DABCO(90% glycerol), produced with oil, glycerine and water immersion optics. We quantified degradations in lateral and axial resolution as well as estimates of size and intensity of known objects, before and after deconvolution. Use of high numerical aperture (NA 1.4) oil-immersion optics results in axial resolution loss of nearly 40% when focussed 10 microns into an aqueous medium, such as PBS. Intracellular PSFs measured inside living macrophages that ingested fluorescently-labeled microspheres were were similar to equivalent extracellular PSFs, but exhibited disturbances that were in some cases severe. The results indicate the advantage of optimizing imaging conditions based on criteria other than lateral resolution, and suggest deconvolution-based approaches to further optimize quantization.

W-Pos130

Single Particle Tracking in Three Dimensions Using an Epifluorescence Microscope Modified with Astigmatic Optics
((H. Pin Kao)) Cardiovascular Research Institute, University of California, San Francisco, CA, 94143.

Previous single particle tracking studies reported the measurement of particle trajectories in two dimensions. We present a novel optical technique for tracking the three dimensional position of a single fluorescent particle using a modified epifluorescence microscope and a cooled CCD camera for image collection. A weak cylindrical lens (focal length ~ 5 m) was introduced into the detection path of an epifluorescence microscope to confer asymmetry to the apparent objective point spread function. When viewed through this modified microscope, a fluorescent particle appears circular in focus but ellipsoidal both above and below focus. However, the major axis of the ellipsoid shifts by 90° in going through focus. The axial position of the particle is determined by the image shape; the lateral position is determined from the position of the image on the CCD array. Three dimensional tracking is achieved by applying image processing to a temporal series of images. Our system resolves the position of a particle to ± 50 nm along the optical axis and to ± 15 nm laterally at a rate of 3-4 Hz. This technique was used to measure the diffusion coefficient of a 264 nm diameter rhodamine-labelled latex bead in free solution and in a glass matrix. In a ~ 60 cP solution, the mean square distance travelled by the particle was linear with time to 10 s (1566 data points measured over 7.5 min). The measured diffusion coefficient was 0.170 ± 0.03 $\mu m^2/s$ SD, in close agreement to the theoretically predicted value of 0.163 $\mu m^2/s$. In a 60 cP solution in a glass matrix (pore size: 0.7 μm), the diffusion coefficient was reduced by 10-40 %. Three dimensional random walks were computer simulated to identify sources of experimental error. The approach for three dimensional single particle tracking developed here can be applied to the analysis of directed and diffusive motions of fluorescent or absorbing particles in cells.

W-Pos131

SATURATION EFFECTS IN POLARIZED FLUORESCENCE PHOTOBLEACHING RECOVERY AND STEADY STATE FLUORESCENCE POLARIZATION. ((E.H. Hellen and T.P. Burghardt)) Dept. of Biochemistry, Mayo Foundation, Rochester, MN 55905

The time resolved anisotropy produced in polarized fluorescence photobleaching recovery experiments has been successfully used to measure rotational correlation times in a variety of biological systems, however the magnitudes of the reported initial anisotropies have been much lower than the theoretically predicted maximum values. This small time zero anisotropy has been attributed to fluorophore motion, wobble and rotation, during the photobleaching pulse. We demonstrate that inclusion of the possibility of saturation of the fluorophore's transition from its ground state to its excited state during the photobleaching pulse leads to the prediction of reduced time zero anisotropy. This eliminates the need to rely solely on the assumption of fluorophore motion during the photobleaching pulse as the cause of the reduced initial anisotropy. We present theoretical and experimental results which show that the initial anisotropy decreases as both the bleach intensity is increased and bleach length decreased so as to keep the total integrated bleach constant. We also show theoretical and experimental results demonstrating that at high excitation intensity the effects of saturation cause the steady state fluorescence polarization to decrease. We estimate that saturation may occur using common photobleaching conditions. Supported by NIH (R01 AR 39288), AHA (GIA 930 06610), and the Mayo Foundation.

W-Pos132

ENDOSOMAL LOCALIZATION OF FLUORESCENT INDICATORS: VACUOLAR SEQUESTRATION OF --AM DYES IN *NEUROSPORA* AND IN CULTURED MAMMALIAN FIBROBLASTS. ((Clifford L. Slayman, Vasiliana V. Moussatos, and Watt W. Webb*)) Department of Cellular and Molecular Physiology, Yale University, New Haven CT, and *School of Applied and Engineering Physics / Biotechnology Resource, Cornell University, Ithaca NY.

The current burgeoning use of fluorescent-probe dyes to monitor intracellular concentrations of inorganic ions prompted us to test bis-(carboxyethyl)-carboxyfluorescein (BCECF), in its permeant acetoxymethylester (-AM) form, to measure cytosolic pH in *Neurospora*. Dye was taken up rapidly, appearing serially in the cell wall, in the cytosol, and finally (after 20-40 min) accumulating in the vacuoles. The punctate distribution of dye in the steady state was systematically enhanced by maneuvers which increase vacuolation. A less highly esterified dye, SNARF-AM (seminaphthorhodafluor) localized in the cytoplasm, but washed out within seconds after removal of extracellular dye. Its more heavily carboxylated derivative, SNARF-calcein(-AM) behaved like BCECF(-AM). Parallel experiments on cultured mammalian fibroblasts which had been modified to have large endosomes (NIH-3T3 cells transfected with the gene for *Neurospora* H^+-ATPase) also showed conspicuously punctate distribution of BCECF, loaded from the -AM derivative.

The most likely cause for vacuolar trapping of -AM dyes is normal localization of the relevant esterases within the vacuoles, at least in fungi. If similar conditions exist for the *submicroscopic* endosomes of most animal cells, then estimates of cytosolic pH made via -AM dyes can be seriously compromised--perhaps even dominated--by *intraorganellar* spaces. Thus, the lipophilic acetoxymethylester derivatives of ion indicator dyes may very well be Trojan horses for the measurement of intracellular ion concentrations and distributions.

W-Pos133

QUENCHING OF CYTOPLASMIC (MAG-)FURA-2 BY MN^{2+} REVEALS INTRACELLULAR STORES OF INTACT FROG NEURONS. ((A.I. Bustamante, M.G. Klein, M.F. Schneider)) Dept. of Biological Chemistry, Univ. of Maryland, Baltimore, MD 21201

Neurons were isolated from frog sympathetic ganglia (*R. pipiens*) by enzyme dissociation and plated on polylysine-coated coverslips as described by Friel and Tsien (J. Physiol. 450:217, 1992). Intracellular calcium ($[Ca^{2+}]$) was monitored by loading the cells with fura-2 or mag-fura-2 (as the acetoxymethyl esters) and measuring the fluorescence at excitation wavelengths of 380 nm and the isosbestic point (358 for fura-2, 350 for mag-fura-2). In agreement with Friel and Tsien, Ringer solution containing 2 mM Ca^{2+} and elevated K^+ (50 mM) could be used to load intracellular stores with Ca^{2+}, and caffeine (10 mM) was able to release Ca^{2+} from intracellular stores, apparently by Ca^{2+}-induced calcium release. In cells heavily loaded with fura-2 or mag-fura-2, extracellular K^+ (100 mM) plus 10 mM Mn^{2+} (and no Ca^{2+}) allowed Mn^{2+} entry via surface membrane Ca channels, and resulted in the quenching of 61 ± 3 % (sem, n = 9) of the cell fluorescence (isosbestic excitation). Using mag-fura-2 in a cell whose stores were loaded by elevated K^+ the % saturation was 14 % before exposure to Mn^{2+}, and 54 % after Mn^{2+}. We are evaluating this technique as a method to selectively quench cytosolic indicator and thus provide a measure the $[Ca^{2+}]$ within intracellular stores of intact neurons.

W-Pos134

Ca^{2+} SUB-COMPARTMENTALIZATION IN CILIATED CELLS. ((T. Nguyen, A Escobar*, J Vergara* y P. Verdugo.)) Ctr. for Bioengineering, University of Washington WD-12, Seattle WA, and Dept. of Physilogy, UCLA.

The precise intracellular localization of changes of fluorescence reported by estirified (permeant) Ca-sensitive probes requires the implementation of optical sections of a thickness equivalent to the size of the cellular sub-compartments where changes of $[Ca^{+2}]$ic are investigated. Otherwise, the fluorescence signals result not only from the focal plane but also from cellular sub-compartments across the whole cone of aperture of the objective lens. Although this problem has been largely ignored by assuming that $[Ca^{+2}]$ic changes take place only in the cytosolic compartment of the cell, there is a potential for a strong artifact in data collected by fluorescence microscopy or by standard fluorimetric methods.

While confocal microscopy can readily avoid out of focus emission, it has severe limitations due to its inherently slow sampling rate which hinders its application in cells where $[Ca^{+2}]$ic undergoes quick changes. The method developed at the Fernandez laboratory (JCB 116:745,1992) allows to discriminate between fluorescence emitted within and outside the depth of field of the objective. Thus, by selecting an objective of high numerical apperture (1.3-1.4) and shallow depth of field (130-160 nm), it is possible to resolve the dynamics of fluorescence at the level of sub-cellular compartments.

This work reports the initial validation of a low-cost system for quick capture and processing of optically sectioned fluorescent images, and its preliminary application to investigate the sub-compartmentalization of intracellular $[Ca^{+2}]$ic in cultured epitheliary ciliated cells of the rabbit trachea. Our results, using double labeling with Rhod-2 AM and $DiOC_6$, suggest that inside the ER and mitochondrial sub-compartments of ciliated cells $[Ca^{+2}]$ic must be at micromolar concentrations. Following 100 µM ATP stimulation, $[Ca^{+2}]$ic inside these sub-compartments undergoes transient increases and oscillations much larger than those detected by Rhod-2 in the cytosol. Supported by NASA NAG-9-604

W-Pos135

FLUORESCENCE LIFETIME IMAGING MICROSCOPY (FLIM). CALCIUM IMAGING IN LIVING CELLS USING QUIN-2. ((H. Szmacinski, J.R. Lakowicz, W.J. Lederer, K. Nowaczyk and M.L. Johnson*)) Univ of Maryland, Sch of Medicine, Center for Fluorescence Spectroscopy, Dept of Biological Chemistry, 108 N. Greene St, Baltimore, MD 21201; *Univ of Virginia, Dept of Pharmacology, Charlottesville, VA 22908. (Sponsored by M.L. Johnson)

We describe our fluorescence lifetime imaging microscopy (FLIM) apparatus which consists of a fluorescence microscopy, high-speed gated MCP image intensifier, and slow-scan CCD camera. To accomplish sub-nanosecond time-resolved imaging, the gain of the image intensifier is modulated with a high frequency signal synchronized to the intensity-modulated excitation. This procedure results in a stationary phase-sensitive intensity image on the output screen of the image intensifier, which is recorded using a cooled slow-scan CCD camera and stored in an image processor. The cellular lifetime images are created from a series of phase-sensitive images at various phase shifts of the gain-modulation signal.

We demonstrate calcium concentration imaging in living COS cells based on Ca^{2+}-induced lifetime changes of quin-2. We create two-dimensional phase angle and modulation images of quin-2 fluorescence in response to intensity-modulated excitation light with a frequency of 49.53 MHz. The phase angle image is mapped to the Ca^{2+} concentration image using an *in vitro*-determined calibration curve. The Ca^{2+} concentration was found to be uniform throughout the cell. In contrast, the intensity image shows significant spatial differences which likely reflects variations in thickness and distribution of the probe within the cell.

W-Pos136

HIGH RESOLUTION DIRECT 3-D FLUORESCENCE MICROSCOPY OF CELLS AND ORGANELLES BY STANDING-WAVE EXCITATION-BASED OPTICAL SUBSECTIONING ((B. Bailey, F. Lanni, D.L. Farkas, D.L. Taylor)) Center for Light Microscope Imaging and Biotechnology, & Departments of Biological Sciences and Physics, Carnegie Mellon University, 4400 Fifth Avenue, Pittsburgh, PA 15213.

We previously demonstrated[1] standing-wave fluorescence microscopy (SWFM) to greatly enhance axial resolution in thin biological specimens by selectively exciting planes within the depth of field. We have expanded the technique to include thicker specimens which require multiple focal plane data sets. For each focal plane, three linearly independent images (a conventional fluorescence image, and two SWFM images with a 90 degree relative phase shift) are acquired. Inspection of the data shows enhanced axial resolution similar to what is observed in thin specimens, limited mainly by refractive index heterogeneity. Processing algorithms for these datasets are under development. A wide variety of biological specimens, including yeast, platelets, leukocytes, fish keratocytes and Swiss 3T3 cells, and their organelles, are currently being investigated with this approach.

[1]B. Bailey, D.L. Farkas, D.L. Taylor and F. Lanni, **Nature** (1993), in press. Work supported by NSF grants BIR- 8920118, 9217217 and 9256343.

W-Pos137

IMAGING OF PHOSPHOLIPASE A2 ACTIVITY IN RBL CELLS USING TWO-PHOTON EXCITED FLUORESCENCE MICROSCOPY. ((Rebecca M. Williams, David R. Sandison and Watt W. Webb*)) Depts. of Physics and *Applied & Eng. Physics, Cornell University, Ithaca, NY 14853.

Unsaturated fatty acid products from phospholipase A2 (PLA2) hydrolysis of membrane phospholipids are hypothesized to be essential components of a wide variety of membrane fusion events. We measure PLA2 product formation in secreting cells using two-photon excited fluorescence laser scanning microscopy, a technique which possesses the non-obtrusive, three-dimensional resolution and sectioning capabilities necessary for differentiating between various membranous regions within a cell. To assay PLA2 activity, we use a UV absorbing bis pyrenylbutanoyl phosphatidylcholine probe which undergoes a fluorescence emission shift upon PLA2 hydrolysis. We trigger secretion in substrate loaded RBL cells (mucosal mast cell line) while scanning them with an 82 MHz train of 100 femtosecond pulsed red light. Fluorescence is detected simultaneously at the two wavelengths corresponding to the excimer and monomer peaks of pyrene. With appropriate substrate concentrations, ratioed pixel values are independent of average fluorophore densities. Images reveal a three-dimensionally resolved cellular distribution of increasing PLA2 product formation. Such studies will be particularly applicable to systems exhibiting a directed secretion.

Supported by grants to the developmental Resource for Biophysical Imaging and Opto-Electronics funded by NSF (DIR8800278), NIH (RR04224) and NIH (R07719).

W-Pos138

A TWO-PHOTON CONFOCAL LIFETIME MICROSCOPE. ((P. T. C. So, Chen Y. Dong, Keith Berland, Todd French and E. Gratton)) Laboratory for Fluorescence Dynamics, Dept. of Physics, Univ. of Illinois at Urbana-Champaign, Urbana, IL 61801.

The combination of two-photon confocal microscopy and lifetime imaging have been shown to be a very promising technique for investigating cellular structures (Piston et. al., *SPIE 1640*, 1992). We have developed a frequency-domain two-photon confocal lifetime microscope utilizing a Ti-Sapphire laser. The high peak power, femtosecond pulses of the laser ensures efficient two-photon excitation. Since the Ti-Sapphire laser is a passive mode-lock system, a simple circuit has been developed to phase-lock the laser to other heterodyne frequency domain apparatus. This microscope has spatial resolution of 0.8 um radially and 2 um axially, which are limited by the diffraction limit of light. The maximum modulation frequency of this microscope is about 1 GHz, which corresponds to a time resolution of about 50 psec. The successful incorporation of the lifetime capability in microscopy also makes other standard spectroscopic techniques such as anisotropy decay and energy transfer measurements possible. Preliminary tests of this powerful instrument in cellular systems, such as drosophila embryos and mouse fibroblast cells, are in progress.

Supported by the National Institutes of Health grant RR03155 and by the University of Illinois at Urbana-Champaign.

W-Pos139

CELLULAR DIFFUSION STUDIES WITH TWO-PHOTON FLUCTUATION CORRELATION SPECTROSCOPY. ((K. Berland, P.T.C. So, C. Dong, and E. Gratton)) Laboratory for Fluorescence Dynamics, Dept. of Physics, Univ. of Illinois at U-C, 1110 W Green, Urbana, IL 61801.

Two-photon fluorescence fluctuation correlation spectroscopy (FCS) is a powerful technique for measuring local molecular diffusion in the cytoplasm of living cells. The advantage of two-photon excitation is that the volume excited is significantly smaller than for single photon excitation. The smaller effective sample volume allows us to perform FCS measurements inside living cells, as well as in bulk (3D) samples. Integration times are also much shorter since there are larger fluctuations in particle number in a smaller volume. We present measurements of the diffusion coefficient for several different size latex beads, dextrans, and proteins in solution. The recovered diffusion coefficients follow the Stoke-Einstein relation. We also present preliminary results of diffusional rates of latex fluorospheres microinjected into the cytoplasm of living drosophila embryos and mouse fibroblasts. Finally, we present the theory describing the autocorrelation function using two photon excitation.

Supported by National Institutes of Health grant RR03155 and University of Illinois at Urbana-Champaign.

W-Pos140

DEVELOPMENT OF AN OPTICAL LOW COHERENCE REFLECTOMETRY MICROSCOPE FOR THREE-DIMENSIONAL IMAGING OF INTERNAL STRUCTURES OF BIOLOGICAL SYSTEMS. ((J.D.B. Sutin, P.T.C. So, T. French and E. Gratton)) Laboratory for Fluorescence Dynamics, Dept. of Physics, Univ. of Illinois at Urbana-Champaign, Urbana, IL 61801.

Coherence microscopy has found wide application for high resolution, three-dimensional surface profiles. Recently, optical low coherent reflectometry (OLCR) has been used to characterize the internal structure of biological systems. However, these measurements were limited to either longitudinal distances or two-dimensional tomographic cross-sectional images produced by scanning a beam laterally across a sample. In this investigation, we report the development of an OLCR microscope which uses full-field illumination and a phase-sensitive CCD camera to record entire three-dimensional images without lateral scanning. This instrument has been constructed through simple modifications to a Zeiss Axiovert 35 microscope illuminated with either a mode-locked titanium sapphire laser or white light sources, achieving a diffraction limited lateral resolution of ~0.5 μm and longitudinal resolution superior to confocal methods. We are optimizing the system to measure internal cellular structures.

Supported by National Institutes of Health grant RR03155 and University of Illinois at Urbana-Champaign.

W-Pos141

FLUORESCENCE PHOTOBLEACHING EFFECTS IN A FLUORESCENCE LIFETIME RESOLVED MICROSCOPE. ((T. French, P. T. C. So, and E. Gratton)) Laboratory for Fluorescence Dynamics, Dept. of Physics, University of Illinois at Urbana-Champaign, 1110 W. Green St., Urbana, IL 61801.

A fundamental advantage of measuring fluorescence lifetime versus fluorescence intensity is that the lifetime is a measure of the state of the fluorophore whereas the intensity also measures other effects such as concentration and excitation intensity. Fluorescence photobleaching, a reduction in the number of excitable fluorophores, is a common occurrence in fluorescence microscopy and causes difficulties for intensity measurements. Fluorescence lifetime measurements should be insensitive to this effect except when the photobleaching rate is on the order of the lifetime measurement rate. As it turns out, photobleaching can occur very rapidly in a fluorescence microscope. It is therefore critical to understand the extent to which photobleaching can effect fluorescence lifetime data if the advantages of lifetime measurements in a fluorescence microscope are to be realized. We will present a study that shows the actual effect of photobleaching on fluorescence lifetime measurements in an imaging fluorescence lifetime microscope.

Supported by National Institutes of Health grant RR03155.

W-Pos142

LOCOMOTION OF TUMOR CELLS IN LIVING TISSUES. ((L.B. Margolis, S.E. Glushakova, B.A. Baibakov, C. Collin and J.J. Zimmerberg)) NICHD & NINDS, NIH, Bethesda MD 20892. (Spon. by R. Berger)

In three-dimensional tissues *in vivo*, cells find themselves in a physically unique microenvironment among various heterogeneous cellular and noncellular elements. Cell behavior in general, and locomotion in particular are greatly affected by microenvironment. Currently cells are studied predominantly in homogeneous monolayer cultures mainly because of the optical properties of the latter system which allows monitoring cells by conventional optical and fluorescent microscopy. We describe a system for studying the behavior of individual cells inside tissues in long-term three-dimentional cultures. We have combined several techniques - native-state histocultures which retain the architecture of tissue explantate and real-time laser confocal fluorescent and reflective microscopy, which overcomes the optical obstacles of these cultures. Using this system, we monitored individual mouse tumor cells invading normal mouse lung, spleen, thymus, etc. in histoculture. We find that (i) tumor cells do locomote within these tissue blocks, (ii) locomotory behavior is different in different organs, and (iii) the invasion goes along certain pathways rather then anisotropically as happens in monolayer cultures. The described system provides new potentials for studying different aspects of cell behavior as a function of the physical and chemical microenvironmental factors of the living tissues.

W-Pos143

CONFOCAL MICROSCOPY STUDIES OF LEPIDOPTERAN CELLS EXPOSED TO *BACILLUS THURINGIENSIS* (*Bt*) TOXINS.

((R. Monette, D. Baines*, L. Potvin+, M. Pusztai-Carey#, R. Laprade+ and J.L. Schwartz)) BRI, National Research Council, Montreal, Que, H4P 2R2, * FPMI, Natural Resources Canada, Sault Ste-Marie, Ont, P6A 5M7, #IBS, National Research Council, Ottawa, Ont, K1A 0R6 and +GRTM, University of Montreal, Montreal, Que, Canada, H3C 3J7.

The exact mode of action of the entomopathic proteins produced by *Bt* is not known. We have shown that these toxins form ionic pores in living cells[1] and planar lipid bilayers[2]. In Sf-9 cells (*Spodoptera frugiperda*, fall armyworm), microspectrophotometric measurements using the Ca^{++} indicator Fura-2 and the pH indicator BCECF have revealed that CryIC triggers an early calcium surge[1] and induces a loss of pH regulation[3]. Calcium signalling in response to CryIC exposure was also observed in UCR-SE-1a cells from *Spodoptera exigua* (beet armyworm)[4]. In an attempt to relate cellular structure changes and signalling mechanisms to *Bt* protein toxicity, confocal microscopy was used on freshly dissociated midgut cells[5] from *Lymantria dispar* (gypsy moth) or on cell lines from *S. frugiperda*, *S. exigua* and *Choristoneura fumiferana* (spruce budworm). The effects of lepidopteran- or coleopteran-specific Cry toxins are visualized on high resolution pseudo-color images.

[1]Schwartz *et al* (1991) BBA 1065:250-260; [2]Schwartz *et al* (1993) J. Membr. Biol. 132:53-62; [3]Vachon *et al* (1993) Biophys.J. 64:A14; [4]Monette *et al* (1993) J. Insect Physiol. (in press); [5]Baines *et al* (1993) J. Insect Physiol. (in press).

MICROSCOPY (OTHER)

W-Pos144

SINGLE MOLECULES OBSERVED BY NEAR-FIELD SCANNING OPTICAL MICROSCOPY (NSOM).

((Eric Betzig and Robert J. Chichester)) AT&T Bell Laboratories, Murray Hill, NJ 07974 USA (Spon. by M. Edidin)

Using NSOM we have been able to image individual carbocyanine dye molecules in a submonolayer spread. We can detect and spatially localize (to $\sim\lambda/50$) molecules repeatedly with a sensitity of at least 0.005 molecules/$(Hz)^{1/2}$ and can determine the orientation of each molecular dipole. We exploit this information to map the electric field distribution in the near-field aperture with molecular spatial resolution.

W-Pos145

IMAGING PLASMA MEMBRANE LIPID DOMAINS AND MEMBRANE BOUND RECEPTORS IN HUMAN SKIN FIBROBLAST CELLS WITH NEAR-FIELD SCANNING OPTICAL MICROSCOPY (NSOM).

((Jeeseong Hwang and Michael Edidin)) Department of Biology, The Johns Hopkins University, Baltimore, MD 21218 USA ((Eric Betzig and Robert J. Chichester)) AT&T Bell Laboratories, Murray Hill, NJ 07974 USA (Spon. by M. Edidin)

We report the application of NSOM to the imaging of submicron size phospholipid domains and HLA-I proteins in the membranes of human skin fibroblasts. Cell plasma membranes were labeled with the fluorescent lipid analogs BODIPY-PC or BODIPY-SM as well as with tetramethylrhodamine-conjugated anti-HLA Fab or IgG. Near field fluorescence and shear force topographic images were obtained simultaneously during scanning. In fluorescence images, patchy distributions of the fluorescent lipid analogs indicative of lipid domains were seen in all cells. Patches of HLA-I antigens were also observed and did not show a correlation with the patches of fluorescent lipids. Cytoskeletal fibers and other features of the leading lamellipodia of intact cells were visible in shear force images.

W-Pos146

FLUORESCENTLY LABELED STRUCTURES IMAGED UNDER SOLUTION USING A NEAR-FIELD SCANNING OPTICAL MICROSCOPE.

((E.J. Seibel and G.H. Pollack)) Center for Bioengineering WD-12, University of Washington, Seattle, WA 98195.

We have constructed a near-field scanning fluorescence microscope designed specifically for imaging fluorescently labeled biological samples in solution at super resolution. The reason for building this new type of microscope is to overcome the resolution-limited conventional optical microscope and the destructive nature of the electron microscope. Our near-field microscope is configured in the transmission mode with the tapered fiber-optic probe as the illuminator and an objective lens as the light collector, located underneath the sample and wet cell. The probe is coated with aluminum, except the very tip, which creates an aperture of 75 to 100 nm diameter for light emission. The light emitted from the probe tip remains collimated at the dimension of the aperture for a limited range, called the near-field. Raster scanning of the fluorescently-labeled sample within the near-field region of the probe generates a fluorescent image of super resolution. We have confirmed that fluorescence near-field scanning images can be obtained under solution by imaging charged, fluorescent microspheres adhered to glass. We are attempting to image single skeletal muscle myofibrils whose thin filaments are fluorescently labeled with FITC-phalloidin. The goal is to develop a means of testing recent models of muscle contraction that predict small changes in thin filament length. We hope to be able to detect 3 to 5 % changes of thin filament length that may accompany transitions between rigor, relaxation, and activation in muscle.

W-Pos147

WALSH AND HAAR TRANSFORM ANALYSIS OF MUSCLE IMAGES

((M.P. Stawnych, L. Morishita, and B.H. Bressler)) Department of Anatomy, University of British Columbia, Vancouver, British Columbia. (Spon. by E. Evans)

Sarcomere length measurements play a central role in the study of muscle mechanics. These lengths are typically obtained in one of two different ways - laser diffraction or image analysis. In terms of the latter, the sarcomere length is obtained by analyzing the Fourier power spectrum. However, there are several other orthogonal transforms that are well suited for analyzing image periodicity, including the Walsh and Haar transforms. The Haar transform is of particular interest since, unlike the Fourier transform, it includes both global and local basis functions and could potentially be used to assess sarcomere inhomogeneity as a function of axial location. In addition, both the Walsh and Haar transfroms are computationally less intensive than the Fourier transform, and thus can readily be used in "real-time" analysis applications.

In general, we found good correspondence between the Fourier and Walsh spectra, as shown below. However, the Haar spectrum tended to be more complicated, making the direct analysis of axial sarcomere inhomogeneity difficult. Because of its edge detection properties, the Walsh transform may also be useful in enhancing muscle images. (Supported by the MRC).

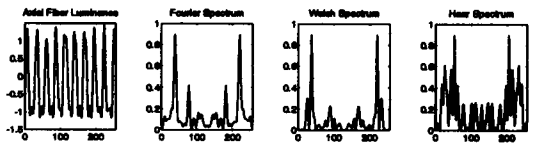

W-Pos148

INTERSTITIAL TRANSPORT OF BINDING AND NON-BINDING ANTIBODIES IN THICK TISSUE MEASURED WITH FRAP. ((D.A. Berk, F. Yuan, M. Leunig, and R.K. Jain)). Radiation Oncology, Massachusetts General Hospital, Harvard Medical School, Boston, MA, 02114. (Spon. by R.M. Hochmuth)

Transport of macromolecules in the extracellular space of tissue can be hindered by binding interactions with various elements of the interstitial matrix as well as by tortuosity and excluded volume effects. It has previously been shown that the technique of fluorescence photobleaching recovery (FRAP) can be used in vitro to measure the effective diffusion coefficient of macromolecules in a three dimensional sample and to quantitate their binding affinity for a fixed substrate in the diffusion-limited and reaction-limited cases. We have extended this experimental approach to investigate the transport of monoclonal antibodies (MAb) in the interstitium of human tumor xenografts (LS174T colon adenocarcinoma implanted in dorsal skinfold chambers in athymic nude mice). Fluorescein-labeled tumor-specific MAb (ZCE025) or a nonspecific control MAb (S1) were administered i.v. at doses ranging from 10^{-3} to 6 mg/g body mass, and the movement of the MAb within the interstitium was measured by FRAP at 24 and 100 h post injection. Control MAb was observed to diffuse at a hindered rate of ≈1/3 compared to diffusion in free solution, and a fraction (≈1/3) of these molecules were immobile within the timescale of the experiment. The relative reduction in diffusion coefficient was similar to that observed for a smaller macromolecule (bovine serum albumin); this suggests that the interstitial volume that is accessible for long-range (10 - 100 μm) macromolecular transport is not strongly dependent on molecule size over this size range (Stokes radius 3.5 to 5.5 nm). The immobile fraction, attributable to nonspecific binding, was independent of MAb concentration. In contrast, the specific MAb exhibited a dose-dependent mobility: at low doses (<0.01 mg/g), the immobile fraction approached 100%, but at high doses (>0.1 mg/g), the immobile fraction was the same as observed for control MAb. We conclude that the in vivo FRAP technique permits detection of binding-site saturation and estimation of in vivo binding avidity or antigen density.

W-Pos149

THE USE OF THE X-RAY MICROSCOPY TO OBSERVE ARTIFICIAL LIPID MEMBRANES AND THEIR ADHESIVE BEHAVIOUR. ((B. Klösgen* and P. Guttmann+)) * Freie Universität Berlin, Institut für Experimentalphysik, Arnimallee 14, D-14195 Berlin; + Forschungseinrichtung Röntgenphysik, Georg-August-Universität Göttingen, Geiststr. 11, D-37037 Göttingen. (Spon. by M.P. Heyn)

X-ray microscopy may develop to be a tool for the investigation of microscopic objects in the resolution gap between light- and electron microscopy. Here we present recent results obtained with vesicles of artificial lipid membranes in a humid observation chamber at normal pressure and at room temperature. Single membranes are distinguishable. Similar to transmission electron microscopy, phase contrast is shown to improve the image quality. Pictures showing detailed views of the contact region of adhering membranes are presented. Also, the method may be used to detect stationary defects in the smooth surface of fluid membranes. The three microscopy techniques are compared as to their principal facilities and especially for their use to investigate the interaction between lipid membranes and observe structural details at the membrane surface.

W-Pos150

DIFFUSION OF LIQUIDS IN NMR MICROSCOPY: MECHANISMS OF CONTRAST AND TISSUE CHARACTERIZATION ((D. Barsky, B. Pütz, K. Schulten, J. Schoeniger, E. Hsu, and S. Blackband)) U. of Illinois, Urbana, IL 61801, Sandia National Laboratories, Livermore, CA 94551, and Johns Hopkins U., Baltimore, MA 21205.

In NMR microscopy the effect of molecular diffusion is usually to degrade resolution and sensitivity due to destructive interference of signals from the moving nuclear spins. In samples there may exist regions that differ markedly in the translational diffusion coefficient of the molecules whose spatial distribution is being imaged, and in particular, samples may contain barriers impermeable to the translating spins. We present an experimental demonstration that, in the presence of a magnetic field gradient, a reduction in the translational mean free path of liquid molecules, due to barriers, results in the enhancement of magnetization near barriers. Monte Carlo simulations are compared with experimental observations. This "phase coherence" edge enhancement may provide a means through NMR microscopy of visualizing small impermeable structures that might otherwise be invisible. In addition, edge enhancement enables one to characterize biological tissue through the inherent sensitivity of edge enhancement to the permeability of cell membranes.

W-Pos151

CALIBRATED SCANNING (ATOMIC) FORCE MICROSCOPY OF EARTHWORM HEMOGLOBIN.
((S. Xu, O.H. Kapp* and M. F. Arnsdorf)), Depts. of Med. and *Radiology, Univ. of Chicago, Chicago, IL 60637. (Spon. by D. Zeng)

Major obstacles to quantitative imaging by scanning force microscopy (SFM) have been distortion and the overestimation of measurements due to tip effect. SFM images of untreated earthworm hemoglobin revealed a donut-shaped hexameric top view and a dumbbell-shaped tetrameric side view. The height measured for the molecule scanned in air was consistent with electron microscope (EM) data (21 ± 0.7 and 31.4 ± 0.6 nm for the top and side views), but the lateral measurements were overestimated tenfold (301.6 ± 8.0 nM for the top view). Calibration of the SFM tips using images of spherical colloidal gold particles (10, 20, 40 nm diameter) allowed recognition of distortion and the correction of raw image dimensions. The grain size of the round images of the gold particles at different image height was analyzed. The radius of the grains was calculated and plotted against the image height. Tip size, shape and semivertical angle were determined from the plot and from the shape of the grain. Corrected lateral measurements were 30.2 ± 3.4 nm which is close to the EM measurement. Wet samples were softer than dried specimens, and the sample was compressed presumably by the pressure of the cantilever. Calibration is rapid and nondestructive to the tip. In conclusion, calibrated SFM imaging allows for the detection of distortion and for the correction of measurements. This is the first report of imaging a biomolecule using calibrated SFM and represents a major step in the development of quantitative SFM imaging of biomolecules.

W-Pos152

MEASUREMENT OF PICONEWTON FORCES USING A SIMPLE OPTICAL FORCE MICROSCOPE. ((Lucien P. Ghislain, Neil A. Switz and Watt W. Webb)) Applied and Engineering Physics, Cornell University, Ithaca, NY 14853. (Spon. by Thomas G. Owens)

The optical trap formed by a strongly focused IR (λ = 1.064 μm) laser can be utilized as a force transducer for micromechanical measurements and as the force sensing element of a novel optical force microscope (OFM) [Ghislain and Webb, Optics Letters, 18, 1678 (1993)]. We report here on an OFM which utilizes a simple, sensitive position sensing device (PSD) that monitors the modulation of the forward scatter of the trapping laser to measure the displacement of a probe particle within the trap, with a dynamic (kHz) sensitivity of ~ 1 nm in the radial and ~ 10 nm in the axial directions. We used viscous drag calibration to measure the force constants of the single-beam optical trap for 0.2 - 2.1 μm diameter microspheres. The calibrated trap with the PSD constitutes a force transducer having a spring constant of ≤ 10^{-4} N/m, capable of (thermal noise limited) sensitivity better than 1 pN at a dynamic lateral spatial resolution of ~ 10 nm. The low spring constant, high force sensitivity, and sub wavelength resolution of this simple instrument should prove useful for delicate surface probe measurements and imaging on biological structures in aqueous media.

Supported by the NIH-NSF Developmental Resource for Biophysical Imaging and Opto-Electronics, under grants NIH (RR04224) and NSF (DIR8800278/DIR9149654).

W-Pos153

ATOMIC FORCE MICROSCOPY OF ATRIAL CELLS: LOCAL VISCO-ELASTIC MECHANICAL PROPERTIES AND IMAGING OF CYTOSKELETON. ((S.G. Shroff, D.R. Saner and R. Lal)) University of Chicago, Chicago, IL 60637.

Atomic Force Microscope (AFM) was used to quantify local visco-elastic properties of adult rat atrial myocytes (7-10 day culture on laminin-coated coverslips) and to image their 3-D surface topology. **Quiescent cells:** Mechanical measurements were made by positioning the AFM cantilever tip at a point on the cell, turning the position feedback off, and recording the cantilever deflection (ΔD) in response to imposed sinusoidal oscillations of the sample holder (ΔZ, 9 nm amplitude @ 0.2 to 200 Hz). The calculated frequency spectrum of the transfer function (ΔD/ΔZ) was consistent with a visco-elastic model of the cell. An increase in extracellular Ca^{2+} caused an increase in cell stiffness and formalin fixation made the cell purely elastic with even higher stiffness (Fig.). **Beating cells:** With ΔZ held constant, changes in ΔD resulting from active contractions could be recorded. These changes responded appropriately to various inotropic stimuli. Using the sinusoidal perturbation of ΔZ as above, dynamic changes in relative cell stiffness during contraction could be quantified. At 200 Hz and 5 mM Ca^{2+}, the modulus of ΔD/ΔZ increased from 0.4 at the onset of contraction to 0.7 at the peak of contraction. **Topology:** 3-D surface images showed well-defined cell morphology and underlying cytoskeleton that corresponded to actin-specific structures as revealed by phalloidin labeling. Thus, regional structure-mechanical function correlation in living cells can be examined using AFM.

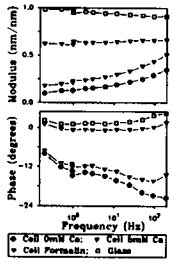

W-Pos154

DIRECT IMAGING OF TWO-DIMENSIONAL BIOMOLECULE ARRAYS USING ATOMIC FORCE MICROSCOPY
((Laura T. Mazzola, Stephen P. A. Fodor)) Affymetrix Research Institute, Santa Clara, CA 95051

We have developed a novel technique using light to direct the immobilization or synthesis of peptides and oligonucleotides in two-dimensional arrays. The spatial distribution and density of these biopolymers can be controlled by light-directed activation of a photoprotected substrate. The coupling chemistry defines the relative orientation of the surface-bound molecules. These spatially-defined arrays can then be used to study a variety of molecular recognition processes.

We have used the above technique in conjunction with atomic force microscopy (AFM) to probe the structure and organization of biological molecules bound to these ligand arrays. For example, AFM images will be shown of streptavidin bound to a 50 μm checkerboard biotin array. The height profile of the protein/ligand pair is ~70 Å over the base substrate, with a 2 μm edge rolloff. High resolution scans indicate a dense packing of ~400 Å globular features in the streptavidin-immobilized regions, which exhibit peaked substructure roughly 100 Å apart. In a second experiment the protein was forcibly cleared from the substrate using the AFM tip, revealing an 8 Å step corresponding to the biotin derivatization. In addition, preliminary results scanning an oligonucleotide array detect a 5 Å height profile for 17mer single strand DNA.

W-Pos155

NEW CANTILEVERS MICROFABRICATED FROM POLYMERIC MATERIALS FOR THE SCANNING FORCE MICROSCOPY OF SOFT BIOLOGICAL SAMPLES.
((R. Pechmann*, J. M. Köhler*, W. Fritzsche#, A. Schaper#, T. M. Jovin#)).*Institute for Physical High Technology, 07743 Jena / F.R.G. #Max Planck Institute for Biophysical Chemistry, Department of Molecular Biology, 37018 Göttingen / F.R.G.

The stable imaging with a scanning force microscope (SFM) of soft materials such as biological specimens requires a force transducer (cantilever) of high sensitivity, i.e. low force constant, and with a sharp tip of known geometry. We have developed a new force sensor element (NovoLever) based on microstructuring with multilayer thin film technology and adapted for optical readout in a conventional SFM. The use of a photoresist (Novolak, widely applied in photolithography) or other polymers as cantilever materials permits the introduction of mechanical properties otherwise not accessible with microfabrication based on Si or Si_3N_4. Indentation measurements on Novolak test structures indicate that it is possible to fabricate more flexible structures than those achieved by silicon technology. We have incorporated the new sensors into a commercial SFM (Nanoscope III) and evaluated their performance with test structures and biological samples such as plasmid DNA spread on mica with a new detergent-based procedure. In addition, a novel approach is presented for the microfabrication of a bifunctional sensor element for near-field scanning optical microscopy (NSOM) combined with the SFM modality.

W-Pos156

DIFFERENT LEVELS OF CHROMATIN CONDENSATION IMAGED WITH SCANNING FORCE MICROSCOPY.
((W. Fritzsche, A. Schaper, T. M. Jovin)). Max-Planck-Institute for Biophysical Chemistry, Department of Molecular Biology, 37018 Göttingen / F.R.G.

The different levels of the chromatin condensation were investigated with the scanning force microscope (SFM) in air and under liquid. Starting from specimen preparation techniques of conventional microscopy we have developed new methods for visualizing the chromatin structure of different cells in the SFM. A beaded substructure of the nucleoprotein filament is observed after spreading the chromatin from chicken erythrocytes and air drying. Such a bead-on-a-string morphology is expected for the basic nucleosomal assembly. In the SFM the nucleosomes appear as round protrusions 3-6 nm in height and 20 nm in diameter. Center-to-center measurements between adjacent nuclesome cores along the chain axis yield a histogram with a peak at 30 nm. After treatment of the cell nucleus with detergent under mild conditions supranucleosomal structures are obtained. The nucleosomes are still distinct but appear more condensed. The fiber dimensions are approximately 5-10 nm in height and 50 nm in diameter. In contrast, a more uniform filamentous morphology of the chromatin fibers of similar dimesions is obtained with a modified droplet diffusion spreading technique applied to the chromatin from Namalwa (a human B-lymphoid cell line). The highest level of chromatin condensation, metaphase chromosomes (e.g. from human lymphocytes) show a very complex morphology that cannot be fully resolved in the SFM. Reversible changes in three-dimensional structure are observed upon exposure of previously air-dried samples (chromatin spreads, metapahase chromosomes) to solutions of different ionic strength.

SEPARATION METHODS

W-Pos157

BREAK-DOWN PRODUCTS vs NONIDEALITY IN A PROTEIN SOLUTION.
((Yujia Xu)) Department of Molecular and Cell Biology, University of Connecticut, Storrs, CT 06269-3125

The dependence of apparent thermodynamic parameters such as molecular weight averages, self-association constants, etc., on the loading concentrations can be used to infer the heterogeneity of a sample preparation examined by equilibrium ultracentrifugation. We observed that, using a least square fitting program, (NONLIN), the data of a heterogeneous system consisting of an ideal main component and smaller molecules (such as break-down products) in a single solution column could be fit very well by a model of nonideal single component: a large apparent second virial coefficient, B_{app}, was estimated by the fitting. In contrast to the constant B_{app} obtained for a nonideal system, the value of B_{app} for the heterogeneous solution increases with loading concentration. Such a concentration dependence of B_{app} could be an indication of the presence of heterogeneity, and thus suggests further least-squares analyses with models involving smaller components to distinguish the two cases. Based on this argument we were able to detect the presence of small amounts of break-down products in a preparation of bovine serum albumin (BSA). Experimental data and computer simulation results will be presented. (Supported by NSF grant #DIR-921867).

W-Pos158

MEASURING SEDIMENTATION, DIFFUSION, AND MOLECULAR WEIGHTS OF SMALL MOLECULES BY DIRECT FITTING OF SEDIMENTATION VELOCITY CONCENTRATION PROFILES.
((J. S. Philo)) Amgen Inc., Amgen Center, Thousand Oaks, CA 91320

Sedimentation velocity experiments have traditionally been used for samples with relatively high sedimentation coefficients and low diffusion. Such samples give sharp boundaries from which it is relatively easy to extract the sedimentation coefficient, and which permit the separation of multicomponent samples into distinct boundaries. However, many proteins of therapeutic interest have molecular masses of only 5-40 kDa, which give very broad boundaries which are difficult to analyze by existing techniques.

We have developed a method where multiple raw data sets of concentration *vs.* radius, taken at various times during the run, are simultaneously fitted to appropriate approximate solutions of the Lamm equation, with *s*, *D*, and the loading concentration as fitting variables. As a bonus, the determination of *s* and *D* from the same experiment allows calculation of the molecular weight with an accuracy of ~2% for 15-70 kDa proteins. This technique can also be used to analyze samples containing multiple non-interacting species, even when they do not resolve into distinct boundaries. By directly fitting the raw data the errors in the fitted parameters may be properly evaluated. Other advantages and drawbacks of this technique will be discussed.

W-Pos159

SEDIMENTATION BOUNDARY ANALYSIS OF INTERACTING SYSTEMS: USE OF THE APPARENT SEDIMENTATION COEFFICIENT DISTRIBUTION FUNCTION. ((Walter F. Stafford)),Boston Biomedical Research Institute, 20 Staniford Street, Boston, MA 02114

The apparent sedimentation coefficient distribution function, g(s*) vs. s*, (where $s^*=\ln(r/r_m)/\omega^2 t$, and g(s*) has units proportional to concentration per svedberg; the other symbols have their usual meaning) can be computed from either the spatial or the temporal derivative of the concentration profile (Stafford,W.F, Anal Biochem., 203,295-301,1992). The plot of g(s*) vs. s* is very nearly geometrically similar to the corresponding plot of dn/dr vs. r (where n is the refractive index) obtained with the schlieren optical system. The distribution function, g(s*), may be used in the same way as dn/dr to analyze self- and hetero-associating systems. For an interacting system, it can be shown, to within a very good approximation, and despite boundary broadening from the interaction or from diffusion, that the weight average sedimentation coefficient is given by

$$s_w = \frac{1}{c_p}\int_m^p s^* g(s^*) ds^* \quad \text{where} \quad c_p = \int_m^p g(s^*) ds^*$$

For example, for a monomer-dimer system, the weight fraction of monomer, α, at any given concentration is given by $\alpha = (s_w - s_1)/(s_2 - s_1)$, where s_1 and s_2 are the sedimentation coefficients of the monomer and dimer, respectively. The equilibrium constant can be obtained from a plot of $(1-\alpha)/\alpha^2$ vs. c_p. Moreover, plots of g(s*) can be compared directly to numerical simulations of sedimenting boundaries for various systems.(Supported in part: NIH grant U01 CA51880)

W-Pos160

AN OPTICAL THERMOMETER FOR DIRECT MEASUREMENT OF CELL TEMPERATURE IN THE BECKMAN INSTRUMENTS XL-A ANALYTICAL ULTRACENTRIFUGE. ((Sen Liu and Walter F. Stafford)) Boston Biomedical Research Institute, 20 Staniford Street, Boston, MA 02114

An optical thermometer has been evaluated for use in the Beckman Instruments Optima XL-A Analytical Ultracentrifuge. A thermochromic solution of $CoCl_2*6H_2O$ (Brenci et al., Proc. Laser '85 Optic-Electronik), was used as the temperature sensing material. The hydration of $CoCl_2$ is temperature dependent resulting a highly temperature dependent absorption peak at 660nm. Spectra of 0.1M $CoCl_2*6H_2O$ in an alcohol-water (92.5%) mixture were measured at different temperature settings of the XL-A. The spectra of the same $CoCl_2*6H_2O$ solution were measured on a Beckman Instruments DU-650 spectrophotometer with a calibrated thermal couple attached to the cell. A standard curve was constructed by plotting the area under the spectrum from 450 to 750nm as a function of the thermocouple temperature. Spectra were obtained on the XL-A at various temperature settings and integrated over the same range. This method allows direct comparison of the cell temperature to the value displayed on the console panel of the XL-A. (Supported in part by NCI grant U01 CA51880)

W-Pos161

ATYPICAL SIEVING OF SPHERES DURING BOTH LOW AND PULSED FIELD AGAROSE GEL ELECTROPHORESIS ((P. Serwer, R. A. Harris, and G. A. Griess)), The University of Texas Health Science Center, San Antonio, TX 78284-7760

Typically, during agarose gel electrophoresis, the electrophoretic mobility (μ) of a particle increases in magnitude as the percentage of agarose in a gel (A) decreases. Here, electrophoresis of spheres 30nm-148nm in radius has revealed conditions that cause an atypical inversion of the μ vs. A relationship, for A values usually between 0.05% and 0.1% agarose (atypical sieving). Atypical sieving occurs in two conditions: (a) The electrical field is comparatively low in magnitude, $\leq$ 0.6 V/cm. (b) The electrical field (6 V/cm) is periodically inverted such that the ratio of the forward to the reverse pulse time is less than 2. As A decreases, the atypical sieving at low constant field is explained by a previously observed (Griess, G.A. et al. [1993] Biophys. J. 65, 138-148) progressive partitioning of agarose gel fibers into zones of comparatively high agarose fiber density. That is, sieving during gel electrophoresis is accompanied by gel exclusion chromatography. At the higher field inversion frequencies, averaging of the field explains atypical sieving. However, atypical sieving is induced by field inversion at pulse times greater than 30 min. For the longer pulse times, field-induced alteration of the structure of the gel appears necessary to explain atypical sieving. Supported by NSF.

W-Pos162

SEPARATION OF DNA AND OBSERVATION OF BANDS IN MICROFABRICATED ARRAYS ((W. Volkmuth[a],T. Strick[a], T. Duke[a], R.H. Austin[a], E.C. Cox[b])) [a]Department of Physics and [b]Department of Biology, Princeton University, Princeton, NJ 08544

Using microlithography, we have designed a pseudo 2-D environment for electrophoresis of DNA. The environment consists of an array of cup-shaped obstacles with openings pointed in the same direction as the E-field. The cups trap the DNA molecules as they move through the array, and short molecules have a longer escape time than long molecules, resulting in a mobility curve in which μ *increases* with length. We show that we can length-separate DNA, observing bands as in conventional electrophoresis, but since longer molecules move faster than shorter ones, the band order is *reversed.* Epi-fluorescence real-time video of the DNA molecules moving in the arrays will be presented.

W-Pos163

IMPROVED HPLC METHOD FOR PURIFICATION OF MEMBRANE-SPANNING POLYPEPTIDES. ((M.L. Jennings)) University of Texas Medical Branch, Galveston, TX 77555.

Biochemical analysis of membrane proteins has been limited in part by the difficulty of isolating hydrophobic fragments. High pressure liquid chromatography (HPLC), a powerful technique for separating small hydrophilic peptides, has been less useful for the isolation of hydrophobic peptides larger than about 20 residues. The main problem is that hydrophobic peptides are eluted as broad peaks with low recoveries. Using slight variations of common methods, the resolution and yield of hydrophobic peptides can be dramatically improved. With a cyanopropyl column and either 1-propanol or 2-propanol in the mobile phase, resolution of erythrocyte membrane protein fragments is far better than with acetonitrile. Integral fragments from pepsin-digested human red blood cell membranes were solubilized in sodium dodecyl sulfate, the excess detergent was precipitated by adding KCl, and the detergent-protein complexes were injected directly onto the column in 20% n-propanol, 0.1% trifluoroacetic acid. Detergent and lipid elute at relatively low propanol (25-35%). At higher propanol (35-65%), various hydrophobic fragments (size 30-80 residues) of the anion transporter and glycophorin were recovered in bands that were well enough resolved to identify by Edman degradation without further purification. This method of preparing hydrophobic fragments is being used to map the topology of the anion transporter. Supported by NIH Grant R01 GM 26861.

W-Pos164

ADAPTATION OF LARGE ZONE ANALYTICAL GEL FILTRATION CHROMATOGRAPHY FOR HPLC ((Elizabeth Nenortas and Dorothy Beckett)) Department of Chemistry and Biochemistry, University of Maryland Baltimore County, Baltimore MD 21228

The method of large zone analytical gel filtration chromatography (AGFC) for determination of the energetics and stoichiometries of protein-protein assembly reactions (1), was adapted for use with a conventional HPLC apparatus. The apparatus included a low flow pulsation HPLC pump, teflon injection valve, UV-Vis detector and 2.3 mL glass column packed with Pharmacia Sephacryl S-200 gel filtration resin. Miniaturization of the column, as compared with the standard column chromatography method, resulted in an 8-fold reduction in the volume of large zones applied to the column. Smaller column size and the use of a 0.15 mL/min flow rate allowed for completion of column calibration and data collection in 2.5 days, a significant time savings over the conventional column chromatography method. Good agreement was observed between measured elution volumes for small and large zones of monomeric proteins. The method was further tested by measurement of the dimer-tetramer equilibrium constant for the well characterized oxy-Hemoglobin A_O system.

Measured values of the equilibrium dissociation constant of 1.8 ± 0.8 μM and Gibbs free energy of -7.8± 0.2 kcal/mol for the oxy-hemoglobin assembly process agree well with the literature values (2). The method should prove to be of general use for measurement of protein association processes.

1. Ackers, G.K., (1975) in *The Proteins* (Neurath, H., Hill, R.L., & Roeder, C., Eds.) Vol 1, pp. 1-94, Academic Press, New York).
2. Pettigrew, D.W. *et. al.* (1982) **Proc. Natl. Acad. Sci.**, 79, 1849-1853.

W-Pos165

SEPARATION OF BIOLOGICAL CELLS USING TRAVELLING ELECTRIC FIELDS. ((X-B. Wang[1], Y. Huang[1,2], M.P. Hughes[2], R. Pethig[2], P.R.C. Gascoyne[1] and F.F. Becker[1])) [1]Univ. of Texas M. D. Anderson Cancer Cr., Dept. of Molecular Pathology, Box 089, 1515 Holcombe Blvd., Houston, TX 77030, USA; [2]Univ. of Wales, Institute of Molecular & Biomolecular Electronics, Dean St., Bangor LL57 1UT, UK

The principle of using travelling electric fields as a possible vehicle for manipulating and separating cells was first described by Masuda et al. We have recently developed a theory to show how the linear motion imparted on a cell is controlled by the geometry of the microelectrodes used to generate the travelling fields and by the electrical properties of the cell. For a particular cell type and electrode geometry, the speed and direction of cell motion, as well as the trapping of cells on the microelectrodes, can be controlled by altering either the phase sequence or the frequency of the travelling field. Furthermore, the induced motion combines the effects of dielectrophoresis and electrorotation.

Using electrorotation and dielectrophoresis measurements, we have shown that the conductivity and capacitance of the plasma membrane of Friend murine erythroleukemia cells alter significantly following treatment with hexamethylene bisacetamide or dimethylsulphoxide, agents that induce terminal differentiation in these otherwise malignant cells. We demonstrate that, by appropriate choice of the electrode geometry and frequency of the travelling electric field, it is possible to facilitate the spatial separation of undifferentiated and differentiated erythroleukemia cells by exploiting the differences in their dielectric properties.

W-Pos166

A. C. ELECTRODYNAMICS OF CELLS: THEORY AND BIOTECHNOLOGICAL APPLICATIONS. ((Y. Huang[1,2])) [1]University of Texas M. D. Anderson Cancer Center, Department of Molecular Pathology, Box 89, 1515 Holcombe Boulevard, Houston, TX 77030, USA; [2]University of Wales, Institute of Molecular and Biomolecular Electronics, Dean Street, Bangor LL57 1UT, UK

The phenomena of dielectrophoresis (DEP, the motion of electrically polarized particles in non-uniform A. C. electric fields) and electrorotation (ROT, the effect of rotational torque exerted on polarized particles by rotating electric fields) can be used to induce a wide range of electrodynamic behavior of bioparticles in suspension. These effects provide not only new techniques for investigating and characterizing the physico-chemical properties of individual cells, but also offer a wide range of possible applications in biomedicine and biotechnology.

In this presentation, the theory relating the dielectrophoretic and electrorotational behavior of cells to their dielectric properties and the applied electric field distribution will be briefly described. Methods by which cellular dielectric parameters can be derived from measurements of these frequency-dependent DEP and ROT effects will then be demonstrated using as an example yeast cells on pin-plate, polynomial and castellated microelectrodes. The applicability of A. C. electrodynamic phenomena to practical problems, including cell manipulation and the separation of dissimilar cell types, will be demonstrated using the examples of yeast cells, erythrocytes and bacteria.

AXONAL TRANSMISSION

W-Pos167

OPTICAL ANISOTROPY ASSOCIATED WITH NERVE IMPULSES. ((David Landowne)) Univ. of Miami Sch. of Medicine Miami, FL 33101.

Molecular conformational changes associated with the passage of nerve impulses were detected as changes in linear birefringence (Δ-LB) and optical activity (Δ-OR). The Δ-LB signal was associated with sodium channels. The origin and nature of the Δ-OR signal is less clear. Δ-OR signals propagate with and have a briefer time course than Δ-LB signals. Δ-OR signals, in contrast to Δ-LB signals, sometimes reverse sign when the direction of action potential propagation is reversed. In order to better characterize the optical properties of nerves the general optical anisotropy of squid fin nerves was measured using modulation spectroscopy and rotation of the nerve azimuth.

Nerves were illuminated with white (tungsten-halogen) light passing through an optical train which included a polarizer (-45°), a photo-elastic modulator (PEM, 0°), the squid fin nerve (angle varied over 180°), an analyzer (crossed or at 45° to the analyzer) and a photodetector. The change in light level in phase with either a 1f or 2f reference signal from the PEM was divided by average light level. This was recorded for both analyzer positions generating four (1fxp, 1f45p, 2fxp, 2f45p) curves as a function of nerve azimuth. Also a xt curve was recorded with crossed polarizers and the PEM off. A 79 nm linear retarder in series with the nerve chamber was a standard.

Fourier series analysis as a function of nerve azimuth was compared to predictions made from the general Mueller matrix for oriented molecules (Schellman & Jensen, 1987,*Chem. Rev.* 87,1359-1399). The 2fxp, 2f45p and xt curves for nerve differ significantly from the simple retarder. In addition the 2f45p curve varied among nerves.

Supported by NIH grant NS26651.

W-Pos168

PREDICTION OF ED_{50}'S FOR PROPAGATED A.P. BLOCK FOR WATER SOLUBLE SOLVENTS. ((R. Hahin and J.J. Larsen)) Northern Illinois University, DeKalb, IL 60115

50% effective doses (ED_{50}) of a series of water soluble solvents to block propagated compound action potentials (A.P.'s) were obtained by characterizing the dose-response relation for each solvent. The solvents studied were: dimethylsulfoxide (DMSO), dimethylformamide (DMF), dimethylacetamide (DMA), acetone, and hexamethylphosphoramide (HMPA); the octanol/water partition coefficents (K_{ow}) for these test substances form an ordered sequence that showed a forty-fold increase from DMSO to HMPA. A.P.'s were recorded from desheathed frog sciatic nerves using the sucrose-gap technique; test solvents were added to Ringer as solutes and applied externally to the nerve. ED_{50}'s for the solutes could be predicted as a function of the molar volume, dV/dn, polarity, P, and the hydrogen bond acceptor basicity, β. Voltage-clamp experiments employing the vaseline-gap technique using single muscle fibers showed that each solute acted to reduce the size of Na currents with little change in their kinetic properties at all voltages studied. Experiments using DMSO or DMF, showed that Na channel block alone is insufficient to explain the respective ED_{50} values of A.P. block. Experiments conducted using a rat pancreatic secretory granule based assay for detecting chloride transport changes caused by bulk membrane fluidizing agents, suggest that each of the solutes act to increase membrane fluidity at doses below and above ED_{50} values; however, fluidity changes can not solely explain the ED_{50} values. Light microscopic observations of fixed thick sections of whole nerves previously exposed to DMSO or DMF show structural changes; however, ED_{50} values also can not be simply explained by osmotic effects on nerve structure. These results suggest that the ED_{50}'s for A.P. block are produced by a combination of effects including osmotically-induced nerve structural changes, ion channel block, and fluidity changes.

W-Pos169

PEPTIDE MODELLING AND FUNCTIONAL ASSAYS OF THE P-REGION OF VOLTAGE-DEPENDENT SODIUM CHANNELS. ((P. Cosette, M. Brullemans and H. Duclohier)). URA 500 CNRS, Université de Rouen, Blvd M. de Broglie, 76821 Mont-Saint-Aignan (France).

In order to contribute towards the elucidation of the structure-function of the P-region, we synthesized a 32 amino acid peptide reproducing positions 1487 to 1518 from domain IV of the electric eel voltage-dependent sodium channel: NFETFGNSMICLFEITTSAGWDGLLLPTLNTG. The peptide was left with a free carboxyl terminal and a N-acetylated N-terminal. Circular dichroism spectra of the peptide in trifluoroethanol yield 35% helical conformation, 37% ß-sheet and 28% random coil. The treatment of CD data, taking into account the chain-length dependence for the helical contribution, is in favor of two helical subsegments presumably separated by the ß-strand whose contribution is likely to be greater in lipid vesicles. After reincorporation of the peptide into DOPE "tip-dip" bilayers bathed by symmetric solutions (0.5 M NaCl, 10 mM HEPES, pH 7.4), a single-channel conductance of 6 pS was found with no voltage-dependence of the open state probability. Surprisingly, there was no significant shift of the reversal potential of macroscopic and single-channel currents under asymmetric conditions (0.5 M NaCl in the bath and 0.45 M KCl + 0.05 M NaCl in the pipette). In this connection, Kontis and Goldin (1993) report no modulation of rat IIA sodium channel selectivity when mutating negatively-charged amino acids, within the P-region of domain II, for neutral ones (Molec. Pharmacol. 43, 635-644). Even with the peptide approach, it may prove rewarding to carry out these functional assays with homologous fragments.

[Supported by GDR 0964 (C.N.R.S.) and ARB of Normandie.]

W-Pos170

A STRUCTURAL MODEL OF THE μ-CONOTOXIN BINDING SITE IN THE SODIUM CHANNEL ((Gregory Lipkind, Harry Fozzard, and Sam Dudley)) Cardiac Electrophysiology Labs, MC-6094, The University of Chicago, 5841 S. Maryland Av., Chicago, IL 60637.

μ-conotoxin, produced by the Piscivorius Cone snails, blocks the adult skeletal and electric organ Na^+ channels from the outside with nanomolar affinity and their binding is in competition with the guanidinium toxins. However, the μ-conotoxin is without effect on highly homologous brain and heart Na^+ channel isoforms. The μ-conotoxin family includes three peptides of 22 amino acids and has structural rigidity conferred by 3 disulfide bonds. The tertiary structure of μ-conotoxin GIIIA has been inferred from 2D-NMR (Wakamatsu et al, *Biochem.* 31:12577, 1992). Studies with analogs demonstrate that Arg-13 is required for activity (Becker et al, *Biochem.* 31:8229, 1992). Combining our recent model of the external vestibule of the Na^+ channel with conotoxin structure, we could account for high affinity binding and isoform specificity. The guanidinium group of Arg-13 in its extended conformation interacts within the vestibule with Asp-384 and Glu-942 of repeats I and II, which are thought to be part of the selectivity filter, and this may be responsible for the toxin block. In the model a conserved Glu in the SS1 region of repeat 4, found in skeletal muscle and electric organ channels but absent in brain and cardiac isoforms, is correctly located to form a salt bridge to one or more of a triad of lysines (Lys-8, Lys-9, Lys-11). This latter may explain the isoform specificity and the absence of effect of substitution of any one of the lysine triad.

W-Pos171

SODIUM CHANNEL AGGREGATION DURING NODE FORMATION IN REMYELINATING AXONS. ((S. Dugandžija-Novaković, A. Koszowski, S.R. Levinson, and P. Shrager)) Depts. of Physiol., Univ. Rochester, Rochester, NY 14642 & Univ. Colorado, Denver, CO 80262

A polyclonal antibody was prepared by immunizing rabbits with a conjugate including a highly conserved 18 residue peptide forming part of the domain III-IV linker of the vertebrate Na^+ channel. Antisera were affinity purified and used to label rat sciatic axons at various stages of lysolecithin-induced demyelination. At one week, prior to appearance of Schwann cells, only heminodes and widely spaced (presumed original) fully demyelinated nodes were seen. Over the next several days, clusters of Na^+ channels appeared at the edges of newly adhering Schwann cells. Aggregates of Na^+ channels at original heminodes remained stable. As the remyelinating Schwann cells grew laterally, the Na^+ channels appeared to move with them since the clusters remained always at the edges. With continued growth (~2 weeks) clusters from adjacent Schwann cells apparently coalesced to complete formation of new nodes of Ranvier. Exposure to mitomycin, which inhibits Schwann cell proliferation, blocked entirely the clustering of Na^+ channels along demyelinated internodes. Original heminodes remained for 1 week, but after 2 weeks, Na^+ channels were absent, indicating that Schwann cells are required at both paranodes for maintenance of nodal structure. Supported by NIH and NMSS.

W-Pos172

THE EFFECT OF CALCIUM ION ON THE EARLY PHASE OF GATING CURRENT. ((Clay Armstrong and Kamran Khodakhah)) Dept. of Physiology, Univ. of Pennsylvania, Philadelphia, Pa. 19104.

Calcium ions slow the opening of voltage-gated Na channels following depolarization in voltage clamp. There are (at least) two hypotheses: I) Ca alters surface potential by binding to the outside of the membrane; or II) Ca selectively affects a late step in activation, tending to close the channel (perhaps by binding in the pore itself). Gating current (Ig) gives the best measure of the velocity of the early steps in activation. Under hypothesis I, the early steps should be slowed, causing a reduction of Ig; while II predicts little or no change in the early phase of Ig. We measured Ig (in the absence of permeant ions, no TTX) and INa (Na current, 40 mM Na) in squid giant axons, and the results for 10 and 100 mM external Ca are in the inset. INa is slowed and reduced, while Ig is unaffected. The results clearly show that Ca does not significantly alter the early steps in activation. By inference, one or more later steps must be slowed selectively.

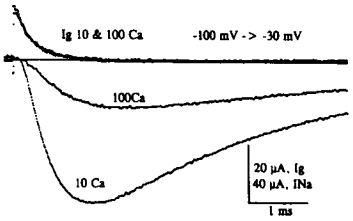

W-Pos173

CLONING AND TISSUE SPECIFICITY OF A MURINE VOLTAGE-GATED NA+ CHANNEL WHICH IS A PUTATIVE MEMBER OF A NEW GENE SUB-FAMILY. ((T.J. Knittle, A. Felipe, K.L. Doyle and M.M. Tamkun)) Dept. of Molecular Physiology and Biophysics, Vanderbilt Medical School, Nashville, TN 37232.

Several laboratories, including our own, have recently presented evidence for the existence of at least two Na+ channel (NaCh) gene subfamilies through the cloning of voltage-gated NaCh isoforms from human muscle ($hNa_v2.1$) and rat glia (Na-G). These two NaChs are 85 % identical to one another, sharing unique amino acid sequence in regions known to be involved in activation, inactivation and ion selectivity. Comparison of these two NaChs with previously cloned voltage-gated NaChs reveals only 40-45% identity which is consistent with inter-family alignments of voltage-gated K^+ channels. We have cloned from mouse heart a voltage-gated NaCh ($mNa_v2.3$) which is an additional member of the newly defined gene subfamily. $mNa_v2.3$ is overall > 80% identical to the other members of the subfamily with nearly identical sequence in functionally relevant regions. Interestingly, both $mNa_v2.3$ and the rat glial NaCh (Na-G) contain a serine residue which substitutes for a highly conserved alanine in the pore-forming segment of domain IV implicated to be important for sodium ion selectivity. Northern hybridization analysis indicated that the $mNa_v2.3$ channel mRNA is present at equivalent levels in mouse heart and myometrium but is not detected in brain which is consistent with the relative distribution of $hNa_v2.1$ in humans. The cloning of this NaCh provides further evidence for the existence of additional NaCh gene sub-families in mammals with a diversity at the molecular level reminiscent to that observed with K^+ channels.

W-Pos174

CHLORIDE CHANNELS IN C FIBERS OF GARFISH OLFACTORY NERVE

((G.R. Kracke, R.K. Shaon, and J.O. Bullock)) Dept. of Anesthesiology, University of Missouri, and Cancer Research Center, Columbia, Missouri 65212.

The olfactory nerve of the garfish contains a uniform population of small, 0.2μ, diameter, unmyelinated axons (C fibers). We have begun to characterize the ion channels in C fibers by reconstituting them into planar lipid bilayers. Axon plasma membrane vesicles were prepared from the nerves. Planar bilayers were formed using a 2:1 mixture of PE and PS, 50 mg/ml in decane. Vesicles were added to one side of the bilayer which was bathed with 130 mM NMG-Cl. The other side contained 10 mM NMG-Cl. Both sides contained 1 mM $CaCl_2$ and 5 mM Tris-Cl, pH 7.4. We observed, in symmetrical 130 NMG-Cl, three types of Cl channels; none were Ca-dependent. Two types of channels had conductances of 18-25 pS and were DIDS-sensitive. One type had a linear IV relationship and the other was outwardly rectifying. The third type of Cl channel had a conductance of about 340 pS, was linear, had a P_o near 1, showed substates, and was DIDS-insensitive. These results indicate the presence of several Cl channels in C fibers. Their role in regulating the excitability of these small nerve fibers is unknown. Supported by NIH grant RR-07790.

W-Pos175

WATER, CHARGES, ENERGY FLUCTUATIONS, AND THE PHYSICAL BASIS OF KINETIC STATES IN AN ION CHANNEL ((Michael E. Green and Jianjun Lu)) Dept of Chemistry, City College of CUNY, New York, NY 10031

Monte Carlo simulation of water in a channel model with charges embedded in the wall shows that for some charge configurations, water is relatively free to move, as in an open state of the channel, while for other configurations the water density rises and the water becomes relatively immobile, as expected for a closed state. This suggests that a charge configuration corresponds to a kinetic state, and transitions among states correspond to changes in position or arrangement of charge. The differences in energy are large compared to kT (> 100 kT) but the energy fluctuations can be 0.2 or more of the energy differences, so the barriers are not impossibly high. The control voltage, in a voltage gated channel, is 2 - 3 kT/q, where q = 1 electronic charge; 5 - 6 charges in these conditions should be marginally sufficient to bias the state of the channel sufficiently to allow control, when fluctuations are considered. The results of simulations will be shown, as will a sample calculation of transitions among states, which will illustrate the importance of fluctuations in making transitions possible.

W-Pos176

THE STOICHIOMETRY OF C-TYPE INACTIVATION ((E.M. Ogielska, W.N. Zagotta and R.W. Aldrich)) Dept. of Molecular and Cellular Physiology and Howard Hughes Medical Institute, Stanford University, Stanford CA 94305.

C-type inactivation in Shaker K channels involves residues near the ion conducting pore and probably occurs by a constriction of the outer mouth of the pore. This inactivation process could result from a concerted conformational change involving all of the four subunits, or a conformational change in a single subunit could be sufficient to cause inactivation. To address this question we constructed and studied channels composed of dimers in which two of the subunits were wildtype and two had either slower or faster C-type inactivtion kinetics. For an independent mechanism the inactivation rate constant of the heteromultimers would be the arithmetic average of the rate constants of the fast and slow homomultimers. In this case a plot of the inactivation rate constant versus the number of fast subunits would be linear. For a concerted mechanism the relationship between the inactivation rate constant and the number of fast subunits would be exponential. Our data for dimers constructed from 3 separate mutations that alter C-type inactivation indicate that the relationship between the inactivation rate and the number of fast subunits is indeed exponential. This supports the idea that C-type inactivation comes about as a concerted conformational change of the four subunits. This mechanism is different from that of N-type inactivation where a single inactivation particle is sufficient to inactivate the channel and the process has been shown to be independent (MacKinnon et al.,1993).

W-Pos177

DETERMINANTS OF GATING KINETICS IN THE S5 REGION OF THE SHAKER POTASSIUM CHANNEL ((Max Kanevsky & Richard W. Aldrich)) Dept. of Molecular and Cellular Physiology and Howard Hughes Medical Institute, Stanford University School of Medicine, Stanford, CA 94305.

Mutagenesis studies have implicated the S4 transmembrane region and the S4-S5 linker region in the voltage-dependent activation gating of K channels. However, the best known mutant *Shaker* allele which affects voltage-dependent gating, Sh^5, differed from wild type by a point substitution (F401I) located in the S5 transmembrane segment (Gautam & Tanouye, 1990; Lichtinghagen *et al.*, 1990). Kinetic analysis of this mutant revealed that changes in the deactivation rate could account for the altered gating behavior (Zagotta &Aldrich, 1990). The Sh^5 results led us to ask whether systematic changes to the gating mechanism could be obtained by making conservative substitutions at residue 401 and surrounding hydrophobic amino acids in S5. Mutant F401I, when expressed in the Shaker background with disrupted N-type inactivation, produced currents that were characterized by a decreased voltage dependence of the deactivation rate. The steady-state conductance-voltage relationship for mutant F401L was similar to wildtype, with activation shifted in the hyperpolarized direction. The most novel gating phenotype resulted from substitution F401A. This mutant gave rise to channels that exhibited extremely shallow voltage dependence: whereas activation began in the wildtype range (ca. -40 mV), the conductance-voltage curve did not saturate at voltage up to 200 mV. Moreover, the kinetics of both activation and deactivation are much faster than in wild type Shaker. Single channel records show a predominance of very brief open durations. Further mutagenesis of this region will help elucidate the roles S5 plays in voltage-dependent gating .

W-Pos178

PROPERTIES OF THE KAT1 CHANNEL EXPRESSED IN *XENOPUS* OOCYTES. ((T. Hoshi)) Department of Physiology and Biophysics, Univ. of Iowa, Iowa City, IA 52242. (Spon. by C.-F. Wu)

KAT1, cloned from the higher plant *Arabidopsis* (Anderson et al., PNAS *89*, 3736-3740, 1992), encodes a potassium channel activated by hyperpolarization. The deduced amino acid sequence suggests that the KAT1 and Shaker channels are similarly organized. Electrophysiological properties of the KAT1 channel expressed in *Xenopus* oocytes were examined using the patch clamp method to compare with the properties of native inward-rectifier channels. Unlike some native inward-rectifier channels, voltage dependence of the KAT1 channel is not markedly dependent on the intracellular Mg^{2+} concentration, suggesting that the KAT1 channel is intrinsically voltage-dependent. Macroscopic pulse and tail G(V) data indicate that the channel activation involves at least 5 to 6 equivalent electronic charges and that the open probability is 0.5 at -120 mV. This voltage dependence is not noticeably influenced by the external K^+ concentration. About 50% of the total charge movement is associated with the closing transitions as indicated by the voltage dependence of the KAT1 tail current. The activation kinetics of the KAT1 channel follows a sigmoidal time course and the sigmoidal behavior is independent of the holding voltage (-50 to +50 mV). When recorded in the excised configuration, the KAT1 channel undergoes rundown. In the inside-out configuration, this rundown is reversed readily by the patch cramming. Application of ATP can at least partially restore the current. The KAT1 macroscopic currents were not affected by internal TEA (20 mM) or by the ShB inactivation "ball" peptide (100 μM). Although the KAT1 channel is activated by hyperpolarization, its electrophysiological properties do not closely resemble those of the native inward-rectifier channels.

W-Pos179

AVAILABILITY OF TRANSGLIAL TUBULAR OPENINGS DETERMINES IMPULSE CONDUCTION VELOCITY IN CRAYFISH GIANT AXON.
((H.M. Digicaylioglu, B. Mock and N.G. Greeff)) Physiology Dept. Univ. Zürich, Winterthurerstr. 190, 8057 CH-Zürich, Switzerland (Spon. by C. Bauer)

In the crayfish (*Proc. clarkii*), both the mesaxonal clefts and the transglial channel system (TGCS) offer candidate ionic current pathways for impulse conduction. Previously we have shown for the squid giant axon, which has a similar TGCS, that (1) the membrane series resistance increases under Na^+-free conditions and (2) this correlates with the disappearance of tubular openings (Greeff et al., Biophys. J, 57:129a; 1990). Here we correlate changes in tubular opening density (TOD) from freeze fracture preparations with conduction velocity measurements on intact crayfish axons under the same extracellular ionic conditions. The control TOD was estimated to be 16 per μm^2 over an area of 409 μm^2. After incubation in Na^+-free TRIS solution the TOD decreased to 10.4 ± 0.76 after 30 min and 1.5 ± 0.15 after 75 min incubation period, respectively. This reaction was reversible when the Na^+-free incubated axons were reincubated in Na^+ containing solution, such that after 120 min reincubation the TOD was 11.8 per μm^2. To determine the influence of decreased TOD on the impulse conduction velocity, the nerve was incubated for 30 min in Na^+-free solution followed by reincubation. Impulse propagation then recovered in two phases. During an initial fast phase Na^+ diffused back into the periaxonal space and allowed impulses to occur with a low conduction velocity. In the second phase velocity recovered slowly to normal values with a time course comparable to the recovery of TOD. These results indicate that the normal TOD is a necessary condition for the normal excitability of the axon and determines its conduction velocity. (Supported by Swiss NF grant 31-27788.89)

EXOCYTOSIS AND ENDOCYTOSIS

W-Pos180

EVALUATION OF DIGITAL FILTERS FOR COMPUTER-BASED MEASUREMENT OF MEMBRANE CAPACITANCE.
((Nenad Amodaj, Frank T. Horrigan, & Richard J. Bookman)) Dept. of Molecular & Cellular Pharmacology, University of Miami, Miami, FL, 33101

The phase sensitive detection or lock-in technique provides a powerful method for measuring changes in cell impedance associated with exocytosis, endocytosis or ion channel gating charge movements. By using a sinusoidal command voltage and analyzing the resulting current signal at orthogonal phase angles, small changes in cell membrane capacitance (C_m) and AC conductance (G) can be determined. Here we evaluate various algorithms for phase-sensitive detection. Software-based stimulus synthesis (sine + pulse) and current analysis provide many advantages over analog lock-in amplifiers including faster recovery of the C_m signal after a voltage pulse, better S/N and efficiency of data collection. We explore the relative advantages and disadvantages of low-pass digital filters with variable decimation using rectangular, triangular and gaussian window functions. In addition, we examine two types of errors that can arise as a result of aliasing. These aliasing effects can occur when the C_m signal bandwidth is greater than the command frequency. In this case, high frequency changes in C_m will appear as lower frequency signals. Less obvious is the result that high frequency changes in C_m can 'cross-over' and appear as changes in the G signal. Methods to prevent, detect, and correct these errors will be presented. (Supported by NSF and AHA/FL)

W-Pos181

MEMBRANE MECHANICS CAN ACCOUNT FOR FUSION PORE DILATION IN STAGES. ((Y.A. Chizmadzhev, F.S. Cohen, J. Zimmerberg, and A. Shcherbakov)) Frumkin Institute of Electrochemistry, Moscow, Russia; Rush Medical College, Chicago; and LTPB, NICHD, NIH, Bethesda, MD 20892. (Spon. by B. Mozayeni)

Fusion pores rapidly enlarge from small conductance values to semi-stable values which represent continuous bilayer membrane structures (Curran et al., J. Memb. Biol., 1993). Enlargement of these pores must involve the work of bending and stretching membranes. Accordingly, we theoretically modelled the expected evolution of fusion pores using the mechanics of homogeneous membranes. We extended previous treatments (Nanavati et al, Biophys. J., 1992), allowing both the length and width of pores to change according to standard dynamical equations of motion. We found that fusion pores, once initiated, rapidly achieve semi-stable dimensions. These dimensions correspond to energy minima located in a canyon between energy barriers. The heights of the barriers decrease as the dimensions of the pore increase. The canyon slopes gently downward along increasing pore dimensions. As a consequence, the pore widens and lengthens slowly as these dimensions migrate along the canyon. When the barriers vanish, the pore rapidly enlarges. This slow, followed by rapid, enlargement occurs for all experimental fusion pores reported to date. Thus, mechanics could be at the root of the phenomenon of fusion pore growth in stages. The functional form of the dynamics of pore dilation are sensitive to surface tension and bending elasticity. The quantitative differences between stages in two biological systems for fusion pores -- mast cell degranulation and cells fusing to planar bilayer membranes -- could be predicted by differences in surface tension between plasma and planar membranes.

W-Pos182

FUSION OF SECRETORY GRANULES WITH PLANAR LIPID BILAYER MEMBRANES. ((A.Chanturiya, #M.Whittaker and J.Zimmerberg)) LTPB, NIH, Bethesda, MD 20892; # Dept. of Physiology UCL, England. (Spon. by K.Ingham)

Fusion of sea urchin egg secretory granules to phospholipid vesicles requires neither cytoplasmic proteins nor plasma membrane proteins (Vogel et al., JBC, 1992). We developed three new assays to monitor the binding and fusion of granules to planar phospholipid bilayer membranes (BLM). DIC microscopy was used for observation of granules binding to BLM. Binding did not require calcium. Membrane merger was monitored by first incubating granules with either amphotericin B or digitonin, then applying them to the BLM and registering co-incident a) jumps in membrane conductance and b) loss of contents of granules by DIC microscopy. Granule content discharge across the BLM was detected by placing the calcium indicator Calcium Green II in the *trans* compartment, and then measuring the increase of fluorescence due to calcium released *trans* from granules. Fusion was detected when calcium was added *cis* or when both calcium and calcium ionophore were added *trans*. Pre-incubation of granules with NEM abolished calcium-induced fusion. No conductance changes accompanied fusion unless granules were treated with exogenous ionophore, so granular membranes are devoid of open channels. Fusion was also detected when granules were osmotically swollen to the point of lysis. In contrast, no fusion of granules to BLM was seen when granules on plasma membrane (native cortices) were applied to BLMs despite good binding of granules to the BLM and fusion of granules to the plasma membrane. We suggest that cortical granules have sufficient calcium-sensitive proteins for fusion to lipid membranes, but in native cortices granular fusion sites are oriented toward the plasma membrane. Removal of granules from the plasma membrane may allow fusion sites access to new membranes.

W-Pos183

CALCIUM SENSITIVITY OF EXOCYTOSIS *IN VITRO* IS HETEROGENEOUS: A RAPID-FLOW STUDY. ((D. Kaplan, P.S. Blank, M.S. Cho, I. Steinberg, and J. Zimmerberg)) LTPB, NICHD, NIH Bethesda, MD 20892.

Why does fusion cease in the presence of a constant level of calcium? Fusion is ultimately irreversible; any finite fusion rate should lead to completion given enough time. However, in the sea urchin egg, secretory granules are docked and ready to fuse for months yet do not fuse. Cooperativity to calcium can explain this, but cannot explain partial fusion at constant low calcium. The extent of fusion is a function of the calcium concentration in the sea urchin egg planar cortex, which is mainly comprised of plasma membrane and docked secretory granules. Alternative hypotheses to explain the cessation of fusion include inactivation to calcium and heterogeneity in granular calcium thresholds. To test these hypotheses, a chamber which allows fast perfusion of solutions was designed. Exocytosis in vitro was measured as light scattering. Following initial fusion at low calcium, no further fusion was seen with repeated stimulation of cortices with the same calcium concentration, with or without intervening EGTA washes. More fusion was obtained only at a higher calcium concentration in a subsequent perfusion. The final extent of fusion after two pulses was nearly the same as that obtained with a single pulse to the same higher calcium concentration. Inactivation is not the cause of the cessation of fusion at low calcium: the fusion machanism is heterogeneous in its response to calcium.

W-Pos184

THE RATE OF EXOCYTOSIS ELICITED BY CALCIUM CURRENT IN PRESYNAPTIC TERMINALS. ((H. von Gersdorff and G. Matthews)) Dept. of Neurobiology, SUNY, Stony Brook, NY 11794.

Calcium-dependent exocytosis was studied by measuring the associated increase in membrane capacitance in single giant synaptic terminals of goldfish retinal bipolar neurons. To drive secretion, Ca current was activated with depolarizing voltage-clamp pulses of varying duration, and the size of the resulting capacitance increase was measured (see Fig.). The capacitance response increased approximately linearly with pulse duration up to ~200 msec; increases in duration beyond 200 msec produced no further increase in capacitance response. The ceiling amplitude was about 150 fF (dashed line), which we take to represent the size of the readily releasable pool of vesicles in the terminal. For 50-nm vesicles, this corresponds to ~2,000 vesicles, or about 30 vesicles for each of the ~60 ribbon-type output sites. The solid line fitted to the data for durations ≤200 msec has a slope of 730 fF/sec, which translates to about 10,000 vesicles/sec. The data could also be fitted, although not as well, by a single exponential with a time-constant of 124 msec; assuming 2,000 vesicles in the releasable pool, this time-constant corresponds to an initial rate of ~16,000 vesicles/sec.

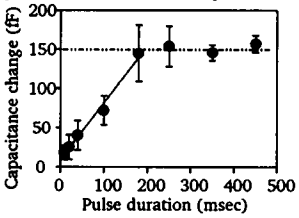

Fig. Relation between duration of depolarisation and size of capacitance increase elicited by a single depolarising pulse. Data points show the mean response (± sem) from 5-27 terminals. For durations ≤100 msec, responses to 5-25 individual pulses were averaged for each terminal to reduce noise.

(Supported by NIH grant EY03821 and NRSA Fellowship EY06506)

W-Pos185

INFLUENCE OF $[Ca^{2+}]_i$ AND GTPγS CONCENTRATION ON DIFFERENT FUSION PROCESSES IN HORSE EOSINOPHILS. ((J. Hartmann and M. Lindau)) MPI f. Med. Research, D - 69028 Heidelberg

In eosinophils intracellular application of GTPγS with a whole cell patch pipette stimulates exocytosis as well as intracellular granule-granule fusion, as indicated by very large (> 0.5pF) capacitance steps during degranulation. At 2 μM $[Ca^{2+}]_i$ the time course of exocytosis is not influenced by the GTPγS concentration but the large steps occur only at 80 μM and not at 20 μM GTPγS [Scepek and Lindau, EMBO J. 12:1811(1993)]. At low $[Ca^{2+}]_i$ (10 mM EGTA, no Ca^{2+} added) both, the average delay before exocytosis of the first specific granule, and the mean time between capacitance steps, are increased about 3 fold, indicating a decreased rate of exocytosis. Furthermore, the initial expansion of the fusion pores is slower at low $[Ca^{2+}]_i$. At low $[Ca^{2+}]_i$ large steps also occur at 20 μM GTPγS such that the contribution of single granules to the capacitance increase is reduced by half and several large steps occur instead. At 80 μM the number of large steps is further increased. These results indicate that granule-granule fusion is also activated by 20 μM GTPγS. However, the rate of granule-granule fusion is slow, such that at high $[Ca^{2+}]_i$ degranulation is complete before significant granule-granule fusion has occurred. At low $[Ca^{2+}]_i$ the slow degranulation allows more time for granule-granule fusion to occur before exocytosis. These results indicate a different sensitivity of these two fusion processes for $[Ca^{2+}]_i$ and GTPγS. In addition an increased number of endocytic events was observed at low $[Ca^{2+}]_i$.

Supported by DFG Sfb 312/B6, Sfb 352/C5.

W-Pos186

Ca^{2+}-INDEPENDENT-RESERPINE-SENSITIVE-^{3}H-NORADRENALINE RELEASE EVOKED BY INTRACELLULAR ACIDIFICATION IN RAT BRAIN SLICES. ((Sergio Sanchez-Armass and Josefina Gonzalez)). Dept. Fisiologia, Fac. de Medicina, Univ. San Luis Potosi, Mexico.

The purpose of this work is to evaluate the effect of the intracellular pH (pH_i) on the release of ^{3}H-noradrenaline (^{3}H-NA) in rat brain slices. Rat brain slices preloaded with ^{3}H-NA were superfused with a HCO_3^- Ringer solution, pH 7.4. The superfusion with sodium acetate (naOAc) 50 mM in Ca^{2+}-free + 100 μM EGTA-Ringer solution (RS) pH_o 6, induces an increment of the release of 0.015 min^{-1}. This increment is not abolished by 20 μM desmetil-imipramine + 10 μM pargiline to inhibit the neuronal reuptake and the monoamine-oxidase. The long superfusion with EGTA rules out the participation of intracellular Ca^{2+}-stores. The superfusion with NaOAc-RS pH_o 7.4 or RS pH_o 6 failed to promote the release of ^{3}H-NA. Reserpine 8 mg/Kg via i.p. 18 hrs before the experiment completely inhibits the ^{3}H-NA release induced by high K^+ or NaOAc. This result show that ^{3}H-NA must be store in the synaptic vesicles to be released by the intracellular acidification induced by NaOAc. These data suggest that H^+ may substitute Ca^{2+} ions in the exocytotic release of ^{3}H-NA.

Supported by CONACYT 06810-N and FAI-UASLP-C92.

W-Pos187

CHARACTERIZATION OF THIOL GROUPS REQUIRED FOR THE GTP-DEPENDENT FUSION OF RAT LIVER MICROSOMES. (A.V.Sokoloff, T.Whalley & J.Zimmerberg) LTPB, NICHD, NIH, Bethesda, MD 20892

GTP-triggered fusion of microsomes was strongly inhibited by sodium periodate and by D_{10}-PDP (2-pyridyl-disulfide-propionate activated dextran, M.W 10K). In both cases, the fusion activity was significantly restored by dithiothreitol. This indicates that the inhibition by periodate and by D_{10}-PDP was due to formation of disulfide bonds between protein thiols or between protein thiols and the reagent respectively. Periodate- and D_{10}-PDP-treated microsomes showed partial and nearly total protection of fusion activity, respectively, against NEM (N-ethylmaleimide), a thiol-specific reagent known to irreversibly inhibit fusion. A comparison of [^{3}H]NEM-labeled protein patterns in control microsomes and those treated with inhibitors revealed one protein, p32.5K, the labeling of which, in both cases was inversely correlated with the inhibition of fusion. These data show that fusion-related thiol groups in microsomal membranes are significantly exposed to the aqueous medium and suggest that p32.5 is a part of the fusion machinery.

W-Pos188

FUSION PORES CONNECTING INFLUENZA HA TRANSFECTED FIBROBLASTS TO PLANAR LIPID BILAYER. EFFECT OF HA SURFACE DENSITY.

((G.B. Melikyan, W.D. Niles, F.S. Cohen)) Rush Medical College, Chicago, IL 60612.

Fusion of influenza HA-transfected fibroblasts, cell lines HAb2 and GP4f, to horizontal planar lipid bilayers was studied by time-resolved admittance measurements. The conductance of the fusion pore connecting a cell to a voltage clamped planar membrane was calculated from in-phase, out-of-phase, and direct current admittance components. The kinetics and extent of transfected fibroblast-bilayer fusion were similar to those obtained previously for MDCK cells infected with influenza virus. After fusion was triggered by acidification, there was a delay time before the first fusion pore transiently formed, followed by repetitive pore flickering before a pore securely and irreversibly opened. Delay times to transient pore formation were less for HAb2 than GP4f cells, consistent with the higher density of HA for HAb2 cells. Also, these delay times decreased with increased extent of HA0 cleavage to its fusogenic form. In contrast, kinetic parameters characterizing pore enlargement after fusion, including the open time distribution of transient fusion pores and dwell time distribution of irreversibly open pores before their final enlargement, were not affected by HA density. We conclude that HA density affects the formation of fusion pores, whereas it is not important for the subsequent dilation of pores. Supported by NIH GM27367.

W-Pos189

RADIOMETRIC CALIBRATION OF VIDEO CAMERAS FOR QUANTITATIVE FLUORESCENCE RESONANCE ENERGY TRANSFER (RET) IMAGING MICROSCOPY.

((W.D. Niles & R.S. Cohen)) Department of Physiology, Rush Medical College, Chicago, IL 60612.

We are developing a RET video microscope to measure donor-acceptor probe distances in images of membrane adhesion and fusion. This requires determining the relation between input radiant intensity and output video brightness for the pair of intensifier-charge coupled device cameras used for recording the donor and acceptor emission images. Light from a 100 W Hg lamp was passed through a monochromator and focused alternately on the faceplate of an intensifier operating at a fixed gain voltage and on a calibrated silicon photodetector with spectral efficiency corrected radiometric output. The CCDs were operated with a preset black level to obviate autoblack correction. We have found that the brightness-radiance relations at all wavelengths are described by brightness = a (radiant intensity)^b, where a and b are constants set by the intensifier gain. These functions are valid over the entire range of input radiances, including within a factor of 10 of the input sensitivity. With these relations, the donor and acceptor brightnesses recorded by the video cameras are transformed to input radiances. After correction for the spectral transfer functions of the separate emission pathways, the input radiances yield RET rate constants at each point in the object plane, and, in a model-dependent fashion, determine donor-acceptor distances. Supported by GM27367.

W-Pos190

ENDOCYTOSIS BY ATRIAL MYOCYTES: REGULATION AND IDENTIFICATION OF ACIDIFIED VESICULAR STRUCTURES IN THE LYSOSOMAL PATHWAY.

((E. Page, G. E. Goings and D. A. Hanck)) University of Chicago, Chicago, IL 60637.

Under conditions in which cytosolic uptake of Lucifer Yellow (LY, 0.5 mg/ml) via plasma membrane channels or carriers was absent, 8-day-old primary cultures of atrial myocytes (PCAM) from adult rats, incubated at 37°C for 10 min in M199 with 10% fetal bovine serum, took up LY into peripheral cytoplasmic structures which were readily distinguishable by fluorescence microscopy from intrinsic perinuclear autofluorescence. Electron microscopy (EM) of PCAM fixed after only 2 min exposure to LY showed classical presumptive early endosomes fused with coated vesicles, which were absent without LY, suggesting that LY turned on endocytosis. Endocytosis of LY could be prevented by a 10 min preincubation in medium containing 1 nM calyculin A or 0.1 μM Na okadaiate or by lowering the temperature to 2°C, consistent with an energy-dependent process and involvement of type 1 and/or type 2a phosphoprotein phosphatases. 1 μM staurospine, 0.1 μM pertussis toxin, 0.1 μM phorbol myristate acetate, or a combination of ryanodine, lowered $[Ca]_o$ and nifedipine, or reducing temperature to 20°C did not prevent LY internalization. Immunofluorescence microscopy of PCAM using four different antibodies (to clathrin, Dictyostelium vacuolar H^+-ATPase, the acidity-indicating weak base DAMP, and atrial natriuretic peptide) and immuno-EM of thin sectioned atria with antibodies against DAMP showed that atrial granules and lysosomes are acidified, and suggested that LY fluorescence does not codistribute with ANP in atrial granules. No evidence for LY internalization via nonclathrin-coated vesicles was obtained. Supported by USPHS-NHLBI 10503.

W-Pos191

TRISKELION STRUCTURE AND CLATHRIN LATTICE TRANSFORMATIONS.

A.J. Jin and R. Nossal. Physical Sciences Laboratory, DCRT, National Institutes of Health, Bethesda, MD 20892

Clathrin triskelion lattice shape transformations give rise to the successive bugging of coated versicles from the interiors of flat coated-pits during *receptor mediated endocytosis*. Recent analysis shows that topological rules strongly constrain such lattice transformations and, in particular, imply that vesicle growth occurs via a mechanism of step-wise, pair addition of triskelions from the cytoplasm [1]. To justify the above proposal, we derive several general topological equations and illustrate their implications. Among these equations is the relationship $\Delta F = \Delta V/2$, where ΔF represents the number of faces added to a growing lattice, and ΔV represents the number of new vertices (which equals the number of added triskelions). The structure of clathrin triskelions determines important energetics relevant to the process. We introduce an elastic modal analysis that explains various structural variations noted when triskelions are observed by electron microscopy.

[1] A.J. Jin and R. Nossal, Topological Mechanisms Involved in the Formation of Clathrin Coated Vesicles, 1993, Biophys. J. 65:1523-1537.

MEMBRANES - BILAYERS AND OTHER MODELS III

W-Pos192

PARTITIONING OF CHOLESTEROL BETWEEN GEL AND FLUID PHASES IN MODEL MEMBRANES.

((Charles Spink and Michael Breed)) Chemistry Department, SUNY-Cortland, Cortland, NY 13045.

Interactions between cholesterol and phospholipids can be studied by examining the thermodynamics of transfer of cholesterol between gel and fluid phases of thermally active lipids. We report here some new measurements of the free energy, enthalpy and entropy of transfer of cholesterol between gel and fluid phases of dimyristoyl-, dipalmitoyl-, distearoyl-, and diarachidoyl-phosphaditylcholine at the corresponding transition temperatures of the phospholipids. The data are obtained from differential scanning calorimetry in dilute mixtures (<0.04% cholesterol). From the concentration dependence of T_t and ΔHc, it is possible to get the transfer parameters using a "regular" solution model. Values of Kp, the gel-fluid partition coefficient vary from 2.3 to over 6. The results will be discussed in terms of the packing of cholesterol in the bilayer and its effects on the thermodynamics of transfer.

W-Pos193

A REINVESTIGATION OF THE PHASE BEHAVIOR OF CHOLESTEROL/DIPALMITOYLPHOSPHATIDYLCHOLINE BILAYERS

((T.P.W. McMullen, R.N.A.H. Lewis and R.N. McElhaney)), Dept. of Biochemistry, University of Alberta, Edmonton, Canada T6G 2H7.

We have reinvestigated the effect of cholesterol on the thermotropic phase behavior of aqueous dispersions of dipalmitoylphosphatidylcholine (DPPC) using high-sensitivity differential scanning calorimetry. In annealed DPPC vesicles the subtransition persists until cholesterol concentrations of 15-20 mol %, but the pretransition is abolished above cholesterol concentrations of 5 mol %. Moreover, the main phase transition consists of overlapping sharp and broad components at all cholesterol concentrations between 1 and 20 mol % (the sharp components arises from the chain-melting of pure DPPC domains and the broad components arises from the melting of cholesterol containing DPPC domains). However, the temperature, enthalpy and cooperativity of both components change monotonically with changes in cholesterol concentration. Thus the apparent increase in cooperativity previously observed at 7.5 mol % cholesterol (Vist and Davis, *Biochemistry* 29 [1990] 451-464) is an experimental artifact. We therefore conclude that there is no eutectic point at 7.5 mol % cholesterol in the cholesterol/DPPC phase diagram and that the "liquid-ordered" phase exists at very low cholesterol concentrations. Our findings will be summarized in a new version of the cholesterol/DPPC phase diagram. (Supported by the Medical Research Council of Canada and the Alberta Heritage Foundation for Medical Research.)

W-Pos194

EFFECTS OF CHOLESTEROL ON THE PACKING DENSITY HETEROGENEITY OF PHOSPHOLIPID BILAYERS STUDIED BY *TRANS*-PARINARIC ACID FLUORESCENCE DECAY.

((C.R.Mateo[1,2], J.C.Brochon[1] and A.U.Acuña[2])). [1]CNRS, URA 1131, Groupe de Biofluorescence, Université Paris Sud Orsay, France and [2]Instituto de Química Física, CSIC, Madrid, Spain. (Spon. by G.Rivas).

The fluorescent probe *trans*-parinaric acid (*t*-PnA) shows a specific fluorescence lifetime distribution depending directly on the lipid phase composition of the bilayer (Mateo et al, *Biophys.J.* 65, 1993). Taking advantage of this property we have investigated the effects of cholesterol in the fluid phase of DMPC and POPC LUVs, over the 0-40 molar % range of cholesterol compositions. Fluorescence decays were measured using the SA1 beam line of the synchrotron radiation machine Super-ACO of Orsay. Data were analysed by the Quantified Maximum Entropy Method. The lifetime distribution of *t*-PnA in both DMPC and POPC LUVs was bimodal at low cholesterol concentrations, and similar to that observed in a pure fluid phase. From 10 to 30 mol % cholesterol the lifetime pattern shows a third long lifetime component. The contribution of this lifetime component was dependent of temperature and cholesterol concentration and reached its maximum value at 30-40 % cholesterol. Results confirm that cholesterol induces in the fluid phase of DMPC the formation of a liquid ordered phase and show that a similar effect is induced in the unsaturated phospholipid POPC. Liquid-ordered phase and fluid phase coexist in a wide range of cholesterol concentrations and become miscible above 30 % cholesterol. The physical properties of both phases have been determined from time-resolved fluorescence anisotropy experiments. DMPC/cholesterol and POPC/cholesterol partial phase diagrams are also proposed.

W-Pos195

EFFECT OF HYDROSTATIC PRESSURE ON THE LATERAL DISTRIBUTION OF CHOLESTEROL IN LIPID BILAYERS:A TIME-RESOLVED FLUORESCENCE SPECTROSCOPY STUDY.

((P.Tauc, C.R.Mateo and J.C.Brochon)). CNRS, URA 1131, Groupe de Biofluorescence, Univ. Paris Sud Orsay, France. (Spon. by M.Velez).

The fluorescence kinetics of the natural lipid *trans*-parinaric acid (*t*-PnA) has been used to study the effect of hydrostatic pressure on the phase behavior of the binary mixture POPC/cholesterol, over the 0-40 molar % range of cholesterol compositions. For this system, at atmospheric pressure and above the transition temperature (-5°C), cholesterol is segregated in cholesterol-rich and poor domains in the lateral plane of the membrane. Pressurized samples were excited with a Ti-sapphire sub-picosecond laser and fluorescence decays were analyzed by the Quantified Maximum Entropy Method. At each temperature and cholesterol concentration, below the transition pressure, the fluorescence lifetime distribution pattern of *t*-PnA is clearly modulated by the pressure changes. From the parameters of these lifetime distributions we have determined, at a given temperature, the partial phase diagram of the POPC/cholesterol mixture as a function of pressure. The diagram shows that pressure increases the fraction of cholesterol-rich domains in the lipid bilayer but it decreases the amount of cholesterol in these domains.

W-Pos196

EVIDENCE FOR TAIL-TO-TAIL CHOLESTEROL DIMERS IN DIPALMITOYLPHOSPHATIDYLCHOLINE BILAYERS ((J.S. Harris, D.E. Epps, S.R. Davio, G.M. Maggiora*, and F.J. Kézdy)). Upjohn Laboratories, 7000 Portage, Kalamazoo, Mich. 49001

The behavior of multilamellar (MLV) liposomes of dipalmitoylphosphatidylcholine (DPPC) was studied by differential scanning calorimetry (DSC) in the presence of ≤ 5 mole% of methyl oleate (MO) or cholesterol (CH). In this concentration range, the melting curves do not indicate any partitioning of the solutes between the s_o and the l_d phases, rather, they suggest that the solutes are soluble only in the l_d phase. The slopes of the T_m versus composition confirm this conclusion: For an ideal cryoscopic system, the melting point depression constant, K_f, can be calculated *a priori* from the experimentally measured heat of fusion per gram DPPC, l_f, and the melting point of pure DPPC, T_o: $K_f = RT_o^2/(1000 \cdot l_f) = 12.3 \pm 0.9$ K•g•M^{-1}•cm^3. With methyl oleate (MO) as the solute, we find that $K_f = 12.9 \pm 0.8$ K•g•M^{-1}•cm^3. Thus MO forms an ideal cryoscopic system with DPPC MLV's: It is fully miscible with the l_d phase but is totally insoluble in the s_o phase. The T_m vs. CH concentration plot yields a straight line and, using the experimental value of K_f, we calculate from the slope of an apparent MW of 715 ± 119 for CH. The simplest interpretation of these results is that CH is insoluble in the s_o phase and it is fully dimerized when dissolved in the l_d phase. From space-filling considerations, we propose that the dimer is an interlamellar one. Such a dimer of CH would be consistent with a variety of observations reviewed by Sankaram and Thompson [*Biochemistry* **29**, 10676-10684 (1990)]. Since CH is insoluble in the s_o phase, it must form below T_m a separate phase or separate domains. The domains, however, should not be too small since the relatively large boundary region of the microdomains would affect the thermodynamic stability of the solid phase. Extrapolation of the interlamellar CH dimer model to biological membranes yields new insights into the physical properties of phospholipid:CH bilayers.

W-Pos197

CHOLESTEROL STABILIZES BILAYER MEMBRANE STRUCTURE AFTER RADIATION DAMAGE. ((T. Parasassi, A.M. Giusti, M. Raimondi, G. Ravagnan, O. Sapora* and E. Gratton**)) Istituto di Medicina Sperimentale, CNR, Roma, Italy; *Istituto Superiore di Sanita', Roma, Italy; **Laboratory for Fluorescence Dynamics, Dept. of Physics, Univ. of Illinois at U-C, Urbana, IL 61801.

X-ray irradiation of unsaturated phospholipid vesicles produces oxidative damage. The width of DPH lifetime distribution is a sensitive reporter of the produced damage at dose as low as 0.5 Gy (Parasassi et al., *Int. J. Radiat. Biol. 59*, 1991, 59-69 & *61*, 1992, 791-796). A linear relationship between the width of DPH lifetime distribution and the logarithm of the radiation dose has been observed. In dioleoyl- and dipalmitoleoyl-phosphatidylcholine vesicles, the width of DPH lifetime distribution decreases from approximately 1 ns to about 0.05 ns after a dose of 110 Gy. This reduction is due to the confinement of DPH molecule deep in the membrane interior, induced by oxidative defects present in the phospholipid acyl chains. In vesicles containing 30 mol% cholesterol, the reduction of the width of DPH lifetime distribution after irradiation has not been observed. This failure in the confinement of the DPH molecule in the bilayer interior is probably due to the homogenizing effect of cholesterol. The cholesterol molecule can compensate for the oxidative damage, promoting a closer packing of the bilayer. The possibility also exists that at 30 mol% cholesterol, oxidative damages are strongly reduced. At this cholesterol concentration we have measured a decreased concentration of water in the bilayer and a decreased oxygen diffusion.

Supported by National Institutes of Health grant RR03155 and CNR.

W-Pos198

CHOLESTEROL MODIFIES PHASE PROPERTIES OF PHOSPHOLIPID BILAYERS AND CREATES LOCAL ORDER AT CRITICAL CONCENTRATIONS. ((T.Parasassi, M. Loiero, A.M. Giusti, G. Ravagnan and E. Gratton*)) Istituto di Medicina Sperimentale, CNR, Roma, Italy; *Laboratory for Fluorescence Dynamics, Dept. of Physics, Univ. of Illinois at U-C, Urbana, IL 61801.

The effect of cholesterol on gel, liquid-crystalline and mixed phases of phospholipid bilayers was studied using the fluorescence of 2-dimethylamino-6-lauroylnaphthalene (Laurdan). Laurdan steady-state excitation and emission spectra change with the polarity and dynamics of molecules in its environment, i.e., with the amount of dipolar relaxation. By Laurdan Generalized Polarization, the coexistence of phospholipid phase domains is detected and each phase is quantitated. After the addition of cholesterol, Laurdan response shows 1) a decrease of polarity and an increase of the amount of dipolar relaxation in gel phase; 2) a decrease of both the polarity and the amount of dipolar relaxation in liquid-crystalline phase; and 3) in bilayers composed of coexisting gel and liquid-crystalline phases, the dynamic properties of both phases are modified to such an extent as to prevent the detection of their coexistence. Above 15mol% and at physiological cholesterol concentrations, ≥30 mol%, no separate Laurdan fluorescence signals, characteristic of distinct domains can be observed. Laurdan excitation and emission spectral contours as a function of cholesterol concentration show some cholesterol concentrations at which Laurdan spectral properties changes discontinuously. These peculiar cholesterol concentrations are in agreement with recent observations of other authors (Somerharju et al., 1985; Tang and Chong, 1992), showing the formation of local order in the liquid-crystalline phase upon addition of pyrene-PC. Supported by National Institutes of Health grant RR03155 and CNR.

W-Pos199

CHOLESTEROL'S INTERFACIAL INTERACTIONS WITH SPHINGOMYELINS, GALACTOSYLCERAMIDES, AND PHOSPHATIDYLCHOLINES: CONDENSATION AND COMPRESSIBILITY MEASUREMENTS. ((J. M. Smaby, H. L. Brockman, S. Ali, and R. E. Brown)) The Hormel Institute, Univ. of Minnesota, Austin, MN 55912.

To evaluate the relative contributions of the headgroup, ceramide, and diacylglycerol regions in interactions of simple sphingolipids and phospholipids with cholesterol (Chol), we measured the mean molecular condensation and compressibility of Chol-sphingomyelin (SM), Chol-galactosylceramide (GalCer), and Chol-phosphatidylcholine (PC) mixed monolayers at 24°C. Various molecular species of SM, GalCer, and PC were studied which exhibit liquid-expanded (LE), liquid-condensed (LC), or both LE and LC phase behavior in their surface pressure versus molecular area (π-A) isotherms. In instances where SM, GalCer, or PC form LE monolayers, cholesterol induces greater condensation and compressibility changes than in LC films regardless of headgroup structure. Maximal interaction of cholesterol was observed in LE species containing saturated acyl chains compared to LE species containing *cis* double bonds at acyl locations that could interfere with chain-chain and chain-cholesterol packing via van der Waals interactions. Headgroup structural effects were then compared under conditions of comparable monolayer phase state and similar acyl structure. Cholesterol's condensation of either SM or PC was 25-30% greater than that of GalCer. However, no difference was observed in cholesterol's condensation of SM compared to PC. (Supported by USPHS Grants GM-45928, HL-49180, and the Hormel Foundation)

W-Pos200

CHOLESTEROL CONDENSATION OF α-LINOLENIC AND γ-LINOLENIC ACID-CONTAINING PHOSPHATIDYLCHOLINE MONOLAYERS AND BILAYERS.
((W. D. Ehringer*, S.R. Wassall# and W. Stillwell*)) Departments of Biology* and Physics#, Indiana University-Purdue University at Indianapolis, Indianapolis, IN 46202

Cholesterol is demonstrated to condense phosphatidylcholine (PC) monolayers and bilayers containing stearic acid in the sn-1 position and α-linolenic acid in the sn-2 position (18:0, α-18:3 PC) but has no effect on PCs where γ-linolenic acid replaces α-linolenic acid (18:0, γ-18:3 PC). Cholesterol-induced condensation is measured by area/molecule determinations made on monolayers using a Langmuir trough while condensation in bilayers is followed by the fluorescent dyes merocyanine (MC540), and dansyl-lysine. Permeability to erythritol is also demonstrated to be diminished by cholesterol for the condensable 18:0, α-18:3 PC bilayer membranes but not the 18:0, γ-18:3 PC membranes. The interaction of cholesterol with the linolenic acids was also monitored by differential scanning calorimetry. α and γ linolenic acid are 18-carbon, three unsaturation isomers which differ only in the location of the unsaturations. Here lipid-cholesterol interaction is used to distinguish the effect of position of unsaturation on membrane structure.

W-Pos201

FORMATION OF SUBGEL IN PHOSPHATIDYLGLYCEROLS.
((Phoebe Dea, Xuemei Huang, and Ma May Chit)), Department of Chemistry, Occidental College, Los Angeles, CA 90041 and Department of Chemistry and Biochemistry, California State University, Los Angeles, CA 90032.

Investigations by high-sensitivity differential scanning calorimetry (DSC) and fluorescence spectroscopy have shown that the subgel (Lc) phase in phosphatidylglycerols may be induced by suspending the phosphatidylglycerol at about 5°C in a 25 mM phosphate buffer, pH 7.4. The subtransition from the Lc phase to the planar gel phase can be observed only on the first heating scan, indicating that the reversibility of the transition is slow. The fluorescence intensity of the fluorescent probe 1,3-diphenyl-1,3,5-hexatriene (DPH) in the phosphatidylglyerol subgel is considerably lower than that observed in the gel phase. The presence of low concentrations of ethanol is found to stabilize the subgel phase.

W-Pos202

KINETICS OF SUBGEL FORMATION IN DPPC: X-RAY DIFFRACTION PROVES NUCLEATION-GROWTH HYPOTHESIS.
((S. Tristram-Nagle*, R.M. Suter+, W.-J. Sun+ and J.F. Nagle*+)) Departments of Biological Sciences* and Physics+, Carnegie Mellon University, Pittsburgh, PA 15213.

Wide-angle and low-angle X-ray diffraction data were obtained during the time course of the gel to subgel phase transformation in fully hydrated dipalmitoylphosphatidylcholine (DPPC) multilamellar vesicles. When the system was kept close to equilibrium by following a temperature-jump protocol (1,2), the X-ray data unequivocally demonstrate the coexistence of growing subgel and shrinking gel domains. When the system was supercooled and held further from equilibrium as in previous studies (3,4), the kinetic behavior was more complicated. These data prove that the basic mechanism for the gel to subgel phase transformation is one of nucleation of subgel domains followed by growth of the domains. It is also interesting to note that the subgel phase transformation kinetics are extremely sensitive to radiation damage.

(1) S. Tristram-Nagle et al. (1987), Biochemistry 26, 4288-4294.
(2) C.P. Yang and J.F. Nagle (1988), Phys. Rev. A 37:3993-4000.
(3) M.J. Ruocco and G.G. Shipley (1982), BBA 691:309-320.
(4) M. Akiyama et al. (1987), J. Appl. Phys. (Japan) 26:1587-1591.
This work was supported by Grant GM-44976 from the US National Institutes of Health.

W-Pos203

COEXISTENCE OF FLUID LAMELLAR PHASES IN A PS/PC MIXTURE.
((A. K. Hinderliter and G. W. Feigenson)) Dept. of Biochem, Cornell University, Ithaca, N.Y. 14853.

We have found fluid-fluid lamellar phase separation in model membrane systems of the binary mixture (12:1,12:1)PC and (16:0,18:1)PS. The experimental method is an equilibrium calcium ion binding procedure (Huang et al., Biophys. J. 64. 1993). The aqueous free calcium ion concentration, $[Ca^{+2}]_{aq}$, is measured as a function of the lipid composition of the mixture. The value of $[Ca^{+2}]_{aq}$ will become invariant if an additional phase appears. $[Ca^{+2}]_{aq}$ was measured using the chromophoric calcium chelator BAPTA or BrBAPTA. This use of the measurement of $[Ca^{+2}]_{aq}$ is analogous to the use of the measurement of partial pressures to detect phase separation and to determine phase boundaries in binary liquid mixtures. The $[Ca^{+2}]_{aq}$ is invariant at 55 nM from PS/PC = 0.65/0.35 to 0.52/0.48 in 100 mM KCl, 20 mM PIPES. The $[Ca^{+2}]_{aq}$ is invariant at 750 nM from PS/PC = 0.80/0.20 to 0.50/0.50 in 800 mM KCl. 20 mM PIPES. The increased ionic strength screens the PS-PS electrostatic repulsion, thereby expanding the region of phase separation. The finding of PS/PC phase separation clearly confirms the analysis of Huang et al. that PS/PC mixtures show clustering of like lipids. The coexisting lipid phases were confirmed to be fluid-fluid lamellar by X-ray diffraction experiments at the Cornell High Energy Synchrotron Source.

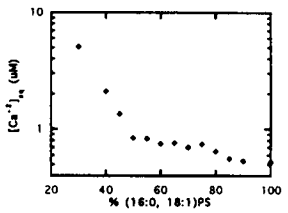

W-Pos204

STERIC INTERACTIONS BETWEEN GEL AND LIQUID CRYSTALLINE PHOSPHATIDYLCHOLINE BILAYERS CONTAINING LIPIDS WITH COVALENTLY ATTACHED POLYETHYLENE GLYCOL
((A. K. Kenworthy[1], T. J. McIntosh[1], K. Hristova[2] and D. Needham[2])) [1]Dept. of Cell Biology, Duke University Medical Center, Durham, NC 27710 and [2]Dept. of Mechanical Engineering, Duke University, Durham, North Carolina 27708

We have measured the range and magnitude of steric interactions between bilayers containing lipids with covalently attached polyethylene glycol (PEG-lipids) as a function of (1) PEG molecular weight, (2) PEG-lipid concentration, and (3) the mechanical properties of the bilayer "surface" to which the PEG is attached. We have used x-ray diffraction of osmotically stressed multilamellar liposomes to measure the distance dependence of the repulsive pressures between phosphatidylcholine/PEG-lipid bilayers as a function of PEG-lipid concentrations up to 20 mol%, for PEG's with molecular weight ranging from 350 to 5000 Da. At a constant applied pressure, the fluid space increased with PEG lipid concentration and PEG molecular weight, while for a given PEG lipid concentration and PEG molecular weight the fluid space decreased with increasing applied pressure. For example, at an applied pressure of $1x10^5$ dyn/cm^2 the fluid space was increased 110 Å over control by 10 mol% PEG-2000. The range and magnitude of the repulsive pressures for gel and liquid crystalline membranes containing PEG 2000 showed a nearly identical dependence on PEG-lipid concentration. The pressure-distance data are being modelled using current theories for the behavior of surface-grafted polymers.

W-Pos205

EFFECTS OF LIPIDS WITH COVALENTLY ATTACHED POLYETHYLENE GLYCOL ON DISTEAROYLPHOSPHATIDYLCHOLINE BILAYER STRUCTURE.
((A. K. Kenworthy[1], S. A. Simon[2] and T. J. McIntosh[1])) [1]Department of Cell Biology and [2]Departments of Neurobiology and Anesthesiology, Duke University Medical Center, Durham, North Carolina 27710

The structural and interactive properties of membranes containing lipids with covalently attached polyethylene glycol, or PEG-lipids, are of interest both for their evolving role as drug delivery vesicles and as a model system for investigating the properties of surface-grafted polymers. We have used x-ray diffraction, differential scanning calorimetry, and ^{31}P NMR to generate phase diagrams for mixtures of distearoylphosphatidylcholine (DSPC) and distearoylphosphatidylethanolamine-PEG lipids, where the attached PEG's ranged in molecular weight from 350-5000 Da. Electron density profiles and wide-angle reflections from x-ray diffraction patterns of osmotically stressed multilamellar vesicles show that up to 15 mol% of all of these PEG lipids can be added to DSPC without changing bilayer structure from the tilted Lβ' gel phase, although the fluid space between apposed bilayers increases dramatically with increasing PEG molecular weight and concentration (see accompanying poster, Kenworthy et al.). Furthermore, these concentrations of PEG lipid do not significantly change the temperature of the main DSPC phase transition. However, at higher PEG-lipid concentrations, the lipid organization depends on the molecular weight of the attached PEG. For instance, dispersions containing either 30 mol % PEG 350 or 20 mol % PEG 750 form an interdigitated LβI gel phase, whereas dispersions containing 20 mol% PEG 1900 or PEG 5000 form a mixed Lβ and isotropic phase.

W-Pos206

PERMEABILITY OF TWO-COMPONENT, TWO-PHASE LIPID BILAYERS.
((Stéphane G. Clerc and Thomas E. Thompson)) Department of Biochemistry, University of Virginia, Charlottesville, VA 22908.

The passive permeation of a small zwitterionic molecule, methylphosphoethanolamine, across two-component phospholipid bilayers (dimyristoylphosphatidylcholine / dipalmitoylphosphatidylcholine (DPPC) mixtures) exhibits a maximum when gel domains and fluid domains coexist. The permeability data of the two-phase bilayers cannot be fitted to single rate kinetics, but are consistent with a gaussian distribution of rate constants. The logarithm of the mean permeability rate constant correlates with the fraction of interfacial lipids, and decreases linearly with the mole fraction of DPPC. The fraction of lipid molecules at the gel-fluid interface can be estimated to a good approximation from the excess heat capacity functions obtained by differential scanning calorimetry, using the deconvolution theory of Freire and Biltonen (*B.B.A.* (1978) 514 54). These experiments suggest that small polar molecules can cross the membrane at the interface between gel and fluid domains at a much faster rate than through the homogeneous phases; the acyl chains located at the domain interface experience lateral density fluctuations that are inversely proportional to their average length, and large enough to allow rapid transmembrane diffusion of the solute molecules. The distribution of the permeability rate constants may reflect temporal and spacial fluctuations of the lipid composition at the phase boundaries. (Supported by NIH grant GM-14628)

W-Pos207

DETERMINATION OF THE PENETRATION DEPTH OF THE PYRENYL MOIETY OF ACYL-LABELED PHOSPHATIDYLCHOLINES IN LIQUID CRYSTALLINE BILAYERS.
((J. Virtanen[1], M. Sassaroli[2], M. Ruonala[3], M. Vauhkonen[3], P. Somerharju[3])) [1]Dept. of Chem., Univ. of California at Irvine, CA. [2]Dept. of Physiol. and Biophys., Mt. Sinai School of Medicine, New York, NY. [3]Dept. of Med. Chem., Univ. of Helsinki, Helsinki, Finland.

1-Palmitoyl-2-pyrene-*n*-acyl phosphatidylcholines (pyr$_n$PC) have been widely used probes of membrane structure and dynamics, to measure lipid translational diffusion, via the excimer formation technique, and as resonance energy transfer acceptors from tryptophan in membrane-protein association studies. Yet, the bilayer depths of the pyrenyl moieties of these probes have never been measured. In an attempt to determine the location of the fluorophores, we have measured the quenching of the fluorescence of a series of pyr$_n$PC (n= 4 to 14) introduced at low mole fraction, x=0.001, in POPC bilayers containing various mole fractions (0 to 1) of 1-palmitoyl-2-dibromostearoyl phosphatidylcholines (BRPC). Three BRPC were used, with Br atoms at positions 6,7 or 9,10 or 11,12. The positions of the Br atoms of these BRPC within the bilayer are known from x-ray diffraction experiments. The quenching was determined to be dynamic by time-resolved fluorescence measurements. By modeling both the Br and pyrene depth distributions as gaussian functions, the center and the width of the pyrene depth distributions were determined. The effect on these parameters resulting from the addition of 50 mol% cholesterol to the bilayers was also investigated.

W-Pos208

STRUCTURAL AND THERMOTROPIC PROPERTIES OF HYDROXY AND NON-HYDROXY FATTY ACID CERAMIDES
((Jyotsna Shah, Josephine Atienza, Anthony V. Rawlings* and G.Graham Shipley)) Department of Biophysics, Boston University School of Medicine, 80 East Concord Street, Boston MA 02118 and *Unilever Research, Edgewater NJ 07020

The structural and thermotropic properties of hydroxy (HFA) and non-hydroxy (NFA) ceramides (CER) have been studied using differential scanning calorimetry (DSC) and x-ray diffraction techniques. The DSC heating curve of the anhydrous HFA-CER shows a single, sharp endothermic transition at 94.6°C (ΔH=15.3 kcal/mol). At intermediate hydrations a double peak endotherm is observed at 86.4°C with a shoulder at 82.0°C. This shoulder increases with increasing hydration and at maximum hydration (72% water) only one endothermic transition is observed at 80.0°C (ΔH=8.5 kcal/mol). The x-ray diffraction pattern of hydrated HFA-CER at 20°C shows a lamellar structure with a bilayer periodicity d=60.7Å and three wide angle reflections at 4.3, 4.0 and 3.7Å, characteristic of a crystalline state. Above the main transition temperature, a reverse hexagonal (H_{II}) phase is observed. However, the heating scans of NFA-CER demonstrate two endothermic transitions at 81.3°C (ΔH=6.8 kcal/mol) and 85.9°C (ΔH=3.5 kcal/mol). With increasing hydration both transitions shift to lower temperatures and at maximum hydration (80% water) the endothermic transitions appear at 73.8°C (ΔH=5.1 kcal/mol) and 84.2°C (ΔH=5.8 kcal/mol). X-ray diffraction of NFA-CER (80% water) at 20°C shows a lamellar crystalline structure with a bilayer periodicity d=58.6Å and three wide angle reflections at 4.6Å, 4.2Å and 3.8Å. At 77°C, again a lamellar structure exists with reduced periodicity d=53.1Å and wide angle reflections at 4.6Å, 4.2Å and 3.8Å. Above the second endothermic transition, the low angle region shows only one reflection at 30.0Å and wide angle region shows a wide diffuse reflection at 4.6Å, indicative of melted chains. Thus, the HFA-CER show a simple phase behavior; below the transition temperature a lamellar crystalline phase exists and above the transition temperature a hexagonal phase is formed. However, the NFA-CER exhibit a more complex polymorphic phase behavior.

W-Pos209

X-RAY DIFFRACTION AND CALORIMETRIC STUDIES OF NON-HYDROXY FATTY ACID (16:0) CERAMIDE.
((Jyotsna Shah, Josephine Atienza, Zheng X. Dong* and G. Graham Shipley)) Department of Biophysics and *Department of Medicine, Boston University School of Medicine, 80 East Concord Street, Boston MA 02118

Differential scanning calorimetry (DSC) and x-ray diffraction techniques have been used to investigate the structural and thermotropic properties of non-hydroxy fatty acid (16:0) ceramide (NFA(C16)CER). NFA(C16)CER was studied as a function of hydration. The anhydrous NFA(C16)CER shows a single, broad endothermic transition at 95.4°C (ΔH=13.8 kcal/mol). On increasing the hydration a broad exothermic transition appears at ~50-60°C and the enthalpy of the main endothermic transition (at 90°C) remains constant at 13.8 kcal/mol. At maximum hydration the broad exothermic transition occurred in a range of 55-72°C (ΔH=4.8 kcal/mol). This polymorphic behavior depends on low temperature incubation time and cooling rate. X-ray diffraction at 26°C shows a well ordered lamellar phase with a bilayer periodicity d=46.9Å. At 70°C, again a lamellar phase is observed with a reduced bilayer periodicity d=41.8Å and an increased number of wide angle reflections indicative of better packing order. Above the main endotherm, the diffraction pattern shows a broad band at ~30Å. The wide angle region shows a diffuse band at 4.6Å, indicative of a melted chain phase. Our data demonstrate that NFA(C16)CER shows polymorphic behavior which involves the conversion of an hydrated liquid crystalline form into an intermediate metastable phase. On heating, this metastable phase converts exothermically into a stable phase and on further heating chain melting into a liquid crystalline phase occurs. Prolonged incubation of the sample at low temperature also facilitates the conversion of the metastable to stable phase.

W-Pos210

LIPID-INDUCED CHANGES IN MEMBRANE CURVATURE IN POPE/LYSOPC BILAYERS
((Wolfgang J. Baumann and Barbara Malewicz)) The Hormel Institute, University of Minnesota, Austin,MN 55912.

We have previously shown that 1-palmitoyl-2-oleoyl-*sn*-glycero-3-phosphocholine (POPC) and 1-palmitoyl-*sn*-glycero-3-phosphocholine (lysoPC) when sonicated in water form stable small unilamellar vesicles (SUV) over a wide range of concentrations (up to ~30 mol% lysoPC). The size of the POPC/lysoPC vesicles formed (250-265Å) was quite independent of the lipid ratio (*e.g.*, Kumar, Malewicz and Baumann, *Biophys. J. 55,* 789-792, 1989). We now found that in 1-palmitoyl-2-oleoyl-*sn*-glycero-3-phosphoethanolamine (POPE)/lysoPC SUV, containing 10-40 mol% lysoPC, membrane curvature is highly responsive to changes in membrane phospholipid composition. Optimal lipid packing in the outer bilayer leaflet of POPE/lysoPC SUV as monitored by ^{31}P NMR was attained at 25 mol% lysoPC at a vesicle size of 270Å when outside phospholipid head group motions were maximally restricted (POPE$_o$, T_2^* 14.5 ms; lysoPC$_o$, T_2^* 22.7 ms). With decreasing lysoPC mole percentage in the POPE/lysoPC SUV, vesicle size increased from 180Å at 30 mol% lysoPC to 535Å at 10 mol% lysoPC as the outer bilayer leaflet became lysoPC depleted. At 10 mol% lysoPC, ^{31}P T_2^* of outside (9.65 ms) and inside (15.9 ms) phospholipid head groups decreased significantly consistent with a decrease in vesicle rotational motion due to the increase in vesicle size. Our observation that in POPE/lysoPC bilayers, but not in POPC/lysoPC bilayers, membrane curvature can be changed by simply changing lipid composition seems relevant to the regulation of various cellular processes that take place in highly curved membrane regions. (Supported by U of M Grant-In-Aid No. 15214, and the Hormel Foundation.)

W-Pos211

STEADY-STATE NONMONOTONOUS CONCENTRATION PROFILES IN THE UNSTIRRED LAYERS OF BILAYER LIPID MEMBRANES.
((Yuri N. Antonenko* and Peter Pohl†)) *A.N. Belozersky Institute, Moscow State University, Moscow 119899, Russia; †Department of Med. Physics and Biophysics, Martin Luther University, 06097 Halle, Germany.

pH gradients of the unstirred layers (USL) near lipid bilayer membranes were measured with pH microelectrode in the presence of transmembrane fluxes and reactions producing or consuming H^+. Under these conditions peculiarities in the pH profiles were observed which with the classical definitions of USL thickness in terms of the concentration gradient at the interface would lead to absurd conclusions. A new equation is proposed which predicts similar USL thickness in the case of exponential concentration profiles and in addition predicts reasonable results under the conditions of nonmonotonous profiles.

W-Pos212

A COMPARATIVE STUDY OF PLANAR LIPID MEMBRANES FORMED BY MONTAL-MUELLER AND MUELLER-RUDIN TECHNIQUES.

((A.N.Chanturiya)) LTPB, NICHD, NIH, Bethesda, MD 20892

Planar phospholipid bilayer membranes formed by two techniques, Montal-Mueller and Mueller-Rudin, were compared in order to determine the difference between these two types of BLMs. The specific capacitance and the morphology of membranes formed from different lipid/solvent combinations were examined using a ramp of voltage and high resolution interference contrast and fluorescence microscopy. It was found that the specific capacitance depends more upon the choice of lipids and hydrocarbons used for membrane formation than upon the method of formation. For diphytanoyl-phosphocholine membranes, capacitance increases with the increase in molecular weight of the hydrocarbon used for hole pretreatment, or for making membrane-forming solution; for phosphatidylethanolamine membranes, the use of squalene results in a lower capacitance than measured for hexadecane-based membranes. No differences were found in the morphology of membranes formed using either technique. Both of them have tori and often contain lenses and/or linear structures. Examination of these structures in membranes formed with the addition of fluorescent lipid indicates that they contain lipid dissolved in hydrocarbon.

W-Pos213

THE CRITICAL MICELLE CONCENTRATION OF DIMYRISTOYLPHOSPHATIDYLGLYCEROL.

((M. Koshinuma, A. Nakamura, K. Tajima, and N.L. Gershfeld)) NIAMS, NIH, Bethesda, MD 20892 (Spon. by R. Horowitz)

We have measured the temperature dependence of the critical micelle concentration (cmc) of the Na salt of dimyristoylphosphatidylglycerol (DMPG-Na) in water by three independent methods: a) surface tension, b) conductivity, and c) Na-ion binding. Micelles do not form at temperatures below 32°C even in saturated solutions of the lipid. The phase diagram of the lipid dispersion indicates this temperature is the Krafft "point", and therefore the cmc ($1.1x10^{-4}$M) equals the solubility of the lipid at this temperature. This temperature is near T* the temperature of the critical unilamellar state for DMPG (1). Above this temperature the cmc of this compound decreases as temperature increases. Thus, at 36°C the cmc is $1.1x10^{-5}$M. Similar phase diagrams can be drawn for the neutral phospholipids DMPC and DPPC where the Krafft temperatures, below which no micelles form, are 29 and 43°C, respectively.

(1) N.L. Gershfeld, W.F. Stevens, R.J. Nossal, Faraday Discuss. Chem. Soc., 81, 19-28 (1986)

W-Pos214

INFLUENCE OF BILAYER CHARGE AND ELECTROLYTE CONCENTRATION ON T* THE CRITICAL TEMPERATURE FOR SELF-ASSEMBLY OF THE UNILAMELLAR STATE OF DIMYRISTOYLPHOSPHATIDYLGLYCEROL.

((K. Fukada, K. Tajima, and N.L. Gershfeld)) NIAMS, NIH. Bethesda, MD 20892

We have previously demonstrated that a multilamellar dispersion of DMPC exhibits a heat capacity (Cp) anomaly between 28.70 and 29.50 °C; this anomaly has been attributed to the transformation from multilamellar to a unilamellar state, at a critical point T* = 28.96±0.01 °C (1). The free energy of the transformation ΔG_{tran} was equal to the work done against the van der Waals force that exists between the neutral bilayers of the multilamellar state. We have now extended the heat capacity studies to dispersions of NaDMPG, an ionized bilayer system, in which T* and the corresponding free energy of the multilamellar-unilamellar transformation was measured as a function of NaCl concentration in the dispersion. With increasing NaCl concentration T* decreases continuously from 31.6 °C in water to 30.0 °C in 0.4 m NaCl. Cp anomalies are observed for all dispersions of DMPG in the region of their respective T*, with ΔG_{trans} values negative at low ionic strength (0.1 m) and positive at higher (0.4 m) NaCl concentrations. The contributions of van der Waals force and the electrical double layer potential of the bilayers to these transformation energies will be presented.

(1) N.L. Gershfeld, C.P. Mudd, K. Tajima, and R.L. Berger, Biophysical J., 65, 1174-1179 (1993).

W-Pos215

DETERMINATION OF THE PHOSPHOLIPID CRITICAL BILAYER CONCENTRATION

((J. T. Buboltz and G. W. Feigenson)) Section of Biochemistry, Mol. and Cell Biology, Cornell University, Ithaca New York 14853

In aqueous suspension, bilayer phase phospholipid will come to equilibrium with monomeric phospholipid. This critical bilayer concentration (CBC) is a valuable thermodynamic parameter, as discussed by Gershfeld [(1989) Biochemistry **28**]. Typical phospholipid CBCs appear to be in the sub-nanomolar regime, and so their measurement presents an experimental challenge. We have characterized several important phenomena that must be taken into account in order to conduct meaningful CBC studies. In particular, the time scale of equilibrium, surface adsorption and trace impurities must be rigorously accounted for. An accurate method for CBC determination has been developed, based on these observations, and we will present results obtained for ^{14}C-labelled dilauroyl-PC. We'll also discuss insights into equilibrium surface binding (at both the air-water and teflon-water interfaces), as well as phospholipid hydrolysis in aqueous solution at pH 7.

W-Pos216

DSC, FT-IR AND ^{31}P-NMR STUDY OF THE INTERACTION OF DIACYLGLYCEROL, PHOSPHATIDYLSERINE AND CALCIUM.

((J. Villalaín, F. López-García and J.C. Gómez-Fernández)) Biochemistry (A), Edf. Veterinaria, Universidad de Murcia, Apdo. 4021, E-30080 Murcia, Spain.

Diacylglycerols are important lipid mediators which activate protein kinase C (PKC) in the presence of phosphatidylserine and Ca^{2+}. We have studied the interaction between DPG with DPPS in the absence and in the presence of Ca^{2+} by using DSC, FTIR, ^{31}P-NMR and $^{45}Ca^{2+}$-binding. DPG increased the phase transition temperature of DPPS in the presence of Ca^{2+}, inducing a rigidification of the complex DPPS/Ca^{2+}. In the absence of Ca^{2+}, DPG induced an increase in the dehydration of the C=O ester groups of DPPS, whereas in its presence, DPG abolished the solid-solid transition of the complex DPPS/Ca^{2+}. Lipid immiscibilities were detected at concentrations of 1,2-DPG higher than 30 mol% and 20 mol% in the absence and in the presence of Ca^{2+}, respectively, where non-lamellar phases were observed by ^{31}P-NMR. DPG induced a dehydration of the PO_2^- group of DPPS at non-saturating Ca^{2+} concentrations, whereas full dehydration was observed at DPPS/Ca^{2+} molar ratios of 3 instead of 2, what is usually found for pure DPPS in the presence of Ca^{2+}. In contrast, $^{45}Ca^{2+}$-binding studies showed that the usual stoichiometry found for DPPS and Ca^{2+} is not altered in the presence of DPG. DSC showed that the DPPS/Ca^{2+} transition observed at 155°C was significantly perturbed by the presence of 1,2-DPG. These results indicate that DPG alters the phase behaviour of DPPS, even at non-saturating Ca^{2+} concentrations, a very important effect to be considered in the activation of PKC by diacylglycerols.

Supported in part by grants No. PM90-0044 and PB920-0897 (DGICYT, Spain).

W-Pos217

FT-IR INVESTIGATIONS INTO THE STRUCTURAL POLYMORPHISM OF LIPID A AND LIPOPOLYSACCHARIDES IN AQUEOUS SOLUTION.

((K. Brandenburg and U.Seydel)) Forschungsinstitut Borstel, D-23845 Borstel, Germany

Lipopolysaccharides (LPS), the endotoxins of Gram-negative bacteria, exert a variety of biological activity in mammals ranging from pathophysiological effects like shock and fever to beneficial ones like cytokine induction (TNF, interleukins). LPS are composed of a saccharide moiety with - depending on the bacterial mutant - varying length and a covalently-linked hydrophobic portion termed lipid A, the 'endotoxic principle' of LPS. For the endotoxin:cell interaction, it can be assumed that the supramolecular structure and the state of order of the acyl chains of LPS aggregates in an aqueous environment are important determinants. Therefore, we have measured the structural polymorphism of lipid A and LPS as function of temperature, Mg^{2+}-concentration, and water content. Depending on these parameters, various lamellar as well as non-lamellar (cubic, H_{II}) structures are observed. The acyl chain melting phase transition shows a clear dependence on the length of the saccharide chain (T_c = 30 to 37 °C) and is well expressed in particular for the IR-vibrations from the hydrophobic region. The supramolecular structures and the transitions between them can be characterized most readily by specific IR-band contours resulting from vibrations from the interface region, the ester carbonyl and amide bands. In contrast, bands from the pure hydrophilic and hydrophobic moieties are, if at all, less structure-sensitive.

W-Pos218

MOLECULAR SOURCES OF NONIDEAL OSMOTIC PRESSURE OF BSA SOLUTIONS AS A FUNCTION OF pH

((K. M. Kanal, G. D. Fullerton and I. L. Cameron)) UTHSCSA, San Antonio, Texas 78284-7800

Nonideal colligative properties of protein solutions are well known. Some researchers explain this due to volume occupancy and/or hydration force. In 1993, Fullerton *et. al.* derived new expressions to describe solution nonideal colligative properties including osmotic pressure. These expressions include a solute/solvent interaction parameter, I and an "effective" osmotic molecular weight, A_e, to describe the nonideality of the solution. We study here the variation in the cosolute osmotic pressure as a function of pH from 3.0 to 8.0, for bovine serum albumin (BSA) solutions, with 50 mmolal sodium chloride concentration. Electrostatic repulsion for pHs away from the isoelectric point (pH=5.4) cause protein denaturation with large increases in osmotic pressure (factor of 5 range). This nonideality change is attributed to two sources: [1] segmental motion leading to lower values of A_e and [2] large solute/solvent interactions for denatured proteins. The significance of either effect depends on the pH region and BSA concentration. It is concluded that the measured "effective" osmotic molecular weight, A_e, is only a true indicator of the molecular weight, A_e, when segmental motion and aggregation effects are prevented. This study shows greater than five-fold changes in osmotic pressure for the same protein concentration at different pHs. The largest nonideality changes are due to segmental motion of denatured filaments at low protein concentrations (< 20 g BSA/ kg water) while hydration due to increased solvent assessible area dominates at high protein concentrations (> 50 g BSA/ kg water). This suggests that factors controlling protein conformation will likely play an important role in tissue (cellular) water content.

W-Pos219

PREDICTION OF PKaS OF IONIZABLE GROUPS IN PROTEINS.

((M.K. Gilson, Jan Antosiewicz[1] and J.A. McCammon)) Dept. of Chemistry, University of Houston, Houston, TX 77204-5641; [1]On leave from Dept. of Biophysics, University of Warsaw, 02-089, Poland.

We describe what may be the most accurate approach currently available for the calculation of the pKas of ionizable groups in proteins, starting from crystallographic coordinates. Accuracy is assessed by comparing computed pKas with 60 measured pKas in 7 proteins. The RMS error is 0.89 pKa units. Linear regression fit of computed vs. measured pKas yields a slope of 0.95, y-intercept of -0.02, and a correlation coefficient of 0.96. The method also picks out many of the shifted pKas of groups in enzyme active sites and strong salt-bridges. The methodology is based upon finite difference solutions of the Poisson-Boltzmann equation. Its success depends upon the use of the rather high protein dielectric constant of 20. However, theoretical considerations and the fact that pKa shifts which result from desolvation are underestimated here implies that the dielectric constant of the protein interior is really lower than 20. We suggest that the high protein dielectric constant improves the overall agreement with experiment because it accounts crudely for phenomena which mitigate pKa shfits, and which are not specifically included in the model. Future models treating such phenomena explicitly, and using a more realistic low protein dielectric constant, should yield improved agreement in calculations of the pH-dependent properties of proteins.

W-Pos220

DIFFUSION OF IONS IN WATER: A SIMPLE CORRECTION THAT ACCOUNTS FOR THE SIGN OF THE IONIC CHARGE.

(J.L. Marin and M. Huerta) Centro de Investigación en Física, Universidad de Sonora, Apdo. Postal 5-088, 83190 Hermosillo, Son, MEXICO and C.U.I.B., Universidad de Colima, Apdo. Postal 199, 28000 Colima, Col. MEXICO.

Experimental observations show that the diffusion coefficients for single charged cations in water are markly different than those for single charged anions, To our knowledge, neither Stokes-Einstein equation nor further improvements on it, account for this fact. Due to the polar nature of water, the microscopic surroundings of a positive ion are different than those for a negative one since in the first case oxigen is closer to the ion than hydrogen and the contrary occurs in the second case. Moreover, as consequence of Pauli's exclusion principle, there is a repulsion between electronic clouds of the ion and the water molecule and it is clearly different whereas the ion is positive or negative. This repulsion can be included, as a correction in the equation for the diffusion coefficient, in the form of a Born-Mayer-type term. In this work we present preliminary results for the diffusion coefficients of single cations and anions calculated following the above consideration

W-Pos221

THE INDUCIBLE MULTIPOLE SOLVATION MODEL: A FAST APPROACH FOR IMPLICIT SOLVENT ELECTROSTATICS

((Malcolm E. Davis))
Macromolecular Modeling, Bristol-Myers Squibb, P.O.Box 4000, Princeton, NJ 08543-4000.

Realistic implicit solvent models are important for long time-scale dynamics simulations as well as conformational and database searching, or any study which requires the calculation of electrostatic energies and forces in solution for large numbers of atomic configurations. Continuum models have a long and surprising record of success in treating solvation phenomena. In recent years, finite-difference methods have been particularly successful by being able to include the detailed shape of the solute. These methods, however, even with powerful numerical techniques like multi-gridding, are too slow for many applications, and suffer from various numerical problems arising from discretizing space. In response, we have developed a new model, the Inducible Multipole Solvation model, which describes the polarization charge, responsible for the reaction field of the solvent, in terms of inducible multipole expansions at the center of each atom of the solute. In this way results as accurate as finite-difference methods can be obtained at the speeds of polarizable *in vacuo* models, and without many of the numerical problems. To demonstrate the methods applicability to a wide range of problems, calculations of small molecule solvation energies, azurin pKa shifts, and SOD fields will be presented.

W-Pos222

EVALUATING ELECTROSTATIC SOLVATION ENERGIES OF BIOMOLECULES USING THE FAST MULTIPOLE ALGORITHM.

((R. Bharadwaj, A. Windemuth, A. Nicholls, S. Sridharan and B. Honig)) Dept. of Biophysics, Columbia University, New York, NY 10032

The Fast Multipole Algorithm (FMA) has been incorporated into the boundary element method (BEM) for solving Poisson's equation for a molecule of arbitrary shape. The BEM involves a tesselation of the molecular surface to yield a set of simple equations that relate the surface charge on each element to the electric field at its position. The equations can be solved self-consistently by repeatedly calculating the field at each surface element from all charges according to Coulomb's law and reiterating the surface charges until convergence is achieved. Direct application of Coulomb's law is very time consuming, with a computation time that scales as the square of the number of surface elements. Instead the FMA is used to calculate the electrostatic fields resulting in a computation that scales linearly with the number of surface elements. Using the FMA in conjunction with a successive over-relaxation technique permits us to calculate solvation energies of large biomolecules at much higher resolutions than is possible with either finite-difference or boundary element methods. We compare the accuracy of solvation energies calculated using the BEM/FMA method to analytical results for a spherical molecule and to results from finite-difference calculations for intermediate and large-sized molecules.

W-Pos223

ROLE OF ELECTROSTATIC INTERACTIONS IN THE COMPLEX FORMATION OF CYTOCHROME C PEROXIDASE AND CYTOCHROMES C.

((H.-X. Zhou)) Laboratory of Chemical Physics, NIDDK, NIH, Bethesda, MD 20892.

Electrostatic calculations are made on the complexes of yeast cotychrome *c* peroxidase (CCP) with yeast and horse cytochromes *c* (cc), taking into consideration salt ions and the low dielectric constant of protein interior. Calculated interaction energies between CCP and cc are consistent with experimental findings about the effects of salt ions and mutations on the binding constant. The binding properties of several mutants are predicted. It is expected that at low ionic strengths, the $Arg^{13} \rightarrow$ Ile and $Gln^{16} \rightarrow$ Lys mutations will decrease the binding constant by 500 and 10 folds, respectively. A single mutation, $Glu^{90} \rightarrow$ Gln, on horse cc is predicted to make this protein bind more strongly to yeast CCP than its native partner yeast cc.

W-Pos224

CALCULATION OF ELECTROSTATIC EFFECTS AT THE AMINO TERMINUS OF AN ALPHA HELIX ((D. Sitkoff, D. J. Lockhart, K. A. Sharp and B. Honig) University of Pennsylvania, Whitehead Institute for Biomedical Research at MIT and Columbia University (Spon. by David Lockhart)

It is generally believed that the electrostatic field arising from the dipolar charge distribution in alpha helices is important for protein structure and function. We report an accurate calculation of the electrostatic potential and field at the amino terminus of an alpha helix in water, obtained using a finite difference solution to the Poisson-Boltzmann equation (FDPB). This method takes into account the detailed helix shape and charge distribution, solvent and generalized ionic strength effects. The accuracy of the calculated potential and field is confirmed through comparison with the experimentally observed helix-induced Stark effect and pK_a shift of a probe at the N-terminus of a stable, monomeric alpha helical peptide (Lockhart, D. J.; Kim, P. S. *Science*, **1992**, *257*, 947; **1993**, *260*, 198.) Ionic screening effects are reproduced up to 0.2 M NaCl. Deviations at higher ionic strengths result from non-Debye-Huckel effects (specific ion-solute and/or ion-solvent interactions.) The FDPB method was used to analyse the per-residue and solvent contributions to the helix potential and field. Backbone contributions come primarily from the first 1-2 helical turns. Charge-charge interactions in the unfolded state contribute significantly to helix-induced pK_a shifts for certain probe-peptide combinations. Additionally, the calculation of Stark effect shifts suggests a previously unexplored application of the FDPB method in computing effects of electrostatic fields on electronic transition energies in the complex environment of a protein and solvent.

W-Pos225

MONOVALENT AND DIVALENT SALT EFFECTS ON THE DRUG BINDING WITH DNA.
((Shu-Wen W. Chen and Barry Honig)) *Department of Biochemistry and Molecular Biophysics, Columbia University, 630W 168th Street, New York, NY 10032.* (Spon. by K. C. Smith)

The effects of monovalent and divalent cations on the binding of antibiotics DAPI with B-DNA in water have been investigated. The dependence of free energy changes in the system on the concentration of monovalent and/or divalent cations is the question of interest in the present work. The free energy change is obtained from electrostatic potentials which are calculated by solving the non-linear Poisson-Boltzmann (PB) equation. A finite difference method is applied to the solution of the PB equation in the 3-dimensional space of the system, where the distribution of mobile ions is described by the Boltzmann distribution and solvent is treated as a dielectric continuum containing mobile ions. The current results show that the presence of salt (both monovalent and divalent cations) weakens the binding of DAPI with DNA. The slope of $\Delta\Delta G$ v.s. $\ln[M^+]$ changes with divalent ionic concentration or vice versa. The product of the slope and the charge on the cation is close to the charge on DAPI. This result is consistent with the previous work.

W-Pos226

SALT EFFECTS ON DNA/LIGAND BINDING: COMPARISON OF POISSON-BOLTZMANN, AND COUNTERION BINDING/RELEASE MODELS
((K. A. Sharp[1], V. Misra[2], R. Friedman[2], J. Hecht[2] & B. Honig[2])), [1]Dept of Biochemistry, U. Pennsylvania, [2]Dept of Biochemistry, Columbia Univ

Binding of charged ligands to DNA depends strongly on non-specific salt effects. Finite difference solutions to the Non-Linear Poisson-Boltzmann equation (FDPB) incorporating detailed molecular shape information, combined with variational methods to evaluate total electrostatic free energies, were used to calculate both the salt dependence and the absolute contribution of salt to binding for three complexes: a cylinder/sphere model, the drug DAPI/DNA and lambda repressor binding domain/DNA. Ion redistribution (cratic) entropy, the ion-polyion and ion-ion electrostatic free energies of interaction each contribute to the salt dependence. The latter two terms contain large previously unrecognized contributions from dielectric (water orientation) entropy. In all systems the absolute effect of salt is to oppose binding, the predominant effect being the more favorable ion-polyion ('solvation') interaction of both ligand and DNA with their respective ion atmospheres in the unbound state. For the cylinder/sphere and DAPI systems FDPB and counterion binding/release models give similar dependences of the binding on salt concentration, but with quite different energetic contributions. The entropy of ion release favors binding but provides only 50% or less of the salt dependence in the FDPB model and does not drive binding. Non-specific anion effects, which are included in the FDPB model by treating the ligand in the same detail as the DNA, contribute significantly to the salt dependence, especially for lambda/DNA binding. In the FDPB model salt dependent enthalpy changes, seen experimentally with some drugs, can arise from the ion-polyion and ion-ion electrostatic terms.

W-Pos227

A SIMPLE TEST OF VALIDITY OF POISSON-BOLTZMANN EQUATION FOR INTERFACIAL REGIONS. ((V.S.Vaidhyanathan)), department of biophysical sciences, S.U.N.Y. at Buffalo, Buffalo, New York, 14221.

The equilibrium Nernst expression, (NE), utilized in the Poisson equation, results in Poisson-Boltzmann equation, (PB), which is the starting point of theories of electrolytes and diffuse double layer. Solutions of PB lead to monotonic concentration and electric potential profiles. Both NE and the Maxwell's Osmotic Balance equation (MOB) are exactly valid, if the limiting expression for electrochemical potential of an ion in solution is valid. The MOB relates the sum of concentrations of solute ions in an inhomogeneous region at two different locations with the difference in electric fields at these two locations. Knowledge of the concentration profiles of ions of the inhomogeneous region system, enables one to compute the charge density profile. NE yields the value of electric potential difference between say the surface and bulk homogeneous region when concentrations at surface and bulk are known. The charge density profile in the system, together with the assumption of constant dielectric coefficient, enables one to integrate, and obtain the value of electric field profile. Thus, with the stipulation that electric field in homgeneous region is zero, the value of electric field at the surface in known, apart from the value, d. Therefore d is known. Integration of the electric field profile, yields the electric potential profile, which leads to specific value of electric potential at the surface. The two values of electric potential at the surface computed using the double integration of charge density profile and NE should tally, if the limiting expression for the electrochemical potential is valid exactly. If there is disagreement, then PB is not valid in inhomogeneous interfacial region, the discrepancy being ascribed as first due to neglect of ion-ion interactions. Use of mass conservation equation to all ions except one, leads to the conclusion that the concentration profiles of all ions in the inhomogeneous region should be oscillatory with respect to position variable. This requires that the electric potential profile be also oscillatory, if NE is valid. Our calculations indicate that in both cases of assumed monotonic concentration profiles and profiles with extrema, the calculated values of electric potential at the surface, using the integrations of charge density profile does not agree with the value computed using Nernst expression.

W-Pos228

NUMERICAL SOLUTION OF THE NONLINEAR POISSON-BOLTZMANN EQUATION AT A MEMBRANE-ELECTROLYTE INTERFACE. ((K. E. Forsten[1], R. E. Kozack[2], D. A. Lauffenburger[1], and S. Subramaniam[2])) [1]Department of Chemical Engineering and [2]Beckman Institute, Department of Physiology and Biophysics, National Center for Supercomputing Applications, University of Illinois, Urbana, IL 61801

In modeling the behavior of biomembranes, it is necessary to account for the large spatial extent of the system without introducing unphysical truncations. Here, the electrostatic potential in the vicinity of the interface between a membrane and an ionic medium is determined through a numerical solution of the nonlinear Poisson-Boltzmann equation. The planar nature of the membrane is simulated by the implementation of periodic boundary conditions. This approach allows for the consideration of complex membrane charge distributions as well as membrane-bound proteins. For a variety of ionic strengths and charge densities, the field produced by a discrete array of charges is compared with Gouy-Chapman theory, which assumes an evenly smeared charge density on the membrane. The transmembrane potential also is investigated. (Supported in part by grants from the NIH and FMC Corporation.)

W-Pos229

THE ROLE OF THERMAL FLUCTUATIONAL BASE PAIR DISRUPTION IN DNA B TO Z CONFORMATION CHANGE. ((Y.Z. Chen and E.W. Prohofsky)) Department of Physics, Purdue University, West Lafayette, IN 47907-1396.

One of the scenarios for the pathway of DNA B to Z transition is that the transition involves base pair separation. It is interesting to note that thermal fluctuational base pair opening has been observed in both B and Z DNA helices. The observed life times for both B and Z DNA base pairs are well within the range of the time scale associated with B to Z transition. This seems to indicate that thermal fluctuational base pair disruption is fast enough to facilitate the transition. We have carried out a calculation to determine the salt and temperature dependent base pair opening probability of both B and Z DNA Poly d(GC)·Poly d(GC). Our calculation is based on a microscopic selfconsistent phonon approach of anharmonic lattice dynamics theory. Our calculated base pair opening probabilities are in fair agreement with the observed probabilities for the B conformation at low salt and Z conformation at high salt respectively. The calculated salt dependence of the probabilities indicates a B to Z transition at a salt concentration close to the observed concentration. We also find a small temperature dependence in the transition over a small region of salt concentration in agreement with some experiments.

W-Pos230

PLANCK-BENZINGER THERMAL WORK FUNCTION: DEFINITION OF TEMPERATURE-INVARIANT ENTHALPY IN BIOLOGICAL SYSTEMS.
((Paul W. Chun)) Department of Biochemistry and Molecular Biology, University of Florida, Gainesville, Florida 32610.

In reexamining the thermodynamic parameters of a number of self-associating protein systems in the standard state near 300 degrees Kelvin, we found that at the stable temperature $\langle T_s \rangle$, the thermodynamic quantities $\Delta G^0(T_s)$ and $\Delta W^0(T_s)$ reach a minimum and maximum, respectively, while $T\Delta S^0(T_s)$ approaches zero. Based on the Planck-Benzinger thermal work function, (Chun, 1988), $\Delta W^0(T) = \Delta H^0(T_0) - \Delta G^0(T)$. Therefore $\Delta H^0(T_0) = \Delta W^0(T_s) + \Delta G^0(T_s)$ at $\langle T_s \rangle$. Values for $\Delta H^0(T_0)$ at $\langle T_s \rangle$ for four self-associating protein systems were found to deviate by less than 0.05% from values for $\Delta H^0(T_0)$ at zero degrees Kelvin. Benzinger's definition (1971) is applied in measuring $\Delta H(T_0)$ for DNA unwinding and protein unfolding in the non-standard state near 340°K. $\Delta H(T) = \Delta H(T_0) + \int \Delta Cp(T)dT$ at the melting temperature, $\langle T_m \rangle$, where $\Delta H(T)$ and $T\Delta S(T)$ are of the same magnitude, $\Delta W(T) = \Delta H(T_0)$ and $\Delta G(T)$ approaches zero. Values for $\Delta H(T_0)$ at $\langle T_m \rangle$ for the proteins we examined deviated by less than 0.04% from values for $\Delta H(T_0)$ at zero degrees Kelvin. The heat of reaction of any biological system consists of two terms, the heat capacity integral between product and reactant, and the temperature-invariant chemical bond energy, $\Delta H(T_0)$, which is a primary, indispensable source of the energy which allows life processes to proceed with quantitative precision. Failure to evaluate $\Delta H^0(T_0)$ or $\Delta H(T_0)$ in assessing any biological system will thus give only a partial picture of the processes taking place within that system.

†This work was supported by a faculty development award, Division of Sponsored Research, University of Florida.

W-Pos231

PROBABILITY DISTRIBUTION FOR SYSTEMS WITH MULTIPLE STATIONARY STATES.
((M. Samoilov)) Biophysics Program, Chemistry Department, Stanford University, Stanford, CA 94305 (Spon. by O. Jardetzky)

Autocatalytic reactions arise frequently in biological processes. A general form for the system with two intermediates could be written as:

$$A + (m-1)X \underset{k2}{\overset{k1}{\rightleftharpoons}} mX$$

$$sX + (r-1)Y \underset{k4}{\overset{k3}{\rightleftharpoons}} (s-1)X + rY$$

$$nY \underset{k6}{\overset{k5}{\rightleftharpoons}} (n-1)Y + B$$

where the chemical potentials of A and B are held constant. If at least one of the coefficients is greater then one, chemical kinetics of these reactions allows for the existence of multiple stationary state solutions. The question of relative likelihood of these states and fluctuations around them could be answered if we consider the system to be stochastic. Stochastic analysis requires finding a stationary probability distribution. A thermodynamic and stochastic theory based on the concept of work was proposed by Ross, Hunt and Hunt (RHH) [J. Chem. Phys. 88, 2719 (1988) and 92, 5272 (1990) and 96, 618 (1992)]. The authors suggest a form for the probability distribution, which makes it proportional to the exponent of the sum of integrals of chemical potential differences (between the actual and the reference system) over the respective concentrations. This formulation depends on the integration path in the concentration space. The extremal action principle applied to RHH formalism gives a way for the numerical evaluation of the probability distribution. The results yield relative probabilities of the various stationary states, as well as predict the likelihood of possible fluctuations away from them.

W-Pos232

DIVALENT EFFECTS ON MONO-VALENT CATION CHANNELS, AN EXTENSION OF POISSON-NERNST-PLANCK THEORY

Duan P. Chen and Robert S. Eisenberg, Department of Physiology, Rush Medical College, Chicago, Illinois 60612, U. S. A.

The Poisson-Nernst-Planck theory of open ionic channels is extended to account for the divalent effects on the mono-valent cation ion channels. We have proved that there is a unique Donnan's potential created by the surface charge on the two sides of the membrane when divalent ions are present. Our numerical results have shown: (1) Micromolar to millimolar divalent cation concentration in the cytoplasmic side will rectify the IV curve from strictly linear to the shape of an inward rectified channel, while the inwardly rectified single channel conductance is slightly increased; (2) Divalent ions do not contribute appreciably to the net current. That is to say that the reversal is mainly determined by the monovalent ion concentrations; (3) More than one steady state solutions to the above set of coupled non-linear equations are found even for uniform permanent charge distribution when divalent ions are present. These results agree well with the experimental facts known about the inwardly rectified potassium channels.

W-Pos233

POLYELECTROLYTE MEDIATED INTERACTIONS BETWEEN OPPOSITELY CHARGED PLANAR SURFACES AND MICELLAR AGGREGATES.
((R. Podgornik and B. Jönsson)) LSB / DCRT, NIH, Bethesda, MD 20892 and Physical Chemistry 2, Chemical Center, POB 124, Lund, SWEDEN (Spon. by D.Juretić)

Using mean - field theory, Monte Carlo simulations and scaling arguments we investigated forces between apposed charged planar surfaces and spherical aggregates, conferred by oppositely charged polymeric chains. In the planar case the most important characteristics of the forces is a region of intersurface separations characterised by net attractive roughly exponentially decaying forces between bounding surfaces, stemming from the bridging of polyelectrolyte chains between the two charged surfaces. The forces conferred by confined polyelectrolyte chains depend in an essential way on the conformation of the chains between the surfaces as can be ascertained from comparison between the monomer intersurface density profile and the concurrent forces. In the case of polyelectrolyte mediated forces between charged spherical aggregates the situation is quite similar. At interaggregate separations comparable to the length of the chain the force is attractive and linear in the interaggregate separation due to a special type of long range bridging attraction mediated by the polyelectrolyte chain, adsorbed to both aggregates. Beyond a certain separation (*capture separation*) there is a symmetry breaking transition in the monomer density distribution, resulting in a preferential adsorption of the chain to one of the aggregates. In both cases the attractive forces can be orders of magnitude stronger than the standard van der Waals attractions.

FOLDING AND SELF-ASSEMBLY II: STRUCTURE OF PROTEINS AND COMPLEXES

W-Pos234

MECHANISMS BASED ON X-RAY STRUCTURES OF TWO $(\beta/\alpha)_8$ BARREL ENZYMES: ADENOSINE DEAMINASE AND ALDOSE REDUCTASE
((David K. Wilson[1] & Florante A. Quiocho[1,2])) Baylor College of Medicine[1] and Howard Hughes Medical Institute[2], Houston, TX 77030.

We have determined the crystal structures of two different enzymes — adenosine deaminase (ADA) and aldose reductase (ALR2)*. Based upon these structures, the mechanism for each has been determined. ALR2 is currently the target of drug design efforts to reduce diabetic complications assocated with a number of tissue types. Aside from the implications for rational drug design, our structure has also shed light on the catalytic mechanism for the enzyme. It catalyzes a simple reaction in which a hydride is donated from an NADPH cofactor to the substrate. Subsequently a proton is abstracted from a general acid on the enzyme. The structure has allowed us to identify the residue most likely to be responsible for this and provided the basis for site directed mutants to test this theory. ADA is an enzyme which functions in the purine salvage pathway and is a critical component in the development and competence of the immune system. The initial structure revealed not only a previously unknown yet necessary Zn^{2+} cofactor but also that the inhibitor which was assumed to be a ground state analog had been converted into a transition-like state which is stable in the enzyme-bound form. Structures of the enzyme bound with a series of inhibitors were then determined. These inhibitors were carefully chosen such that the reaction "stalled" at different points along its course. This has painted a very clear picture of all of the detailed steps in the reaction pathway.

*In collaboration with J.M. Petrash, University of Washington Medical School.

W-Pos235

CRYSTAL STRUCTURE OF PORCINE RIBONUCLEASE INHIBITOR, A PROTEIN WITH LEUCINE-RICH REPEATS: A NOVEL CLASS OF ALFA/BETA STRUCTURE.
((Bostjan Kobe and Johann Deisenhofer)) Department of Biochemistry and Howard Hughes Medical Institute, University of Texas Southwestern Medical Center, Dallas, TX 75235. (Spon. by J. Deisenhofer)

Ribonuclease inhibitor (RI) is a 49-kDa protein that inhibits neutral and alkaline ribonucleases and angiogenin by very tight binding. The primary structure of RI consists of 15 leucine-rich repeats (LRR), alternately 28 and 29 residues long. RI belongs to a large family of proteins that all seem to be involved in protein-protein or protein-membrane interactions. The crystal structure of porcine RI was solved by multiple isomorphous replacement using ten heavy atom derivatives. The model has been refined to 2.5 Å resolution with an R-factor of 18.2% and contains all 456 residues. RI is a horseshoe-shaped protein with dimensions 70 x 62 x 32 Å. Individual LRR correspond to right-handed β–α structural units, similar to those found in many α/β proteins. The β–α units are, however, arranged in a way different from other known α/β structures. β-strands form a parallel β-sheet on the inner circumference of the horseshoe, while helices align on the outer circumference. The structure of RI and the available biochemical data suggest a possible ribonuclease binding region incorporating the surface formed by the parallel β-sheet and the neighboring loops. The crystal structure of RI represents the first three-dimensional structure of any protein containing LRR.